The role of exchange interactions in the formation of the magnetic structure in rare-earth orthoferrites $RFeO_3$ (R=Ho, Tb, Yb)

From the Faculty of Georesources and Materials Engineering of the

RWTH Aachen University

to obtain the academic degree of

Doctor of Natural Science

approved thesis

submitted by

Aleksandr Ovsianikov, M.Sc.

Advisors: **Herr Univ.-Prof. Dr. rer. nat. Georg Roth**
Herr Univ.-Prof. Dr. rer. nat. Thomas Brückel

Date of the oral examination: 22.02.2023

Acknowledgements

First and foremost, I would like to express my sincere gratitude to my advisors, Prof. Dr. rer. nat. Georg Roth (Institut fuer Kristallographie, RWTH Aachen University, Aachen) and Dr. rer. nat. Martin Meven (Institut fuer Kristallographie, RWTH Aachen University, Aachen) for their invaluable support, guidance, and encouragement.

I would also like to thank my colleagues Vladimir Hutanu (Institut fuer Kristallographie, RWTH Aachen University, Aachen) and Wolfgang F. Schmidt (Jülich Centre for Neutron Science at Institut Laue-Langevin, Grenoble, France) for their help in carrying out the experiments.

Above all, I would like to express my profound gratitude to my family and dear friends for making the period of my doctorate such a wonderful experience.

Abstract

The rare earth orthoferrite family RFeO$_3$, where R is a rare earth element, demonstrates a remarkable variety of magnetic properties. Its compounds crystallize in an orthorhombic perovskite structure with the space group Pnma. Different combinations of Dzyaloshinsky-Moriya interactions (DMI) and rare-earth ions with different ionic radii and filling of outer shells lead to a variety of magnetic effects. Rare earth orthoferrites are nowadays well known as multiferroics - materials with typically large magnetoelectric (ME) coupling and show the magnetocaloric effect (MCE). This cumulative dissertation investigates various orthoferrites RFeO$_3$ (R=Ho, Tb, Yb) using neutron scattering methods.

The orthoferrite HoFeO$_3$ was studied by single crystal inelastic neutron scattering. It was shown that the spin dynamics of the Fe subsystem does not change through the spin reorientation transitions. The observed spectrum of magnetic excitations was analyzed in the framework of linear spin-wave theory. Within this approach the antiferromagnetic exchange interactions of nearest neighbors and next nearest neighbors were obtained for the Fe subsystem. Parameters of DMI at the Fe subsystem were refined. The temperature dependence of the gap in the Fe spin-wave spectrum indicates the temperature evolution of the anisotropy parameters. Estimations for the values of the Fe-Ho and Ho-Ho exchange interactions were made as well.

Using the new polarized neutron diffraction (PND) setup of the instrument POLI at MLZ the spin reorientation transition in the HoFeO$_3$ was studied at different wavelengths. The various experiments provided reproducible results demonstrating high reliability of the used setup. It was shown that during the phase transition at T_{SR}=53 K in an external magnetic field applied along the crystal c-axis, the ordered magnetic moment of the Fe sublattice rotates from the crystallographic direction b to a not just in the ab plane, but through the z axis. This means that the applied field breaks the orthorhombic symmetry allowing some magnetization parallel to z within a small temperature region. Interestingly, this is the same temperature region where the large magnetocaloric effect for HoFeO$_3$ was previously reported. A general model of the magnetic structure of HoFeO$_3$, unconstrained by the orthorhombic symmetry, would allow the magnitudes and directions of the moments on each of the 8 magnetic sublattices in the unit cell to be independent of one-another, leading to 24 independent magnetic parameters. PND measurements were used to determine the absolute sign of the DMI in the ab plane for the Fe magnetic sublattice at 65 K. DMI plays an important role in the energy balance of the system.

Neutron diffraction studies of HoFeO$_3$ single crystals were performed under external magnetic fields. The interplay between the external magnetic fields, Dzyaloshinsky-Moria antisymmetric exchange, isotropic exchange interactions between Fe and Ho sublattices and within the Fe sublattice provides a rich magnetic phase diagram. As result of the balance of exchange interactions inside the crystal and external magnetic fields, eight different magnetic phases were found, which are induced or suppressed dependent on the external field.

Investigations of the orthoferrites TbFeO$_3$ and YbFeO$_3$ were performed by neutron inelastic scattering and neutron single crystal diffraction in magnetic fields. The low temperature evolution of energy gaps was explored for both compounds and considered from the point of view of changes of rare earth ion anisotropy. Exchange parameters between nearest neighbors for Fe^{3+} in TbFeO$_3$ were obtained. The magnetic phase diagram for YbFeO$_3$ was obtained and discussed as a result of the energy balance between Heisenberg exchange interactions, Dzyaloshinsky-Moriya interaction, anisotropy and external magnetic field.

Abstrakt

Die Orthoferrit-Familie der Seltenen Erden $RFeO_3$, bei der *R* ein Element der seltenen Erden ist, weist eine bemerkenswerte Vielfalt an magnetischen Eigenschaften auf. Seine Verbindungen kristallisieren in einer orthorhombischen Perowskitstruktur mit der Raumgruppe Pnma. Verschiedene Kombinationen der Dzyaloshinsky-Moriya-Wechselwirkung (DMI) und Seltene-Erden-Ionen mit unterschiedlichen Ionenradien und Füllungen der äußeren Schalen führen zu einer Vielzahl von magnetischen Effekten. Orthoferrite der Seltenen Erden sind heute als Multiferroika bekannt - Materialien mit typischerweise großer magnetoelektrischer Kopplung (ME) und magnetokalorischem Effekt (MCE). In dieser kumulativen Dissertation werden Orthoferrite $RFeO_3$ (*R*=Ho, Tb, Yb) mit Hilfe von Neutronenstreuungsmethoden untersucht.

Mit Hilfe der inelastischen Neutronenstreuung an Einkristallen wurde der Orthoferrit $HoFeO_3$ untersucht. Es wurde gezeigt, dass sich die Spindynamik des Fe-Subsystems durch die Spinumorientierungsübergänge nicht ändert. Das beobachtete Spektrum der magnetischen Anregungen wurde im Rahmen der linearen Spin-Wellen-Theorie analysiert. Im Rahmen dieses Ansatzes wurden die antiferromagnetischen Austauschwechselwirkungen der nächsten Nachbarn und der nächstgelegenen Nachbarn für das Teilsystem Fe ermittelt. Die Parameter der DMI im Fe-Subsystem wurden verfeinert. Die Temperaturabhängigkeit der Lücke im Fe-Spinwellenspektrum zeigt die Temperaturentwicklung der Anisotropieparameter. Es wurden auch Schätzungen für die Werte der Fe-Ho und Ho-Ho Austauschwechselwirkung vorgenommen.

Mit dem neuen Setup für polarisierte Neutronenbeugung (PND) des Instruments POLI am MLZ wurde der Übergang der Spinumorientierung in $HoFeO_3$ bei unterschiedlichen Wellenlängen untersucht. Die verschiedenen Experimente lieferten reproduzierbare Ergebnisse, die die hohe Zuverlässigkeit des verwendeten Aufbaus belegen. Es wurde gezeigt, dass während des Phasenübergangs bei T_{SR}=53 K in einem externen Magnetfeld, das entlang der *c*-Achse des Kristalls angelegt wird, das geordnete magnetische Moment des Fe-Untergitters von der kristallographischen Richtung *b* zu *a* nicht nur in der *ab*-Ebene, sondern durch die *z*-Achse rotiert. Das bedeutet, dass das angelegte Feld die orthorhombische Symmetrie bricht und eine gewisse Magnetisierung parallel zu *z* innerhalb eines kleinen Temperaturbereichs ermöglicht. Interessanterweise ist dies derselbe Temperaturbereich, in dem zuvor ein großer magnetokalorischer Effekt für $HoFeO_3$ berichtet wurde. Ein allgemeines Modell der magnetischen Struktur von $HoFeO_3$, das nicht durch die orthorhombische Symmetrie eingeschränkt ist, würde es ermöglichen, dass die Größen und Richtungen der Momente auf jedem der acht magnetischen Untergitter in der Einheitszelle unabhängig voneinander sind, was zu 24 unabhängigen magnetischen Parametern führt. PND-Messungen wurden verwendet, um das absolute Vorzeichen der DMI in der ab-Ebene für das magnetische Fe-Untergitter bei 65 K zu bestimmen. Die DMI spielt eine wichtige Rolle für die Energiebilanz des Systems.

Neutronenbeugungsstudien an $HoFeO_3$-Einkristallen wurden unter externen Magnetfeldern durchgeführt. Das Zusammenspiel zwischen den externen Magnetfeldern, dem antisymmetrischen Dzyaloshinsky-Moria-Austausch, den isotropen Austauschwechsel-wirkungen zwischen Fe- und Ho-Untergittern und innerhalb des Fe-Untergitters ergibt ein reichhaltiges magnetisches Phasendiagramm. Als Ergebnis des Gleichgewichts der Austauschwechselwirkungen innerhalb des Kristalls und der externen Magnetfelder wurden

acht verschiedene magnetische Phasen gefunden, die in Abhängigkeit vom externen Feld induziert oder unterdrückt werden.

Untersuchungen der Orthoferrite $TbFeO_3$ und $YbFeO_3$ wurden mittels inelastischer Neutronenstreuung und Neutronen-Einkristallbeugung in Magnetfeldern durchgeführt. Die Entwicklung der Energielücken bei niedrigen Temperaturen wurde für beide Verbindungen erforscht und unter dem Gesichtspunkt der Änderungen der Anisotropie der Seltenerdionen betrachtet. Die Austauschparameter zwischen den nächsten Nachbarn für Fe^{3+} in $TbFeO_3$ wurden ermittelt. Das magnetische Phasendiagramm für $YbFeO_3$ wurde als Ergebnis der Energiebilanz zwischen Heisenberg-Austauschwechselwirkungen, Dzyaloshinsky-Moriya-Wechselwirkung, Anisotropie und externem Magnetfeld ermittelt und diskutiert.

List of publications

1. A.K.Ovsyanikov, I.A.Zobkalo, W.Schmidt, S.N.Barilo, S.A.Guretskii, V.Hutanu, «Neutron inelastic scattering study of rare-earth orthoferrite HoFeO3», Journal of Magnetism and Magnetic Materials, Volume 507 (2020).

2. A. Ovsianikov, H. Thoma, O. Usmanov, P. J. Brown, T. Chatterji, A. Sazonov, S. Barilo, L. Peters, and V. Hutanu, "Breaking the magnetic symmetry by reorientation transition near 50 K in multiferroic magnetocaloric $HoFeO_3$" IEEE Transactions on Magnetics, Volume: 58, Issue: 2 (2022).

3. A.K. Ovsianikov, O.V. Usmanov, I.A. Zobkalo, V. Hutanu, S.N. Barilo, N.A. Liubachko, K.A. Shaykhutdinov, K. Yu Terentjev, S.V. Semenov, T. Chatterji, M. Meven, P.J. Brown, G. Roth, L. Peters, H. Deng, A. Wu, «Magnetic phase diagram of HoFeO3 by neutron diffraction», Journal of Magnetism and Magnetic Materials, Volume 557 (2022).

4. A. K. Ovsianikov, O.V. Usmanov, I. A. Zobkalo, W. Schmidt, A. Maity, V. Hutanu, E. Ressouche, K.A. Shaykhutdinov, K. Yu Terentjev, S.V. Semenov, M. Meven, G. Roth, L. Peters, «Inelastic neutron studies and diffraction in magnetic fields of $TbFeO_3$ and $YbFeO_3$», Journal of Magnetism and Magnetic Materials, Volume 563, 1 December 2022, 170025.

Contents

1. Introduction

An analysis of the current state of research in condensed matter physics shows that, in recent years, magnetically active materials with pronounced effects of interactions between different order parameters have become the focus of increasing attention [1-3]. These include multiferroics of complex structures, compounds with magnetoresistance and giant magnetocalorimetric effects as well as high-temperature superconductors, etc. Compounds of this type have the potential to create new functional materials or to improve their properties, allowing for technological breakthroughs in high-tech areas of industry. Studies of the microscopic mechanisms responsible for the interactions in such compounds can provide progress in the understanding and creation of new materials.

The discovery of the possibility to control electric polarization by magnetic ordering gave a new impulse to the development of the theory of magnetoelectric phenomena [4-6]. A necessary part of the problem of the interaction of magnetic and electrical order parameters in multiferroics is the study of magnetic interactions, the competition of which leads to various complex structures and to the appearance of ferroelectric polarization. The main purpose of this dissertation is to study the specifics of exchange interactions in RFeO$_3$ orthoferrites (R is a rare-earth element).

To complete this task, studies of RFeO$_3$ orthoferrites with different rare-earth elements R = Ho, Tb, Yb were planned and performed. The study of the crystalline and magnetic properties focused on various neutron scattering techniques. The specific features of complex magnetic structures and their evolution under changing external conditions – temperature and magnetic fields – were studied by neutron diffraction methods. Magnetic dynamics studies were performed by inelastic neutron scattering, which made it possible to obtain the parameters of exchange interactions in these compounds. These experiments were proposed as the magnetic structures realized in orthoferrites and the provided magneto-electric interactions are complex and non-collinear. Both symmetric (Heisenberg) exchange interactions of the species 3d-3d, 3d-4f, 4f-4f, and antisymmetric Dzyaloshinsky-Moriya interactions (DMI) between the same magnetic subsystems were studied using the inelastic neutron scattering method. One of the directions of research was a detailed study of the crystal structure of these compounds, the search for structural distortions in the low-temperature phase, which may indicate a decrease in crystal symmetry.

It is also important to note that the study of multiferroics is increasingly influencing neighboring research fields such as complex magnetism and ferroelectricity, oxide heterostructures and interfaces, as well as seemingly distant objects such as green ceramic synthesis [7, 8].

1.1 Motivation and research-relevant topics

This section contains a short history of multiferroics, magnetocalorics and rare-earth orthoferrites RFeO$_3$, their main properties and possibilities for the realization of technical applications.

1.1.1 **Multiferroics**

The first ideas about the possibility of the parallel existence of magnetic and electric order in one crystal were proposed by Pierre Curie [9], who showed that magnetic and electric ordering can coexist in crystals with a specific symmetry. Experiments confirming this theory were performed after the linear magnetoelectric (ME) effect for Cr_2O_3 [4-6] was predicted in 1957. In 1961 first experiments were performed on the polycrystal $Pb(Fe_{2/3}W_{1/3})O_3$, which showed the presence of ferroelectric and antiferromagnetic ordering [10]. The term "multiferroics" was proposed by Hans Schmidt in 1994 for materials possessing at least two of the three ordering types simultaneously: electrical, magnetic and elastic [11].

The relationship between magnetic and electrical ordering leads to different physical effects: magnetoelectric, magnetodielectric, electric polarization of magnetic domain boundaries, controlled chirality of Neel walls and others. There are several mechanisms leading to the appearance of multiferroic properties. For example, in "mixed" perovskites with ferroelectricity active d_0 ions and magnetically active d_n ions, the dislocation of d_0 ions from the centers of O_6 octahedrons leads to polarization, which coexists with magnetic ordering in octahedrons with d_n ion which are in the center of the octahedrons. In materials such as $BiFeO_3$ and $PbVO_3$, the Bi^{3+} and Pb^{2+} lone pair-ions have two outer 6s electrons that do not participate in chemical bonds. It is their ordering that contributes to polarization [12, 13]. In a charge-ordered material, the coexistence of non-equivalent positions with different charges and non-equivalent bonds (long and short) leads to ferroelectricity. In addition, multiferroics are classified into the first and second type. Multiferroics of the type I are materials in which ferroelectricity and magnetism have different origins and appear largely independent of each other. In such materials, ferroelectricity usually appears at higher temperatures than magnetism, and the spontaneous polarization P is often quite large (on the order of 10-100 μC/cm^2). For example, $BiFeO_3$ (T_{FE} ~ 1100 K, T_N ~ 643 K, P ~ 90 μC/cm^2) [14, 15] and $YMnO_3$ (T_{FE} ~ 914 K, T_N ~ 76 K, P ~ 6 μC/cm^2) [16]. In multiferroics of type II, magnetism is the cause of ferroelectricity. The polarization in these materials is usually much lower (~10^{-2} μC/cm^2) than for type I multiferroics. In such compounds, in addition to the linear ME effect, nonlinear effects of higher order in electric and magnetic fields (quadratic, cubic), as well as switching of electric polarization by magnetic fields are observed [17-19].

This variety of different physical effects makes multiferroics a good material for use in technology: magnetic field sensors, magnetic memory and spin electronics devices, non-volatile memory, microwave signal processing and more [1]. For example (figure 1), magnetic sensors are created based on composite materials, where the optimal sensor geometry is selected depending on the magnetic field [20]. Magnetoresistive random access memory based on the magnetoelectric effect allow to combine the speed of semiconductor memory with the non-

volatile characteristic of magnetic memory [2, 21]. However, it should be noted that most of these technologies are still under development and are not yet available for mass use.

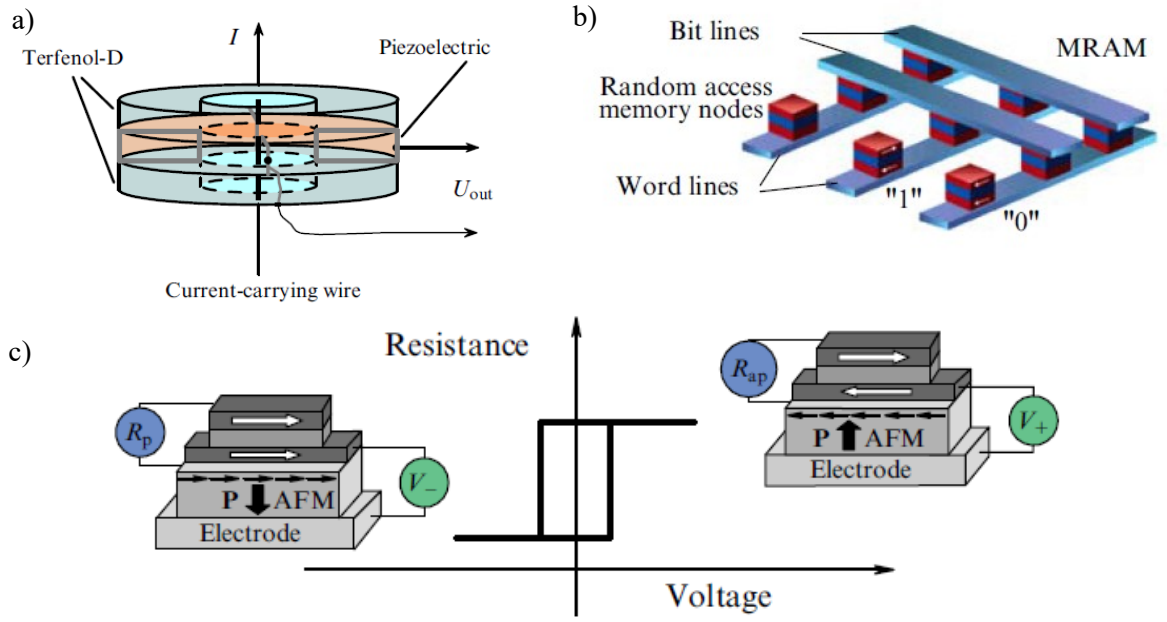

Figure 1. Some examples of the realization of technical devices based on multiferroics: a) magnetic field sensors [20]; b) Schematic of magnetic random access memory [2]; c) ME memory element [21];

1.1.2 **Magnetocalorics**

The magnetocaloric effect (MCE) [22] is the change in temperature of a magnetic material when an external magnetic field is applied to it. Heat is produced or absorbed in this process. If the process is carried out under adiabatic setting, for example by switching fastly a magnetic field on or off, this effect is demonstrated by a change in the temperature of the material. This phenomenon is usually called the magnetocaloric effect and compounds with large MCE are called magnetocalorics. This effect is characterized in two ways - by measuring the temperature change and by analyzing isotherms of magnetization and entropy change ΔS [23]. A material demonstrating the magnetocaloric effect usually heats up when a magnetic field is applied and cools down when the field is no longer applied - this is due to structural modifications of the material's magnetic domains - their configuration in correspondence with the magnetic field direction when it is applied and their disorder when it is absent.

Emil Warburg was the first who noticed the release of heat when iron is magnetized in 1881 [24]. Materials with a phase transition show a large magnetic entropy change within a small temperature range. For example, $Gd_5Si_2Ge_2$ is a material with a "giant" MCE that shows a transition accompanied by a structural phase transformation from an orthorhombic to a monoclinic crystal structure [25].

An important practical application of magnetocalorics is their use in magnetic coolers and magnetothermal pumps. Magnetic cooling using the magnetocaloric effect has high potential for environmentally friendly and energy efficient temperature control. The first room

temperature refrigeration (figure 2) units were built after 1997 at several research centers: Ames Laboratory [26], Mater. Science Institute Barcelona [27], Toshiba [28] and others [29]. Thus, an understanding of the physical mechanisms associated with the magnetocaloric effect will allow us to significantly optimize already available technical devices.

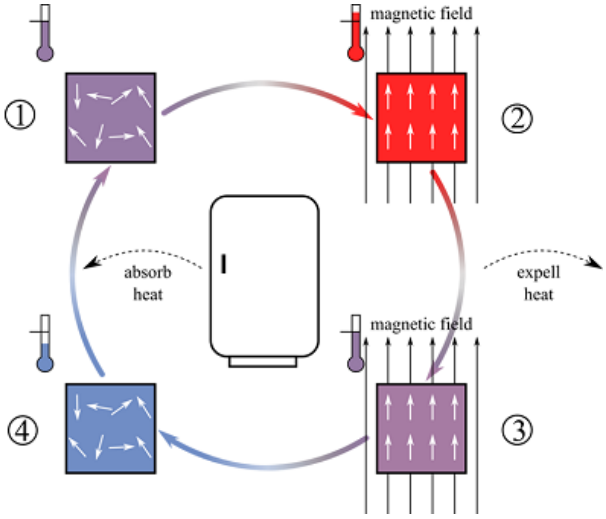

Figure 2. The magnetocaloric cooling cycle: First the refrigerant is exposed to a magnetic field (1) which results in a heating of the material (2). This excess heat is expelled to the surroundings (3). The removal of the magnetic field causes a cooling of the refrigerant and heat can be absorbed from the cooling compartment (4) [3].

1.2 Rare-earth orthoferrites

Rare-earth orthoferrites RFeO$_3$ have been studied since the 60s of the last century [30 – 32]. These compounds belong to the orthorhombic *Pnma* space group and have high Néel temperatures in the region T_N = 620 – 740 K (see figure 3). Below T_N, the iron subsystem orders antiferromagnetically with a weak ferromagnetic component. With temperature decrease, the influence of the R ion leads to spin-reorientation (SR) transitions, which take place in the case of magnetic rare-earth ions. There are no such transitions for the non-magnetic ions R = Y, La, Lu [33]. The amount and features of SR transitions vary for different magnetic R ions, as well as the characteristic temperatures T_{SR}. The temperature of spin-reorientation transitions ranges from T_{SR} = 37 K for DyFeO$_3$ [34] to T_{SR} = 480 K for SmFeO$_3$ [35]. For compounds with R= Dy, Sm, Tm, Er, Yb, only one SR transition is reported while in TmFeO$_3$ and ErFeO$_3$ an additional intermediate mixed phase [36, 37] is observed. Several SR transitions were detected in crystals with R = Ho, Tb [38, 39]. Spontaneous ordering of the rare-earth sublattice takes place below T_{NR} ~ 10 K.

Rare-earth orthoferrites show the properties of multiferroics and magnetocalorics. Electric polarization in DyFeO$_3$ was observed at higher temperature, around T_{SR} = 50 – 60 K [40]. In HoFeO$_3$ spontaneous electric polarization emerges at ~ 210 K [41]. In other orthoferrites like SmFeO$_3$, YFeO$_3$ and LuFeO$_3$, electric polarization was reported even at room temperature [42 – 44]. This brings these compounds close to being useful for potential applications in switching elements, sensors, memory and other advanced technical devices with low energy consumption [45-47]. In addition, orthoferrites RFeO$_3$ show interesting anisotropic

magnetocaloric phenomena. The magnetocaloric effect describes the temperature change of magnetic materials in an adiabatic process caused by magnetic entropy change ΔS_M under external magnetic field. In $TmFeO_3$, the entropy change ΔS_M has a maximum of ~ 12 J/kg K at 17 K under applied field of 7 T along the *c* axis; in $TbFeO_3$ ΔS_M reaches a value of ~ 25 J/kg K at ~ 12 K in an applied field of 7 T along the *a* axis [48]. In $HoFeO_3$ the entropy change ΔS_M has some extrema with values equal to 9 J/kg K at a temperature T = 53 K, ΔS_M = 15 J/kg K and ΔS_M = 18 J/kg K in an external field of 7 T at the temperatures T = 10 K and T = 3 K respectively [49].

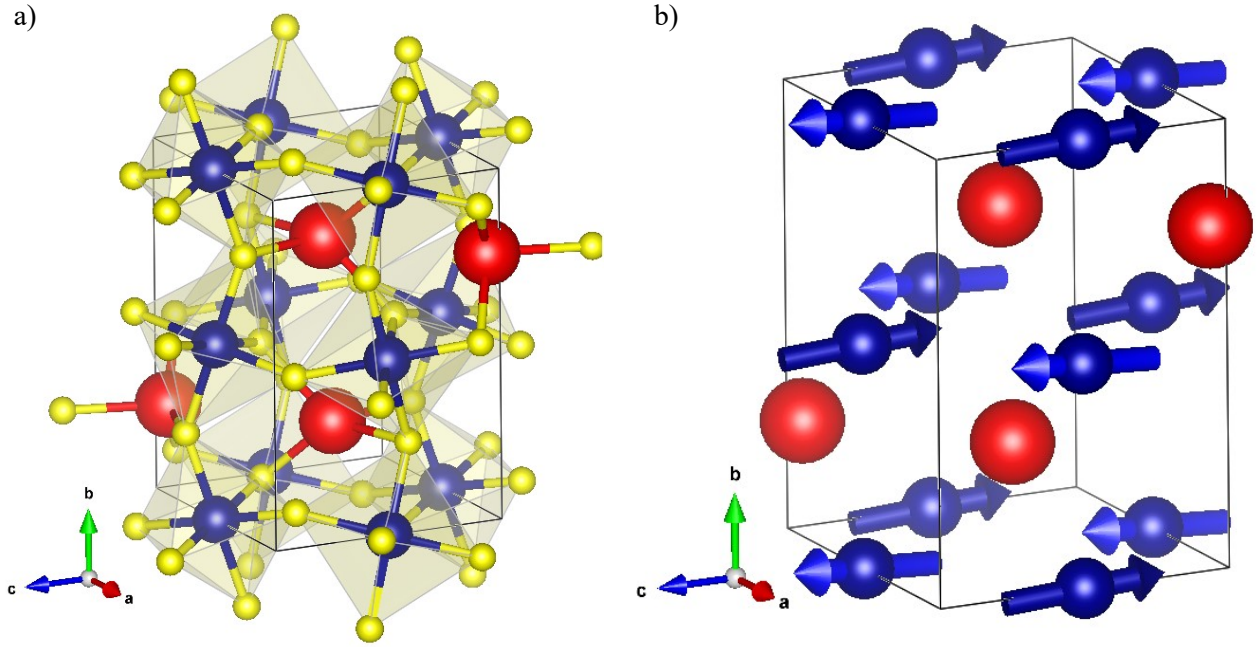

Figure 3. a) Crystal structure of $RFeO_3$ (blue spheres - Fe^{3+} ions, red – Ho^{3+}, yellow – O^{2+}). b) Magnetic structure of $HoFeO_3$ in the high-temperature phase.

1.3 Exchange Interactions and the Hamiltonian of the System

Rare earth orthoferrites have a complex crystal and magnetic structure, and in the analysis of exchange interactions, their magnetic symmetry plays an important role. Magnetic symmetry groups are usually used to classify possible types of magnetic order. In orthoferrites, the crystallographic and magnetic unit cells are identical. Due to the antiferromagnetic nature of the ordering of the Fe^{3+} ions' spins, the contribution of isotropic exchange is almost completely compensated. Thus, the magnetic properties of a crystal are determined mainly by non-Heisenberg terms such as the DMI and anisotropy. The interaction between *R* and Fe ions appears by two mechanisms: exchange and dipole. Interaction *R*-*R* appears only at very low temperatures T_{NR} < 10 K.

The linear theory of spin waves was used to calculate exchange interactions. Spin waves are collective magnetic excitations. They can be described in the classical Heisenberg model based on the approximation of localized moments [51, 52]. The energy of exchange interactions can be described using the Heisenberg Hamiltonian:

$$H = \sum_{ij} J_{ij} \vec{S}_i \cdot \vec{S}_j$$

where J_{ij} is the exchange coupling constant between two spin vectors $\vec{S}_i$ and $\vec{S}_j$ located at the lattice point i and j. Using the Holstein-Primakoff approach and Fourier transforms, it is possible to obtain the energy of spin waves [53]. In the case of rare-earth orthoferrites, the total Hamiltonian of the system can be written in the form:

$$H = H^{Fe-Fe} + H^{R-R} + H^{Fe-R}$$

$$H = \sum_{ij} J_{ij}^{Fe}\, \vec{S}_i^{Fe} \cdot \vec{S}_j^{Fe} + \sum_i A_i^{Fe} \left(\vec{S}_i^{Fe}\right)^2 + \sum_{mn} D_{mn}^{Fe} \left[\vec{S}_m^{Fe} \times \vec{S}_n^{Fe}\right] + \sum_{kl} J_{kl}^{Fe-R}\, \vec{S}_k^{Fe} \cdot \vec{S}_l^{R} + \sum_{gc} J_{gc}^{R-R}\, \vec{S}_g^{R} \cdot \vec{S}_c^{R}$$

where $\vec{S}$ – spin operator; J – isotropic exchange interactions; A - single ion anisotropy; D – DMI parameter; $\vec{s}^R$ – the R spin moment operator: $\vec{s}^R = \left(g_j - 1\right)\vec{\mathbf{J}}$; g_j - Landé factor; $\vec{\mathbf{J}}$ - total angular moment. In this work, all calculations were performed using the SpinW library that can plot and numerically simulate magnetic structures and excitations of given spin Hamiltonian using classical Monte Carlo simulation and linear spin wave theory [54].

1.4 Neutron diffraction

1.4.1 Basic principles of instrument configuration

Neutron diffraction is an excellent method for studies in condensed matter physics. This is due to the fact that the neutron easily penetrates the volume of matter, as it is electrically neutral and the neutron interacts with both nuclear and magnetic moments [55-57]. There are two main types of neutron-matter interactions: nuclear and magnetic scattering. Nuclear scattering occurs due to interaction with the force field of the nucleus. Magnetic scattering occurs due to the Zeeman interaction between the magnetic moment of the neutron with the internal magnetic field in the sample.

There are two types of neutron sources for scientific experiments. Nuclear reactors using fission with a constant neutron flux and neutron channels (MLZ, ILL) [58, 59] or pulsed neutron flux realized by mechanical modulation of neutron flux from the core by moving reflectors (IBR-2M) [60] and spallation sources generating on proton acceleration (ESS) [61].

At neutron sources with a constant flux, neutron diffraction experiments are mostly performed on neutron diffractometers with constant wavelengths [62]. The schematic diagram of a diffractometer is shown in figure 4a. Neutron diffractometers copy the scheme of an X-ray diffractometer. A small line is extracted from the Maxwell wavelength distribution of neutrons with the help of a crystal monochromator. Detector is used to catch the intensities of Bragg reflections along 2theta. During scanning, the detector angle between the incident neutron beam and the scattered neutron beam changes or instead of scanning by scattering angle 2θ, multi-detector systems or position-sensitive detector can be used.

In the case of inelastic neutron scattering, there are two main types of instruments: triple-axis (TAS) and time-of-flight (TOF) spectrometers. In this work, all inelastic experiments were

performed on TAS. The schematic diagram of the TAS is shown in figure 4b. The incident neutron wavevector $\vec{k}_i$ is selected by Bragg reflection on a monochromator (angles A1 and A2). The orientation of the vector $\vec{k}_i$ in the reciprocal space is controlled by the orientation of the sample (angle A3). The scattered neutron wavevector $\vec{k}_f$ is selected by Bragg reflection on analyzer (angles A5 and A6). The orientation of the vector $\vec{k}_f$ in the reciprocal space is determined by the value of the scattering angle at the sample position (A4). It is also should be noted that the experiments can be performed using two modes of operation at constant total momentum transfer $\vec{Q}$ scan and constant energy E scans. In the constant-$\vec{Q}$ and constant-$\vec{k}_i$ mode the angles A3, A4, A5 and A6 change for each measurement point, for constant-$\vec{Q}$ and constant-$\vec{k}_f$the angles A1, A2, A3 and A4 change. In the constant-E scans, only angles A3 and A4 change [63].

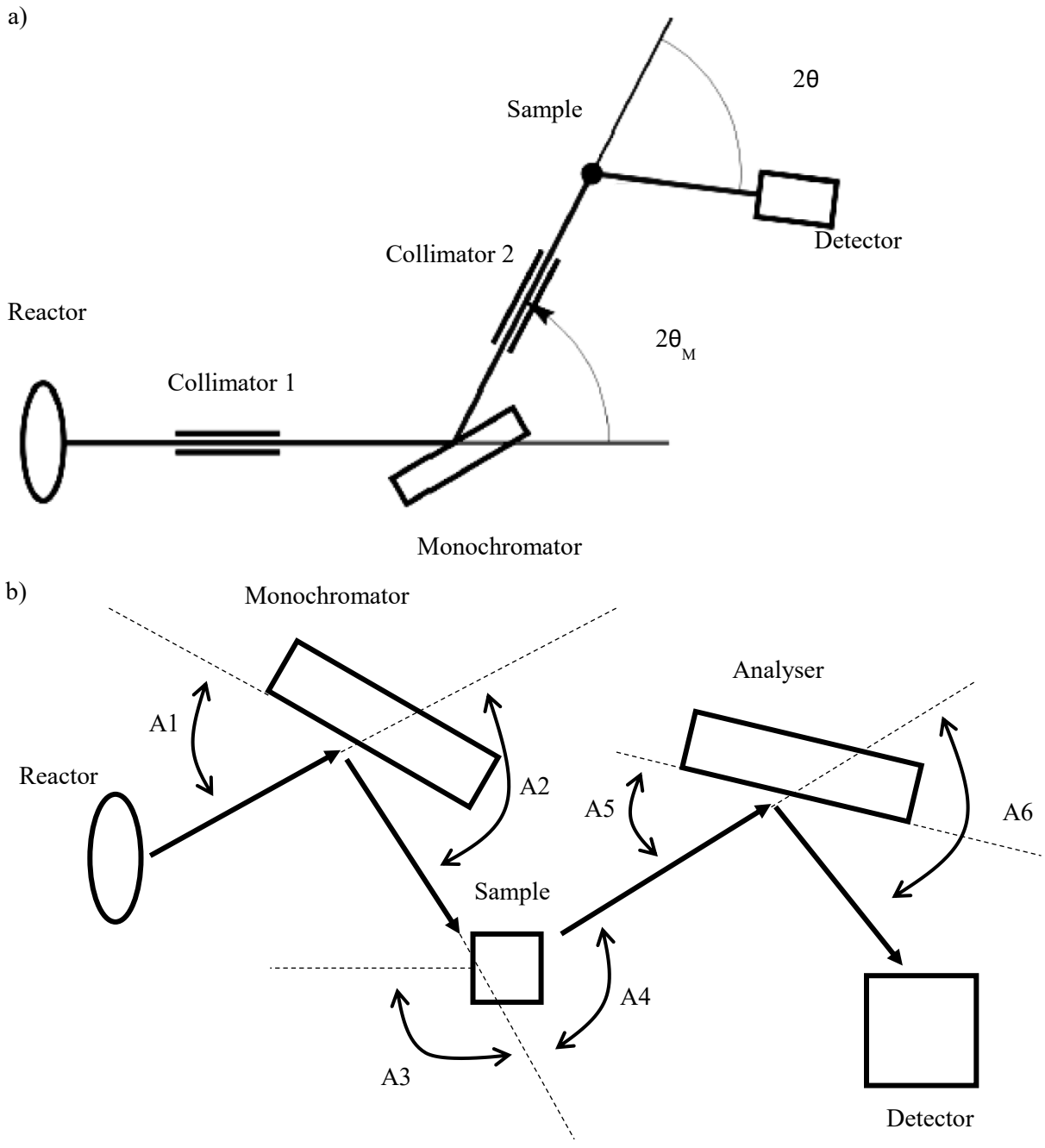

Figure 4. a) Schematic diagram of a diffractometer where the wavelength of neutrons incident on the sample is fixed. θ_M: Bragg's angle, 2θ: scattering angle. b) Schematic diagram of a triple-axis spectrometer. The comments on angles A1-A6 are given in the text.

1.4.2 Description of the experiments

Magnetic neutron scattering techniques were used in this dissertation, and all of the experimental instruments were at reactors with a constant neutron flux. In this dissertation, experiments on the diffraction of non-polarized neutrons were performed at the thermal neutron lifting-counter two-axis diffractometer D23 at the Institut Laue-Langevin (ILL). The diffractometer configuration scheme for this experiment is shown in figure 5. The monocrystal was placed in a vertical cryomagnet with a maximum magnetic field of 12 Tesla. The experiments measured the intensities of Bragg reflections as a function of temperature in a constant magnetic field. Sets of reflections were chosen that include each type of magnetic mode corresponding to the Bertaut notation [64] for collinear magnetic ordering (see table 1). A typical Bragg peak is shown in figure 6a. The peak fitting was done in the program OriginPro [65]. In the experiment performed on this instrument, which is presented in this dissertation, most parts of the measurements were concentrated in the temperature range from 3 to 15 K where the spin reorientation transition occurs. However, a higher temperature range was also checked to make sure that there were no reorientation transitions, which had not been investigated before (figure 6b).

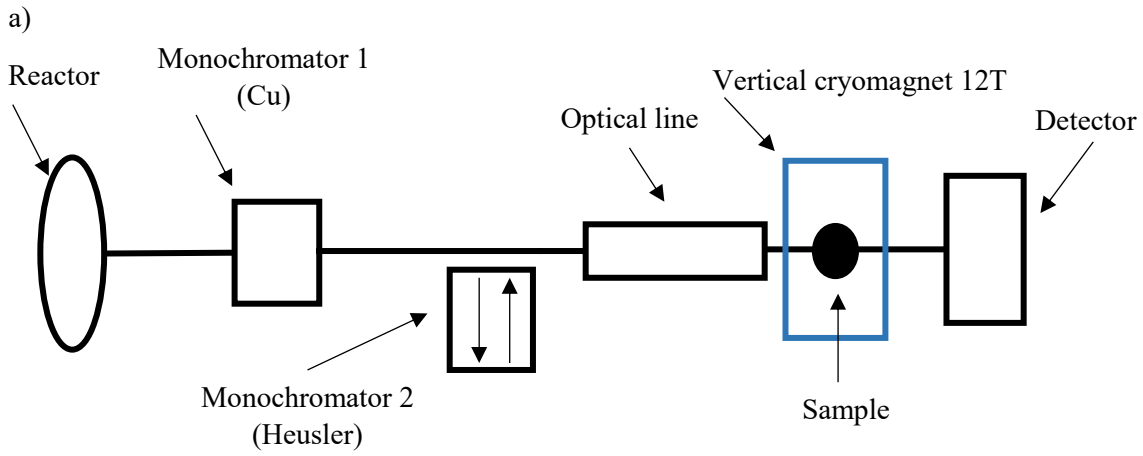

b)

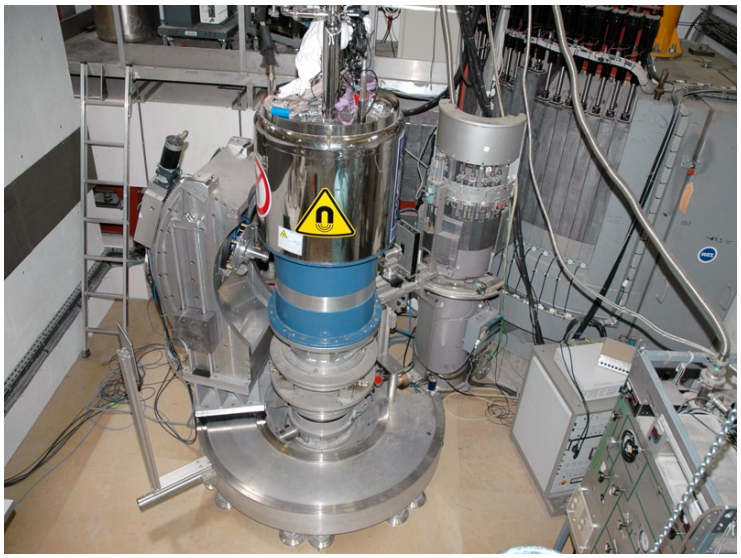

Figure 5. a) Block diagram representation of the diffractometer D23, in the configuration used in the experiments in this thesis. b) Photo of the diffractometer D23.

Table 1. List of reflection sets that were measured on instrument D23 for $YbFeO_3$.

№	Field || [100]	Field || [110]			type
1	0 -2 2	2 -2 0	1 -1 0	0 0 2	F
2	0 -2 0	1 -1 2	1 -1 2	1 -1 -2	F
3	0 -2 1	2 -2 1	1 -1 1	1 -1 -1	A
4	0 -4 1	1 -1 3	1 -1 3	1 -1 -3	A
5	0 1 -1	2 -1 -3	0 1 -1	1 -2 1	G
6	0 -3 1	4 -3 -3	0 1 -3	0 1 -3	G
7	0 -3 0	2 -1 -4	0 1 0	0 1 -2	C
8	0 -3 2	4 -3 -2	0 1 2	1 -2 0	C

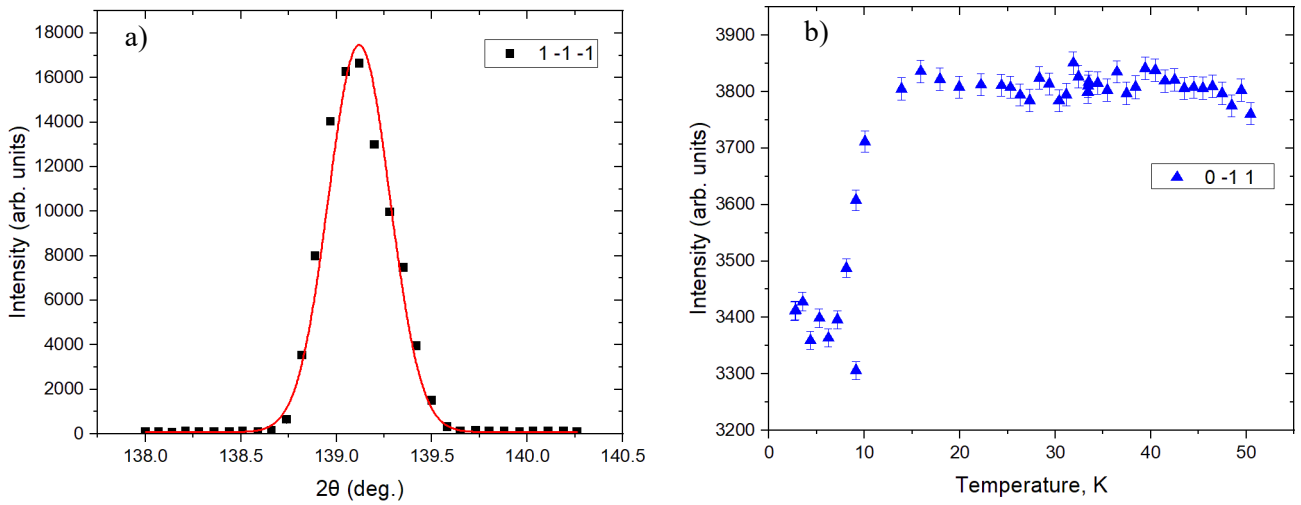

Figure 6. a) Typical Bragg reflection of the $YbFeO_3$ crystal at the temperature T=10 K. Black squares - measured intensity, error - point size, red line is the result of the fitting. b) Temperature dependence of the intensity for reflection (0 -1 1).

Experiments on the diffraction of polarized neutrons were performed at the versatile two axes single crystal diffractometer POLI [66] (see figure 7a) at the Heinz Maier-Leibnitz Zentrum (MLZ) on the monocrystal of $HoFeO_3$ (see section Publication 2). In this technique the ratio between the diffracted intensity of a Bragg reflection for spin-up neutrons ($I+$) to the same measured intensity when the incoming neutrons are spin-down ($I-$) is measured, the quantity $R=I+/I-$ is called flipping ratio (FR) [67]. These data are used to construct spin density maps and make it possible to determine the sign of the DMI by the asymmetry of the peaks intensities [68]. During the experiment, the sample was in a zero magnetic field at high temperature and cooled to the temperature point of measurement and then the field was activated. After measurements, the field was returned to zero, the sample was heated to a high temperature and cooled again to the next temperature point of measurement. This approach made it possible to avoid the effect of phase transition temperature changes during heating and cooling in an external magnetic field. To avoid sample movement in strong magnetic fields, the crystal is fixed in the holder: glued on both sides, mechanically clamped with a stronger tightening and additionally fixed with aluminum wire, as shown in figure 7b.

a)

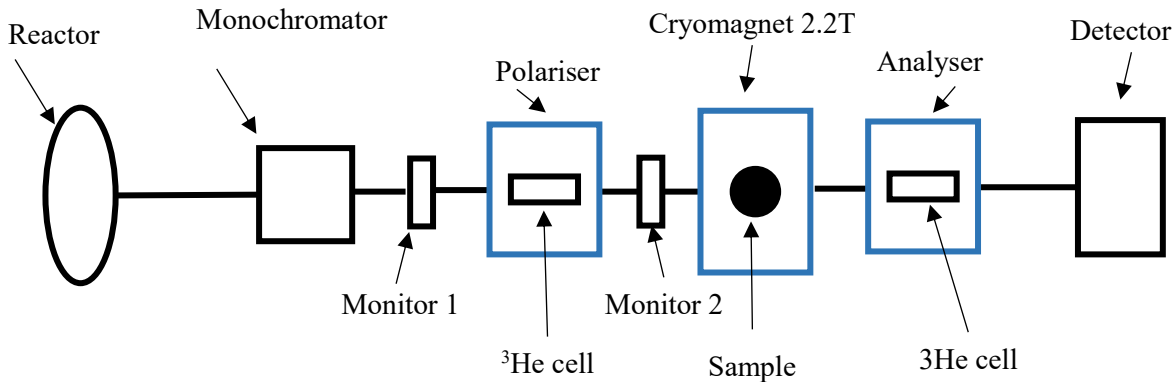

b)

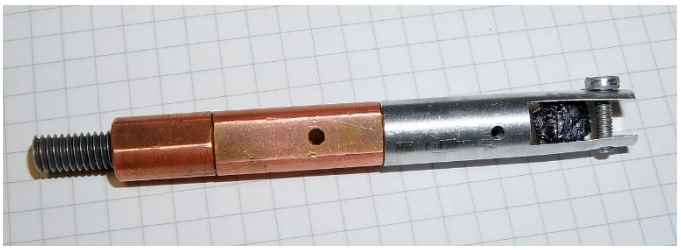

c)

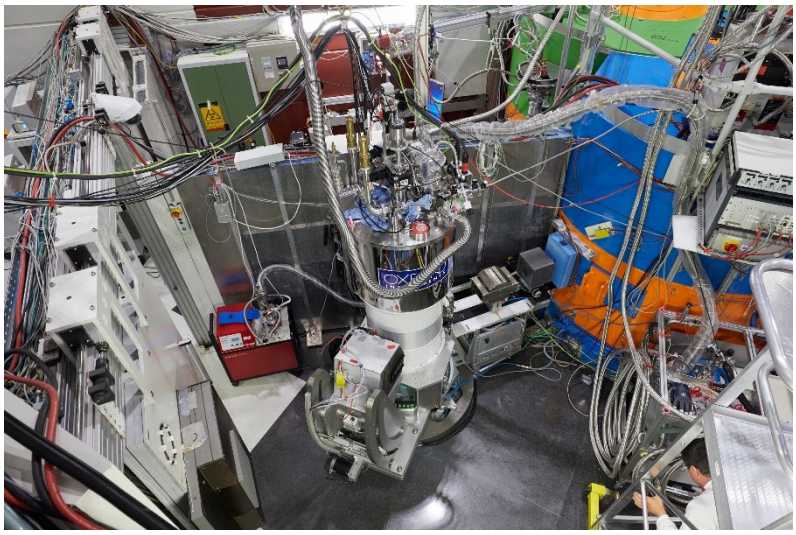

Figure 7. a) Block diagram representation of the diffractometer POLI, in the configuration used in the experiments in this thesis. b) Sample in the sample holder. c) Photo of the diffractometer POLI.

Inelastic neutron scattering experiments were performed on the three triple-axis spectrometers IN12, IN20 at ILL [69, 70] and PUMA [71] at MLZ. The crystal pairs PG (002) and PG (002), Si (111) and PG (002), and PG (002) and PG (002) were used as monochromators and analyzers for the instruments IN12, IN20 and PUMA, respectively. All monochromator units are double focussing devices that allow for optimum focussing conditions over a wide range of incident wavevectors $\vec{k}_i$. The basic spectrometer configuration scheme for experiments is shown in figure 8. Cryostats with temperature ranges of 1.5 (3.5K for PUMA)-300 K were used in the experiments. IN20 and PUMA are thermal triple-axis spectrometers, which allow to measure excitations at high energies. In the case of the experiments presented in this dissertation, this energy range is 7-70 meV. The experiments were performed using two modes of operation at constant-$\vec{Q}$ scan and constant-E scans. IN12 is a cold neutron triple-axis spectrometer. Available measurement range there is 0.4-7 meV. Thus, the full possible range of energies in which magnons can be found in rare-earth orthoferrites was investigated.

a)

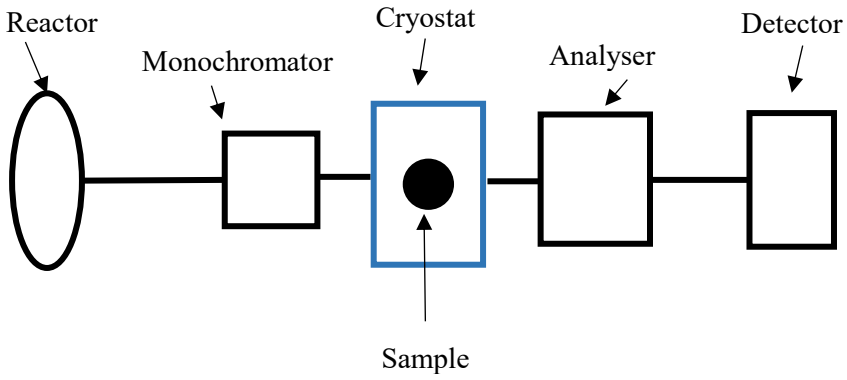

b) c)

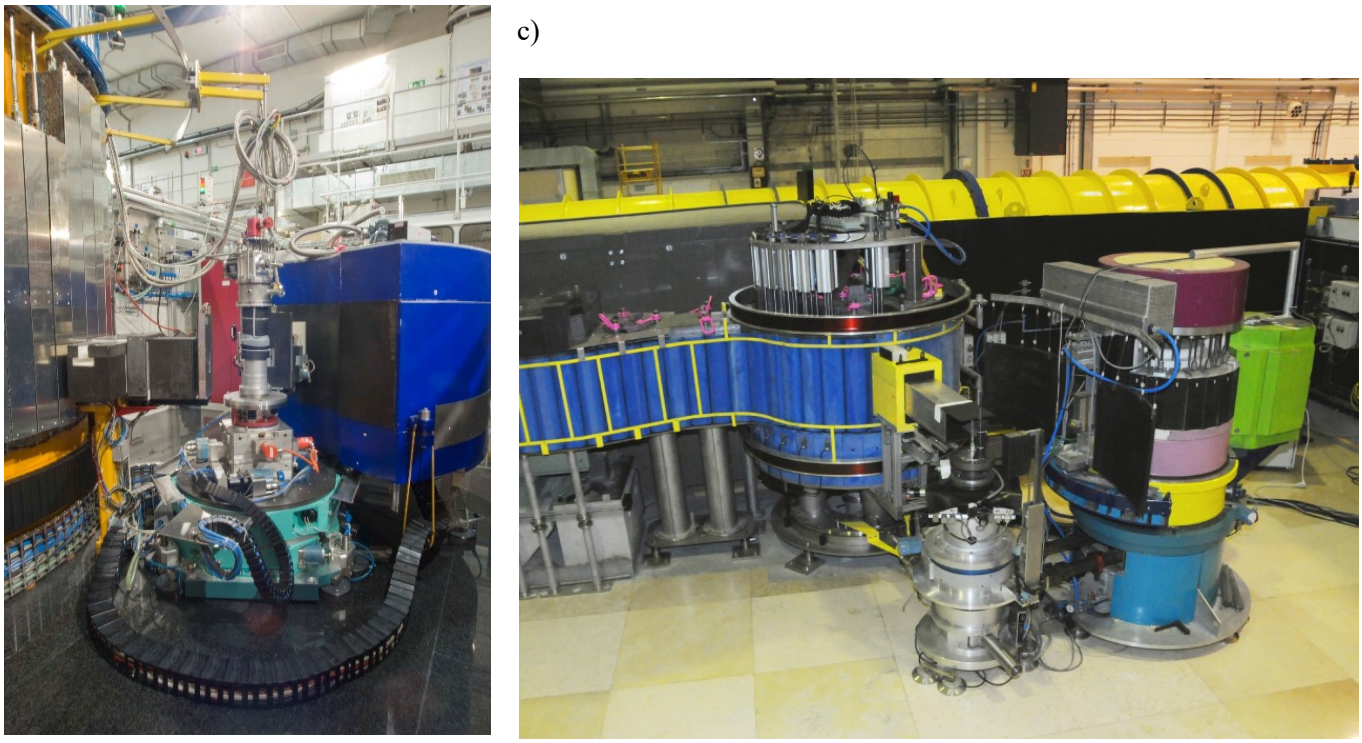

Figure 8. a) Block diagram representation of the triple-axis spectrometer, in the configuration used in the experiments in this thesis. b) and c) Photos of spectrometers PUMA and IN12, respectively

2. Cumulative part of the dissertation

This section shows the cumulative part of the thesis. Four publications are presented. A summary of each publication is given below.

2.1 Publication 1

- Title: Neutron inelastic scattering study of rare-earth orthoferrite $HoFeO_3$

- Authors: A.K. Ovsyanikov, I.A. Zobkalo, W. Schmidt, S.N. Barilo, S.A. Guretskii, V. Hutanu

- Reference: A.K. Ovsyanikov, I.A. Zobkalo, W. Schmidt, S.N. Barilo, S.A. Guretskii, V. Hutanu, «Neutron inelastic scattering study of rare-earth orthoferrite $HoFeO_3$», Journal of Magnetism and Magnetic Materials, Volume 507, 1 August 2020, 166855, https://doi.org/10.1016/j.jmmm.2020.166855

- Research methods: X-ray diffraction, inelastic neutron scattering, linear theory of spin waves.

- Own contribution: Creating a model of exchange interactions, writing a Hamiltonian, and modeling energy maps. Writing a proposal for an experiment. Performing the experiment together with W. Schmidt (ILL). Calculation of the values of exchange interactions. Analysis of the results and article preparation for publication together with I.A. Zobkalo and V. Hutanu.

The compound $HoFeO_3$ is part of the rare-earth orthoferrites family and stands out because it has several spin reorientation transitions. The cause of these transitions is the competition of exchange interactions, which leads to various complex magnetic structures including the appearance of ferroelectric polarization and magnetocaloric effect.

Research Questions: The purpose of this work was to study the exchange interactions in orthoferrite of $HoFeO_3$. Their influence at different temperatures in different magnetically ordered phases.

Main Results: Studies were made using the inelastic neutron scattering method. The linear theory of spin waves was used for the theoretical analysis. As a result, using the inelastic neutron scattering method, the first time numerical values of the exchange interactions were obtained within the iron subsystem: interaction along the *b* direction J_b^{Fe}, the interaction within the *ac* plane J_{ac}^{Fe} and the interaction between next nearest neighbors J_{nnn}^{Fe} for different magnetic phases. Estimates of the values of exchange interactions between the holmium and the iron subsystems J_{ij}^{Fe-Ho}, within the holmium subsystem J_{mn}^{Ho-Ho}, and parameters D_1 and D_2 of the DMI are given. The values of exchange interactions parameters are in a good agreement with similar values in other orthoferrites. It is also shown that the parameter of easy plane single-ion anisotropy of iron A_{ab}^{Fe} almost does not change at temperatures above the temperature of magnetic ordering of holmium $T_{N,Ho}$, and the energy of easy-axis anisotropy increases at temperatures below $T_{N,Ho}$.

These data allow us to determine the causes of spin reorientation transitions and show the effect of energy balance on the whole system. Unfortunately, our experiment does not allow us to determine with sufficient accuracy the parameters of exchange interactions within the holmium subsystem and the parameters of the DMI. However, this can be done with polarized neutron scattering experiments. This was done to improve the parameters of the DMI (see Publication 2). In addition, to expand our understanding of the influence of the balance of energies, we can add an additional energy parameter to the system, for example an external magnetic field (see Publication 3). It is also to be noted that the use of polarized neutrons for the inelastic scattering experiment will allow us to separate the peaks corresponding to the levels of the crystal electric field and rare-earth magnons, which can significantly improve our results.

2.2 Publication 2

- Title: Breaking the magnetic symmetry by reorientation transition near 50 K in multiferroic magnetocaloric $HoFeO_3$

- Authors: A. Ovsianikov, H. Thoma, O. Usmanov, P. J. Brown, T. Chatterji, A. Sazonov, S. Barilo, L. Peters, and V. Hutanu

- Reference: A. Ovsianikov, H. Thoma, O. Usmanov, P. J. Brown, T. Chatterji, A. Sazonov, S. Barilo, L. Peters, and V. Hutanu, «Breaking the magnetic symmetry by reorientation transition near 50 K in multiferroic magnetocaloric $HoFeO_3$», IEEE Transactions on Magnetics, Volume: 58, Issue: 2, Feb. 2022, doi:10.1109/TMAG.2021.3082324.

- Research methods: Polarized neutron diffraction (PND).

- Own contribution: Calculation of the sign of the DMI together with H. Thoma. Analysis of the results and article preparation for publication together with P.J. Brown and V. Hutanu.

This work is a continuation of our research on the orthoferrite $HoFeO_3$ which focuses on the study of the spin reorientation transition at 55 K and the influence of the DMI. As noted earlier, the polarized neutron diffraction method makes it possible to determine the components of the magnetic moment. This allows us to better define the components of the antisymmetric DMI, which is one of the main interactions leading to the relationship between the magnetic order parameters. The transition at 55 K was chosen because it avoids the strong influence of the rare-earth subsystem and shows an increase in magnetic entropy change, which corresponds to the appearance of the magnetocaloric effect.

Research Questions: The purposes of this work were to test a new polarized neutron diffraction (PND) setup on the instrument POLI, the determination of the DMI sign and studying the spin reorientation transition at 55 K where a large magnetocaloric effect for $HoFeO_3$ was previously reported.

Main Results: We show that during the phase transition at T_{SR}=53 K in an external magnetic field applied along the crystal *c*-axis, the ordered magnetic moment of the Fe-sublattice rotates from the crystallographic direction *b* to *a* not in the *ab* plane, but through the *z* axis. This means that the applied field breaks the orthorhombic symmetry allowing some magnetization parallel to *z* within a small temperature region. This intermediate phase breaking of the magnetic symmetry could not be explained as a linear combination of the irreducible representations Γ_4 and Γ_1. Therefore, it should be considered as a new low-symmetry magnetic phase. Using PND, a mapping of the new phase the absolute positive sign of the DMI for the Fe-Fe interaction in the Γ_4 phase was determined. The appearance of a new magnetic phase at such a small external field B~0.1 T, led us to the further study of the orthoferrite $HoFeO_3$ and the construction of the phase diagram (see Publication 3). In addition, this experiment was done at temperatures above $T_N^{Ho} = 10$ K, so we cannot say anything about the DMI on the rare earth subsystem. Thus, this is the goal of future studies.

2.3 Publication 3

- Title: Magnetic phase diagram of $HoFeO_3$ by neutron diffraction

- Authors: A.K. Ovsianikov, O.V. Usmanov, I.A. Zobkalo, V. Hutanu, S.N. Barilo, N.A. Liubachko, K.A. Shaykhutdinov, K. Yu Terentjev, S.V. Semenov, T. Chatterji, M. Meven, P.J. Brown, G. Roth, L. Peters, H. Deng, A. Wu

- Reference: A.K. Ovsianikov, O.V. Usmanov, I.A. Zobkalo, V. Hutanu, S.N. Barilo, N.A. Liubachko, K.A. Shaykhutdinov, K. Yu Terentjev, S.V. Semenov, T. Chatterji, M. Meven, P.J. Brown, G. Roth, L. Peters, H. Deng, A. Wu, « Magnetic phase diagram of HoFeO3 by neutron diffraction», Journal of Magnetism and Magnetic Materials, Volume 557, 1 September 2022, 169431, ISSN 0304-8853, https://doi.org/10.1016/j.jmmm.2022.169431.

- Research methods: X-ray diffraction, neutron diffraction, magnetization measurement, magnetic symmetry analysis.

- Own contribution: Calculation of bond lengths from X-ray scattering data. Performing magnetic symmetry analysis. Construction of the phase diagram, calculation of the values of the magnetic moments in each phase. Analysis of the results and article preparation for publication together with V. Hutanu, M. Meven and G. Roth.

This work is a continuation of our research on the orthoferrite $HoFeO_3$. The external magnetic field is a new parameter and breaks the energy balance of the system. For example, this can be clearly seen in our experiments with polarized neutrons or in graphs magnetic entropy change as a function of temperature for a field variation from 0–1 T to 0–7 T.

Research Questions: The purpose of this work was the construction of the magnetic phase diagram.

Main Results: Our studies demonstrate that $HoFeO_3$ has a rich phase diagram in an external magnetic field. We can outline eight different magnetic phases, induced or suppressed by the magnetic field. Thus, the competition between the external magnetic field, the antisymmetric DMI and isotropic exchange interactions between the Fe- and Ho-sublattice and within the Fe-sublattice leads to a complex picture of phase transitions in the rare-earth orthoferrite $HoFeO_3$. This work is the final one in our study of $HoFeO_3$ orthoferrites. In the future, the obtained results of the balance of the values of exchange interactions can be used for comparison with other orthoferrites (see Publication 4). It should also be noted that if an external magnetic field leads to new spin reorientation transitions by influencing the energy balance of the exchange interactions, then a mechanical change in the bond lengths by pressure can also lead to the appearance of new phases. However, such experiments require special cells, which are currently to be realized on the instrument POLI.

2.4 Publication 4

- Title: Inelastic neutron studies and diffraction in magnetic fields of $TbFeO_3$ and $YbFeO_3$

- Authors: A.K. Ovsianikov, O.V. Usmanov, I.A. Zobkalo, W. Schmidt, A. Maity, V. Hutanu, E. Ressouche, K.A. Shaykhutdinov, K. Yu Terentjev, S.V. Semenov, M. Meven, G. Roth, L. Peters

- Reference: A.K. Ovsianikov, O.V. Usmanov, I.A. Zobkalo, W. Schmidt, A. Maity, V. Hutanu, E. Ressouche, K.A. Shaykhutdinov, K. Yu Terentjev, S.V. Semenov, M. Meven, G. Roth, L. Peters, «Inelastic neutron studies and diffraction in magnetic fields of $TbFeO_3$ and $YbFeO_3$», Journal of Magnetism and Magnetic Materials, Volume 563, 1 December 2022, 170025

- Research methods: X-ray diffraction, neutron diffraction, magnetic symmetry analysis, inelastic neutron scattering, linear theory of spin waves.

- Own contribution: Creating a model of exchange interactions, writing a Hamiltonian, and modeling energy maps. Writing a proposal for experiments. Performing the inelastic neutron scattering experiments together with W. Schmidt (ILL) and A. Maity (MLZ). Performing the neutron diffraction experiment together with V. Hutanu and E. Ressouche (ILL). Calculation of bond lengths from X-ray scattering data. Performing magnetic symmetry analysis. Calculation of the values of exchange interactions. Analysis of the results and article preparation for publication together with M. Meven and G. Roth.

The two compounds $TbFeO_3$ and $YbFeO_3$ have a similar phase transition scheme, where the Fe-sublattice has a spin reorientation transition from the high-temperature (HT) phase to the low-temperature (LT) phase at T_{SR1}^{TbFeO3}=8.5 K and T_{SR1}^{YbFeO3}=8 K for $TbFeO_3$ and $YbFeO_3$, respectively. However, $TbFeO_3$ has a second spin reorientation transition at T=3 K, which is absent in $YbFeO_3$. Thus, it would be interesting to study these two compounds in terms of the competition of exchange interactions and the influence of an external magnetic field, as done for $HoFeO_3$.

Research Questions: The purposes of this work were to determine the values of exchange interactions, analyze their effect on spin reorientation transitions, and the influence of an external magnetic field on the energy balance of the system.

Main Results: Combining both methods of inelastic neutron scattering and neutron diffraction in external magnetic fields allowed us to show the influence of the energy balance on the phase transitions in the two compounds. The exchange within the Fe-subsystems is the strongest one, playing the main role, DMI leads to a spin canting, the interaction within the *R*-subsystems leads to additional spin-reorientation transitions. Thus, the orthoferrites $TbFeO_3$, $YbFeO_3$, and $HoFeO_3$ have similar mechanisms of spin reorientation transitions. But the

difference in the rare-earth ions determines the difference in these transitions. At the moment there is still an open question about the influence of DMI within the *R*-subsystem.

3. Conclusions

In this thesis, a cycle of studies of rare-earth orthoferrites $RFeO_3$ with different rare-earth elements R = Ho, Tb, Yb was performed, focusing on the crystalline and magnetic properties of the $RFeO_3$ family by neutron scattering techniques. One of the areas of research was a detailed study of the crystal structure of these compounds, the search for structural distortions in the weakly ferromagnetic phase, which may indicate a decrease in crystal symmetry. This was done by X-ray diffraction. Experimental results showed that the crystal structure is described by space group Pnma and there is no reason to use a space group of lower symmetry. Magnetic symmetry analysis was performed using the concept of Shubnikov groups, which allowed us to determine the possible magnetic structures consistent with the parent symmetry of the crystal group and gives symmetry constraints on possible magnetic structures of crystals.

Specific characteristics of complex magnetic structures and their evolution under changing external conditions - temperature and magnetic field - were studied by neutron diffraction methods. The parameters of the magnetic structure were studied using a neutron diffractometer POLI (MLZ) and D23 (ILL). Phase diagrams for orthoferrites $HoFeO_3$ and $YbFeO_3$ in an external magnetic field were constructed for the first time. The effect of an external magnetic field on spin reorientation transitions in terms of the energy balance of the system is described.

Magnetic dynamics studies were performed by inelastic neutron scattering, which made it possible to obtain the parameters of exchange interactions in these compounds. Magnetic dynamics studies were performed on the triple-axis cold neutron spectrometer IN12 (ILL) and on the triple-axis thermal neutron spectrometers IN20 (ILL) and PUMA (MLZ). Numerical calculations of the magnetic excitation spectra were performed using the SpinW package, which can build and numerically simulate the magnetic structures and excitations of a given spin Hamiltonian using classical Monte Carlo simulation and linear spin wave theory. As a result, numerical values of exchange interaction parameters, DMI and anisotropy for the orthoferrites $HoFeO_3$, $TbFeO_3$ and $YbFeO_3$ were obtained. These values are in good agreement with parameters in other orthoferrites and data obtained by other methods. The influence of exchange interactions on spin reorientation transitions was analyzed. The results show that the exchange within the Fe-subsystems is the strongest one, playing the main role, DMI leads to a spin canting, single-ion anisotropy stabilizes the system and exchange interactions *R*-Fe and *R*-*R* lead to a change in the energy balance of the system, which causes spin reorientation transitions.

It is noted that the family $RFeO_3$ includes various rare earth ions. Thus, similar complex studies can be performed for other orthoferrites or for similarly structured orthochromites $RCrO_3$. It may also be of interest to change the exchange bonds under mechanical influences. Such studies can contribute not only to the understanding of the processes inside the compounds, but also to the construction of high-pressure cells for neutron experiments.

Bibliography

[1] A. P. Pyatakov and A. K. Zvezdin, Phys.-Usp. 55 557 (2012).

[2] Fert A., Rev. Mod. Phys. 80 1517 (2008).

[3] D. Liu, M. Yue, J. Zhang, T.M. McQueen, J.W. Lynn, X. Wang, Y. Chen, J. Li, R.J. Cava, X. Liu, Z. Altounian and Q. Huang, Physical Review B. Vol. 79, 014435 (2009).

[4] Dzyaloshinskii I. E., Sov.Phys. JETP 10 628 (1960).

[5] Astrov D. N., Sov.Phys. JETP 11 708 (1960).

[6] Folen V. J., Rado G. T., Stalder EWPhys. Rev. Lett. 6 607 (1961).

[7] X. X. Zeng, R. Wang, X. Q. Xi, B. Li, and J. Zhou, "Terahertz rare-earth orthoferrite metamaterials by 3-D direct writing technology," Opt. Express 26, 17056-17065 (2018).

[8] P.Mehdizadeh, Y.Orooji, O.Amiri, M.Salavati-Niasari, H.Moayedi, Journal of Cleaner Production, Volume 252, 119765, (2020).

[9] Curie P., J. Physique III 393 (1894).

[10] Smolenskii G.A., Sov. Phys. JETP. 25 1333 (1961).

[11] Schmid H Ferroelectrics 162 317 (1994).

[12] Smolenskii G. A., Chupis I. E., Sov. Phys. Usp. 25 475 (1982).

[13] Agal'tsov A. M. et al. Sov. Phys. Lebedev Inst. Rep. (5) 48 (1989).

[14] Teague J. R., Gerson R., James W. J., Solid State Commun. 8 1073 (1970).

[15] Fischer P., Polomska M., J. Phys. C Solid State 13 1931(1980).

[16] P. J. Brown and T. Chatterji, J. Phys.: Condens. Matter 18 10085 (2006).

[17] Popov Yu. F., et al. Ferroelectrics 204 269 (1997).

[18] Srinivas A., Sritharan T., Boey F. Y. C., J. Appl. Phys. 98 036104 (2005).

[19] Matsui T., et al. Appl. Phys. Lett. 86 082902 (2005).

[20] Dong Sh, Li J-F, Viehland D., Appl. Phys. Lett. 85 2307 (2004).

[21] Bibes M., Barthelemy A., Nature Mater. 7 425 (2008).

[22] Joseph R. Sootsman, Duck Young Chung, Mercouri G. Kanatzidis, Angew. Chem. Int. Ed. (2009).

[23] V.K. Pecharsky, K.A. Gschneidner, J. Magn. Magn. Mater. 200, 44 (1999).

[24] E. Warburg, Ann. Phys. 249, 141 (1881).

[25] V. K. Pecharsky and K. A. Gschneidner, Jr., Phys. Rev. Lett. 78, 4494 (1997).

[26] Zimm, C; Jastrab, A.; Sternberg, A.; Pecharsky, V.K.; Gschneidner, K.A. Jr.; Osborne, M.; Anderson, I., Adv. Cryog. Eng. 43: 1759. (1998).

[27] Bohigas, X.; Molins, E.; Roig, A.; Tejada, J.; Zhang, X. X., IEEE Transactions on Magnetics. 36 (3): 538. (2000).

[28] Hirano, N., AIP Conference Proceedings. Vol. 613. pp. 1027–1034, (2002).

[29] Shir, F.; Mavriplis, C.; Bennett, L. H.; Torre, E. D., International Journal of Refrigeration. 28 (4): 616, (2005).

[30] W.C. Koehler, E.O. Wollan, M.K. Wilkinson, Phys. Rev. 118 58 (1960).

[31] M. Marezio, J.P. Remeika, P.D. Dernier, Acta Cryst. B 26 2008 (1970).

[32] R. White, J. Appl. Phys. 40 1061 (1969).

[33] K. Park, H. Sim, J. C Leiner, Y. Yoshida, J. Jeong, S. Yano, J. Gardner, P. Bourges, M. Klicpera, V. Sechovský, M. Boehm and J. Park, J. Phys.: Condens. Matter 30 (2018).

[34] Y. Tokunaga, S. Iguchi, T. Arima, and Y. Tokura, Phys. Rev. Lett. 101, 097205 (2008).

[35] S. Chaturvedi, P. Shyam, A. Apte, J. Kumar, A. Bhattacharyya, A. M. Awasthi, and S. Kulkarni, PHYSICAL REVIEW B 93, 174117 (2016).

[36] A. Bombik, B. Leśniewska, A.W Pacyna, JMMM, 214, 243 (2000).

[37] L. T. Tsymbal, et al. Low Temp. Phys. 31 (3–4), (2005).

[38] T. Chatterji, M. Meven, P.J. Brown, AIP Adv. 7 045106 (2017).

[39] Artyukhin, S., Mostovoy, M., Jensen, N. et al. Solitonic lattice and Yukawa forces in the rare-earth orthoferrite TbFeO3. Nature Mater 11, 694–699 (2012).

[40] B. Rajeswaran et al., EPL 101 17001 (2013).

[41] K. Dey, A. Indra, S. Mukherjee, S. Majumdar, J. Strempfer, O. Fabelo, E. Mossou, T. Chatterji, and S. Giri. Phys. Rev. B 100, 214432 – Published 26 December 2019.

[42] J.-H. Lee, Y.K. Jeong, J.H. Park, M.-A. Oak, H.M. Jang, J.Y. Son, J.F. Scott, Phys. Rev. Lett. 107 117201 (2011).

[43] P. Mandal, V.S. Bhadram, Y. Sundarayya, C. Narayana, A. Sundaresan, C.N.R. Rao, Phys. Rev. Lett. 107 137202 (2011).

[44] U. Chowdhury, S. Goswami, D. Bhattacharya, J. Ghosh, S. Basu, S. Neogi, Appl. Phys. Lett. 105 052911 (2014).

[45] Zvezdin, A. K. & Kotov, V. A. Modern Magnetooptics and Magnetooptical Materials (IOP, Bristol, 1997).

[46] Kimel, A., Kirilyuk, A., Usachev, P. et al. Ultrafast non-thermal control of magnetization by instantaneous photomagnetic pulses. Nature 435, 655–657 (2005).

[47] X. X. Zeng, R. Wang, X. Q. Xi, B. Li, and J. Zhou, "Terahertz rare-earth orthoferrite metamaterials by 3-D direct writing technology," Opt. Express 26, 17056-17065 (2018) [18] I. E. Dzyaloshinsky, J. Phys. Chem. Solids 4 241 (1958).

[48] Ke, YJ., Zhang, XQ., Ma, Y. et al. Anisotropic magnetic entropy change in $RFeO_3$ single crystals(R = Tb, Tm, or Y). Sci Rep 6, 19775 (2016).

[49] M. Shao et al., Solid State Communications 152 947–950 (2012).

[50] C. Kittel, Introduction to Solid State Physics, seventh edition, John Wiley and Sons Inc., New York Chichester Brisbane Toronto Singapore, (1996).

[51] F. Bloch, Zeitschrift fur Phys. 61, 206 (1930).

[52] J. C. Slater, Phys. Rev. 35, 509 (1930).

[53] P.A.Lindgård, A.Kowalska, P.Laut, Journal of Physics and Chemistry of Solids, Volume 28, Issue 8, Pages 1357-1370 (1967).

[54] S. Toth and B. Lake: Linear spin wave theory for single-Q magnetic structures, JPCM, 16, 166002 (2015).

[55]C. G. Shull and M. K. Wilkinson Rev. Mod. Phys. 25, 100 (1953).

[56] Thomas F. Koetzle, Garry J. McIntyre, Single-Crystal Neutron Diffraction, Characterization of Materials [0-471-26882-8; 0-471-26696-5] J.:2002.

[57] A. K. Cheetham, A. P. Wilkinson, Synchrotron X-ray and Neutron Diffraction Studies in Solid-State Chemistry Angewandte Chemie International Edition in English [0570-0833] Bd.:31 H.:12 S.:1557 -1570 J.:1992.

[58] https://mlz-garching.de/

[59] https://www.ill.eu/

[60] http://flnph.jinr.ru/en/facilities/ibr-2

[61] https://europeanspallationsource.se/

[62] Cassels, J. M., The Scattering of Neutrons by Crystals, edited by O. R. Frisch, Prog. Nucl. Phys. 1, 185–215 (1950).

[63] R. Currat, Neutron and X-ray Spectroscopy, pp 383–425, Springer, Dordrecht (2006).

[64] E. F. Bertaut, Magnetism (Academic, New York, 1963).

[65] https://www.originlab.com

[66] V. Hutanu, Journal of large-scale research facilities, vol. 1, p. A16, (2015).

[67] C.Frontera, J.Rodríguez-Carvajal, Physica B: Condensed Matter, Volume 335, Issues 1–4, Pages 219-222 (2003).

[68] H. Thoma, V. Hutanu, H. Deng, V. E. Dmitrienko, P. J. Brown, A. Gukasov, G. Roth, and M. Angst, Phys. Rev. X, (2021).

[69] https://www.ill.eu/users/instruments/instruments-list/in12/description/instrument-layout

[70] https://www.ill.eu/users/instruments/instruments-list/in20/description/instrument-layout

[71] Heinz Maier-Leibnitz Zentrum. PUMA: Thermal three axes spectrometer. Journal of large-scale research facilities, 1, A13 (2015). http://dx.doi.org/10.17815/jlsrf-1-36

Appendix A

This appendix includes the text of all the publications used in the thesis.

Journal of Magnetism and Magnetic Materials 507 (2020) 166855

Contents lists available at ScienceDirect

Journal of Magnetism and Magnetic Materials

journal homepage: www.elsevier.com/locate/jmmm

Research articles

Neutron inelastic scattering study of rare-earth orthoferrite $HoFeO_3$

A.K. Ovsyanikov[a], I.A. Zobkalo[a,*], W. Schmidt[b], S.N. Barilo[c], S.A. Guretskii[c], V. Hutanu[d]

[a] Petersburg Nuclear Physics Institute named by B.P. Konstantinov of National Research Centre "Kurchatov Institute", Orlova Roshcha, Gatchina 188300, Russia
[b] Julich Centre for Neutron Science Outstation at Institut Laue-Langevin, 71 Avenue des Martyrs, CS 20156, 38042 Grenoble, France
[c] Scientific-Practical Materials Research Centre NAS of Belarus, 19 P. Brovki str., Minsk, 220072, Belarus
[d] Institute of Crystallography, RWTH Aachen University and Jülich Centre for Neutron Science at Heinz Maier- Leibnitz Zentrum, 85747 Garching, Germany

ARTICLE INFO

Keywords:
Inelastic neutron scattering
Orthoferrites

ABSTRACT

By the single crystal inelastic neutron scattering the orthoferrite $HoFeO_3$ was studied. We show that the spin dynamics of the Fe subsystem does not change through the spin-reorientation transitions. The observed spectrum of magnetic excitations was analyzed in the frames of linear spin-wave theory. Within this approach the antiferromagnetic exchange interactions of nearest neighbors and next nearest neighbors were obtained for Fe subsystem. Parameters of Dzyaloshinskii-Moriya interactions at Fe subsystem were refined. The temperature dependence of the gap in Fe spin-wave spectrum indicates the temperature evolution of the anisotropy parameters. The estimations for the values of Fe-Ho and Ho-Ho exchange interaction were made as well.

1. Introduction

The remarkable magnetic properties of rare-earth orthoferrites $RFeO_3$ result from complex interactions between the moments of 3*d* electrons of the transition metal and 4*f* electrons of the rare-earth. Investigations of these magnetic compounds were started several decades ago [1], including neutron powder diffraction investigations of the crystal and magnetic structures [2,3]. The space group was reported to be orthorhombic *Pbnm* (or *Pnma* in another setting). It was shown that these compounds have high Néel temperatures $T_N \approx 600$–700 K, below which Fe^{3+} moments are ordered antiferromagnetically with a weak ferromagnetic component. With decreasing temperature, the importance of the Fe–*R* interaction increases (certainly for magnetic rare earth ions) leading to the spin-reorientation (SR) transition. This latter takes place at temperature T_{SR}, which is often in the range $50 \div 60$ K; though SR transition occurs at much lower temperatures, close to the Neel temperatures of rare-earth alignment for some rare-earth ions like Tb, Yb, or at such a high temperature as ~456 K for Sm. The rare-earth subsystem with relatively weak R–R interactions remains paramagnetic at elevated temperatures, or it is weakly polarized by the exchange field of the ordered Fe^{3+} moments. The spontaneous ordering of the rare-earth sublattice takes pace below $T_{NR} \approx 5$–10 K. Complex magnetic properties of the $RFeO_3$ system are governed by the presence of various competing exchange interactions. They include Heisenberg-type super exchange of type Fe–Fe, Fe–R, R–R, and also Dzyaloshinskii-Moriya (DM) interaction [4,5] which has an important influence on the magnetic properties and leads to weak ferromagnetism.

Recently, the interest in the $RFeO_3$ family of compounds has been greatly renewed because of the discovery of their multiferroic properties. Emergence of ferroelectricity in orthoferrites at temperatures below T_{NR} has been predicted in theoretical work [6] on the basis of a symmetry analysis of the crystal structure. The ordering of the R^{3+} moments takes place in accordance with the $\Gamma 1 - \Gamma 8$ irreducible representations, which are not compatible with inversion symmetry and thus allow for a linear magnetoelectric effect as well as for a dynamic magnetoelectric effect i.e. an electric-dipole-active magnetic excitations.

In the subsequent experiments on $DyFeO_3$ and $GdFeO_3$ the emergence of a ferroelectric polarization was observed below the magnetic ordering $T_{NR} \approx 5$–10 K of the rare-earth subsystem indeed [7,8]. Later, however, electric polarization in $DyFeO_3$ was found at much higher temperatures, above $T_{SR} \approx 50$–60 K [9]. In other orthoferrites like $SmFeO_3$ [10], $YFeO_3$ [11] and $LuFeO_3$ [12], electric polarization was reported even at room temperature. This brings these compounds close to being useful for potential applications in switching elements, sensors, memory and other advanced technical devices with low energy consumption. Macroscopic investigations show a strong influence of external fields on the magnetic and/or ferroelectric properties of these compounds [7,12,13,14].

There is an indication that the DM interaction could be responsible for the emergence of ferroelectric ordering in $DyFeO_3$, $YFeO_3$ and $LuFeO_3$ at high temperatures [12]. It should be noted also that the

* Corresponding author at: Condensed Matter Research Department, PNPI, Orlova Roshcha, Gatchina, St. Petersburg distr., 188300, Russia.
E-mail address: zobkalo@pnpi.nrcki.ru (I.A. Zobkalo).

https://doi.org/10.1016/j.jmmm.2020.166855
Received 23 October 2019; Received in revised form 12 March 2020; Accepted 30 March 2020
Available online 31 March 2020
0304-8853/

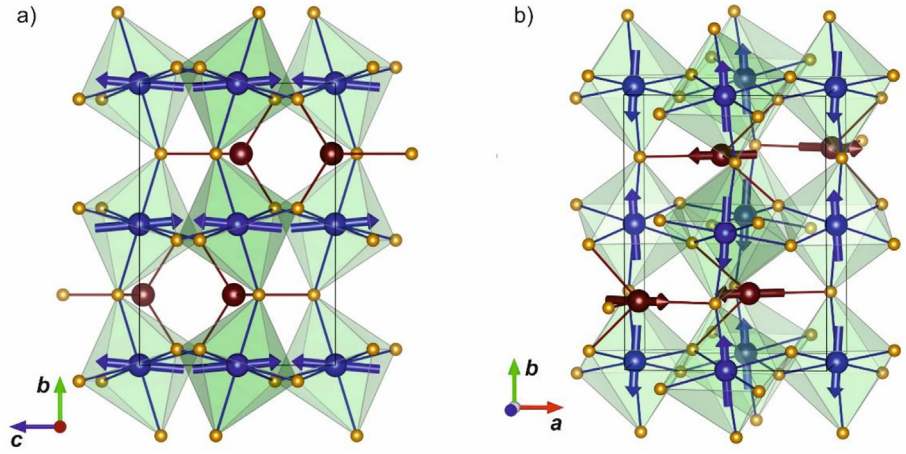

Fig. 1. The magnetic structure: a) in phase Γ4 and b) in phase Γ2. Blue spheres - Fe^{3+} ions, red – Ho^{3+}, orange – O^{2+}. (For interpretation of the references to color in this figure legend, the reader is referred to the web version of this article.)

orthorhombic space group *Pbnm* is centrosymmetric and therefore does not allow spontaneous electric polarization. Therefore, more precise and detailed studies of the crystal and magnetic properties of the $RFeO_3$ compounds required in order to search for the physical origin of the symmetry lowering. Rare-earth orthoferrites $RFeO_3$, with a ferroelectric moment induced presumably by the magnetic DM interaction, are very promising candidates for the realization of such an effect that will also serve to a better understanding of the interplay between ferroelectric polarization and magnetic order.

According to recent precise single-crystal neutron diffraction studies of $HoFeO_3$ below T_N = 647 K Fe sublattice has antiferromagnetic order described by symmetry representation Γ_4 [15] with the strongest component along *a*-axis, and weak ferromagnetic component along *c*-axis. The first spin-reorientation phase transition to the antiferromagnetic order with Γ_1 takes place at T_{SR1} = 55 K and the second reorientation transition from Γ_1 to Γ_2 – at T_{SR2} = 35 K, where the strongest component of Fe magnetic moments directed along *c* [15]. Fig. 1 shows the magnetic structures in phases Γ4 and Γ2. Ho order happens at temperatures 3.3–4.1 K as it was shown by the works on the heat capacity, magnetization, and Mössbauer studies [16–18]. The magnetic moments of Ho lie in *a*-*b* plane, the ordering also could be described by Γ2 representation [15] which does not impose any restriction on the moment orientation along c for Ho site 4c.

The spin dynamics of *R*FeO3 orthoferrites have been previously studied with inelastic neutron scattering [19–21], Raman spectroscopy [22–24], Faraday balance [25–27], far-IR [28,29], and submillimeter [30] spectroscopies. These studies made it possible to determine the parameters of exchange interactions in some orthoferrites, and also discovered a number of unexpected interesting properties of spin dynamics in these materials. Thus the recent study $YbFeO_3$ reveals rich quantum spin dynamics of Yb magnetic sublattice [31]. At temperatures below T_{SR} = 7.6 K the Yb subsystem changes the its excitation spectrum, demonstrating the transition between two regimes with magnon and spinonlike fluctuations. The electromagnon excitations were detected in $DyFeO_3$ and TbFeO3 in magnetic phases, which are compatible with a spontaneous electric polarization [28,29]. In $TbFeO_3$ was found that the specific exchange of magnons can lead to new magnetic states [32]. Ultrafast control of the spin dynamics by polarized femtosecond laser pulses was observed in $DyFeO_3$ [26] and in $TmFeO_3$ [27].

Inelastic neutron scattering is the only direct method to investigate the dynamics of a magnetic lattice and, therefore, the most reliable way to obtain the magnetic interaction parameters. This could provide an essential input for the theoretical description of the magnetic properties as well as for developing the model responsible for the multiferroicity. Just a few earlier works were performed on the orthoferrites with Er, Tm [19] and Tb [20] by this technique and the parameters of exchange interactions have been determined, using incomplete models for the calculations. These considered only the strongest exchange interactions of Heisenberg-type like Fe-Fe super exchange interactions between the nearest and next-nearest neighbors, whereas DM antisymmetric exchange almost never have been taken into account. Just recently, the DM interaction and single-ion anisotropy of Fe were considered in the studies of magnetic dynamics of $YFeO_3$ [21] and $YbFeO_3$ [31]. Despite its weakness, the DM-interaction could strongly influence on the magnetic properties of a system. As mentioned above, in the case of $RFeO_3$ orthoferrites, the DM interaction is the origin of weak ferromagnetism and definitely needs to be taken into account. Therefore, we plan to study both the symmetric exchange interactions 3*d*–3*d*, 3*d*–4*f*, 4*f*–4*f* as well as the antisymmetric interaction in the same magnetic subsystems.

2. Experimental

High quality twins-free single crystal of $HoFeO_3$ has been grown using fluxed melt method [33]. The shape of the crystal used in experiment is close to parallelepiped with approximate dimensions 5 × 4 × 6 mm^3 with the longest dimension along c-axis The parameters of the unit cell were refined at room temperature and at 65 K and appeared to be the same at both temperatures. The obtained structure should be attributed to space group *Pbnm* with cell parameters a = 5.280 Å, b = 5.591 Å, c = 7.602 Å, which corresponds completely to those obtained earlier [2].

The inelastic neutron scattering experiments were performed at ILL on the spectrometers IN12 and IN20. High energy excitations were studied at IN20 – thermal neutron triple axis spectrometer, and low energy range was explored at IN12 – cold neutron triple-axis spectrometer.

The experiment at IN20 was performed at some temperatures corresponding to different magnetic phases: at 65 K – weak ferromagnetic phase Γ_4, at 35 K – antiferromagnetic phase Γ_1, at 15 and 2.5 K – weak ferromagnetic phase Γ_2. During the experiment we used the measurements in "constant-*q*" mode consisted in series of energy scans with sequential steps along *h* or *l* directions in the reciprocal space (conditionally *h*-scan or *l*-scan in the following text). For the high energy studies the energy step was taken ΔE = 1 meV along the scan in the energy range 10–70 meV. The *q*-step was Δh, Δl = 0.2 rlu. And the measurements were made in the vicinity of node *q* = [3 0 5] along *h* direction in the range from *q* = [1 0 5] to *q* = [3 0 5] and along *l* direction from *q* = [3 0 3] to *q* = [3 0 5].

For low energy transfer the measurements at IN12 were made in the range 0–7 meV with the energy step ΔE = 0.1 meV along the scan with

the step Δh, $\Delta l = 0.2$ rlu. Scans were made in the vicinity of node $q = [1\ 0\ 1]$ along h direction in the range from $q = [0\ 0\ 1]$ to $q = [2\ 0\ 1]$ and along l direction from $q = [1\ 0\ 0]$ to $q = [1\ 0\ 2]$. In this way we obtained a maps of the intensity, reflecting different kinds of inelastic scattering.

For more accurate determination of the energy gap and separation of the tale from elastic peak and inelastic peak intensity at energy transfer range $0 \div 1$ meV, the scans with better energy resolution $\Delta E = 0.05$ meV were performed in the energy range from 0 to 2.5 meV. In this mode the wave vector of scattered neutrons was kept $k_f = 1.25$ Å^{-1} and the momentum transfer varied from $q = [0.6\ 0\ 1]$ to $q = [1.6\ 0\ 1]$.

In the course of data treatment the positions, intensities and half widths of the measured peaks were calculated using the Winplotr program included in the FullProf Suite [34]. For the INS treatment the preliminary calculations for the description of the Fe subsystem were made using our own code performed in the Wolfram Math environment. All final results are obtained using the SpinW software [35]. For the determination of the uncertainty of the fitted parameters we took the maximum parameter range, at which convergence R-factor did not change its value.

3. Experimental results

The typical results of the measurements at high-energy transfer are presented at Fig. 2, where q-constant scans for 65 K and 2.5 K obtained at IN20 are shown. As it can be seen, a significant number of inelastic peaks maxima can be found on the measured spectra.

Measured in this way scans were then combined into energy maps and these ones obtained at IN20 for the higher energy range are presented at Fig. 3. The dispersion branches of Fe^{3+} magnon excitations is clearly visible here. The number of dispersionless branches are also clearly observed on the maps. The energies of these lines correspond to the transitions in molecular field, which was obtained by the estimations within the mean-field approach. The details of this consideration will follow in the separate article soon. Dispersionless branches at ~10 meV, ~15 meV correspond also to CEF levels reported in the works by optical spectroscopy [36,37]. It can be seen also that not all these q-dependences are straight lines, that can really be related to some hybridization with magnon or phonon scattering. The low energy transfer results obtained at IN12 are presented at Fig. 4, where the maps along h direction around point [1 0 1] from q = [0 0 1] to q = [2 0 1] at temperatures of 65 K, 35 K and 2.5 K are shown. The peak intensities at energy transfer of 0 meV correspond to elastic scattering. At 35 K and 2.5 K one can see doubled dispersionless (or almost dispersionless) lines in the range $0 \div 1$ meV which should be attributed to split level of the crystal field and Ho-originated magnon branch. At $q = [1\ 0\ 1]$, dispersion curves with the energy gap are observed, which definitely should be associated with the spin waves in the Fe^{3+} sublattice. In order to elucidate the nature of the signal, we have checked all measured peaks with respect to reasonable resolution widths. For the description of the peaks shape, pseudo-Voight function was used. Analysis shows that different widths of the peaks originate solely from the instrument, excluding any broadening effects from real physics.

4. Spin waves modeling and calculation

For the analysis of magnetic excitations observed in $HoFeO_3$ the standard linear spin-wave approach was used. In the general case, a Hamiltonian must contain the following terms:

$$H = H^{Fe-Fe} + H^{Ho-Ho} + H^{Fe-Ho} \quad (1)$$

where the first two terms describe exchange interactions and single-ion anisotropies within Fe^{3+} and Ho^{3+} subsystems, respectively. The third term describes the interaction between the Fe and Ho subsystems.

At $T = 65$ K subsystem Ho^{3+} supposed to be non-ordered, i.e. has zero ordered magnetic moment and the second and third terms in the Hamiltonian (1) are zero. Then dispersion curves can be described using interactions within the Fe^{3+} sublattice only:

$$H^{Fe-Fe} = \sum_{ij} S_i^{Fe} \bullet J_{ij}^{Fe} \bullet S_j^{Fe} + \sum_i S_i^{Fe} \bullet A_i^{Fe} \bullet S_i^{Fe} + \sum_{mn} S_m^{Fe} \bullet D_{mn}^{Fe} \bullet S_n^{Fe} \quad (2)$$

where S – spin operator, J – isotropic exchange interactions, A – single ion anisotropy, D – DM interaction parameter. In the expression (2), the parameters of exchange interactions, anisotropy and DM are written as a 3×3 matrix, as it was used in the calculations. In this Hamiltonian (2), the first term dictates an overall shape and maximum energy of the Fe excitations. For the simulation of the exchange interactions in Fe subsystem it is reasonable to include in the analysis the interactions between nearest neighbors (J_{nn}) and next-nearest neighbors (J_{nnn}). The nearest neighbors exchange interactions along the axis c – J_c^{Fe} and in the plane ab – J_{ab}^{Fe} (see Fig. 5a, b) describe the exchange between ions that are at different distances. In the studies [19–21], these exchanges are considered as the equal interactions between the nearest neighbors and are described by one common exchange parameter. However, the latest work [38] on $YFeO_3$ showed that difference in the distance between the ions such a small as ~0.03 Å, may result in an appreciable energy difference between the exchange parameters of about ~0.4 meV. The similar situation arises when considering the interaction between next-nearest neighbors, where several interactions between ions with close exchange paths distances were described by one common parameter J_{nnn}^{Fe} (Fig. 5c–e).

The anisotropy determines a magnetic ground state [39] and gives rise to the gap in the Fe magnon spectrum [21]. Due to the orthorhombic symmetry of the Fe^{3+} environment, the anisotropy must be described by two nonequivalent constants Aab and Ac. In $RFeO_3$ with nonmagnetic R-ions, a dominating Aab stabilizes the Γ4 phase. In $HoFeO_3$, the Ho-Fe interaction induces renormalization of the effective anisotropy constants. At $T \approx T_{SR1}$, Aab and Ac become approximately equal [39]. Below T_{SR2} $Ac > Aab$ that stabilizes the Γ2 phase.

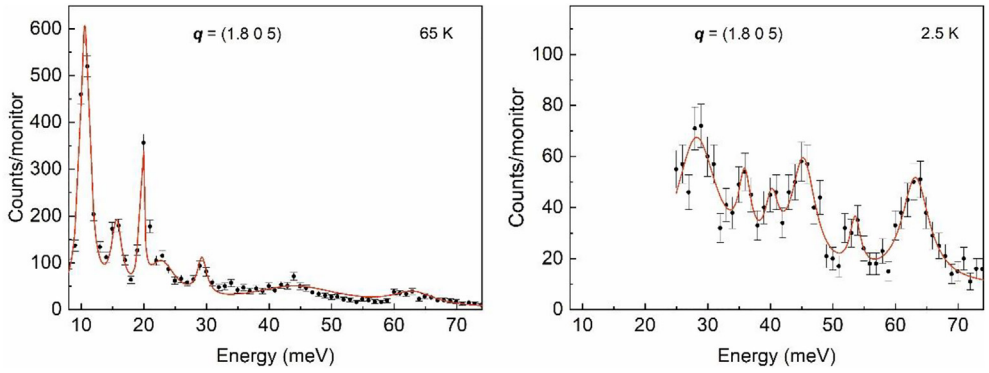

Fig. 2. Typical scans of inelastic neutron scattering, obtained at IN20 at T = 65 K and T = 2.5 K. Solid lines – fitting results.

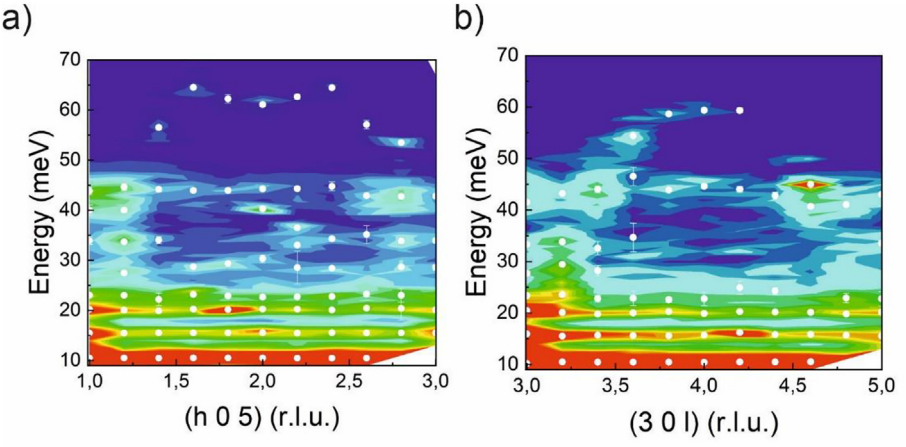

Fig. 3. Energy maps, obtained at IN20 at temperature of 65 K: a) *h*-scans with $l = 5$ and b) *l*–scans with $h = 3$. The colors show the intensity, the white dots – positions of the inelastic peaks.

At temperatures above $T_{SR1} = 55$ K the moments of Fe are directed along *a* axis and are ordered antiferromagnetically with the propagation vector $\boldsymbol{k} = (0\ 0\ 0)$. The DM antisymmetric exchange interaction leads to a weak canting of the sublattices, which is described by two constants *D1* and *D2*, responsible for the canting along *c* and *b* axes, respectively. Since DM interaction is very small, for its determination we consider only two pairs of the nearest neighbors in Fe subsystem (Fig. 5a, b). The DM exchange parameters were calculated in the following way: as in [21], initial DM values were obtained based on the canting angles of the sublattices. The values of the canting were taken from [40]. These DM values were used then as starting parameters when fitting our model.

In order to describe the dispersion at lower temperatures at T = 2.5 K, when the moments of Ho^{3+} are ordered, and the system is in the magnetic phase Γ2, it is necessary to take into account exchange interactions between Fe^{3+} and Ho^{3+} subsystems -J^{Fe-Ho}, and interactions within Ho^{3+} subsystem J^{Ho} (Fig. 6). Then we the following terms should be added to the expression (1):

$$H^{Fe-Ho} + H^{Ho-Ho} = \sum_{ij} S_i^{Fe} \bullet J_{ij}^{Fe-Ho} \bullet s_j^{Ho} + \sum_{mn} s_m^{Ho} \bullet J_{mn}^{Ho} \bullet s_n^{Ho} \quad (3)$$

where s^{Ho} – the Ho spin moment operator:

$$s^{Ho} = (g_j - 1)\boldsymbol{J} \quad (4)$$

where g_j – Lande factor, $\boldsymbol{J}$ – total angular moment. Since the crystal structure and distances between iron ions have not changed, it is reasonable to fix in fitting procedure the parameters included in H^{Fe-Fe} which were obtained from the data at T = 65 K. For J^{Ho} calculation in order to simplify the model we restrict ourselves to the R-R interaction between the nearest neighbors. This is because the value of exchange interaction within the Ho sublattice is small, and at the same time in our experiment we cannot distinguish the dispersion curves corresponding to Ho.

Experimental and calculated dispersion curves are shown at Fig. 7. Calculated values of all parameters are presented at the Table 1. The obtained values of the exchange parameters inside the Fe sublattice are in good agreement with those ones in other similar compounds [21,31,38]. At the same time, the difference between nearest neighbors exchange interactions J_c^{Fe} and J_{ab}^{Fe} is noticeable. With regard to next-nearest neighbors, the results of our calculations show that there is no sense in separation of the parameters because the values of the exchange parameters appeared to be the same within the calculation error.

5. Discussion

The results confirm that the exchange interactions J_c^{Fe} and J_{ab}^{Fe} are the strongest in the system and they are crucial in the formation of structure with antiferromagnetic ordering in $HoFeO_3$, and also these interactions determine the maximum excitation energy of the Fe^{3+} magnetic sublattice.

At high temperatures ordered Fe^{3+} sublattice polarizes Ho^{3+} subsystem, giving rise to Ho-Fe exchange interaction, which in turn, leads to the exchange splitting of the ground state of Ho^{3+}. This could be seen on the energy maps at Fig. 4 where the energy level that corresponds to Zeeman splitting of the ground state of Ho lies in the energy

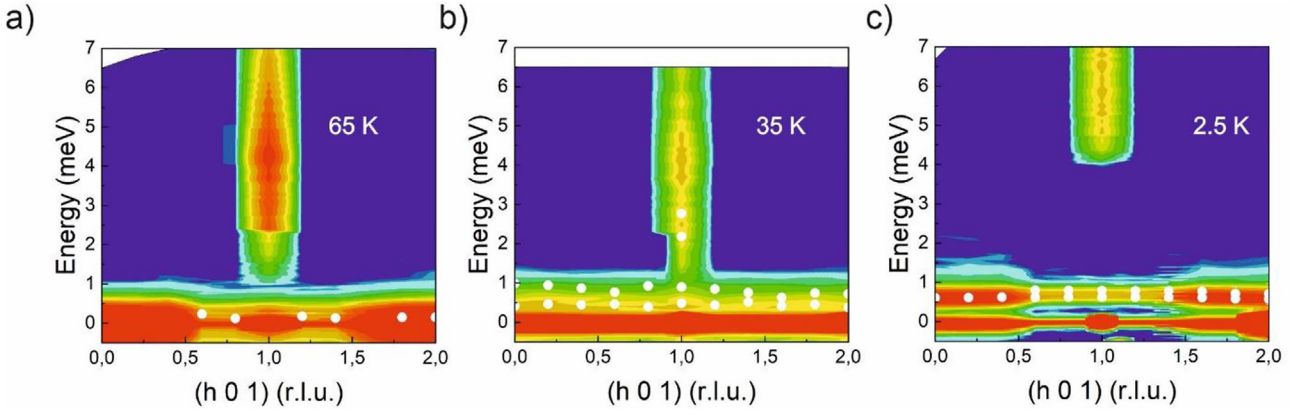

Fig. 4. Energy maps obtained at IN12 by *h*-scans with $l = 1$ at temperatures a) 65 K, b) 35 K and c) 2.5 K. The color indicate the intensity, the white dots are the positions of the inelastic peaks.

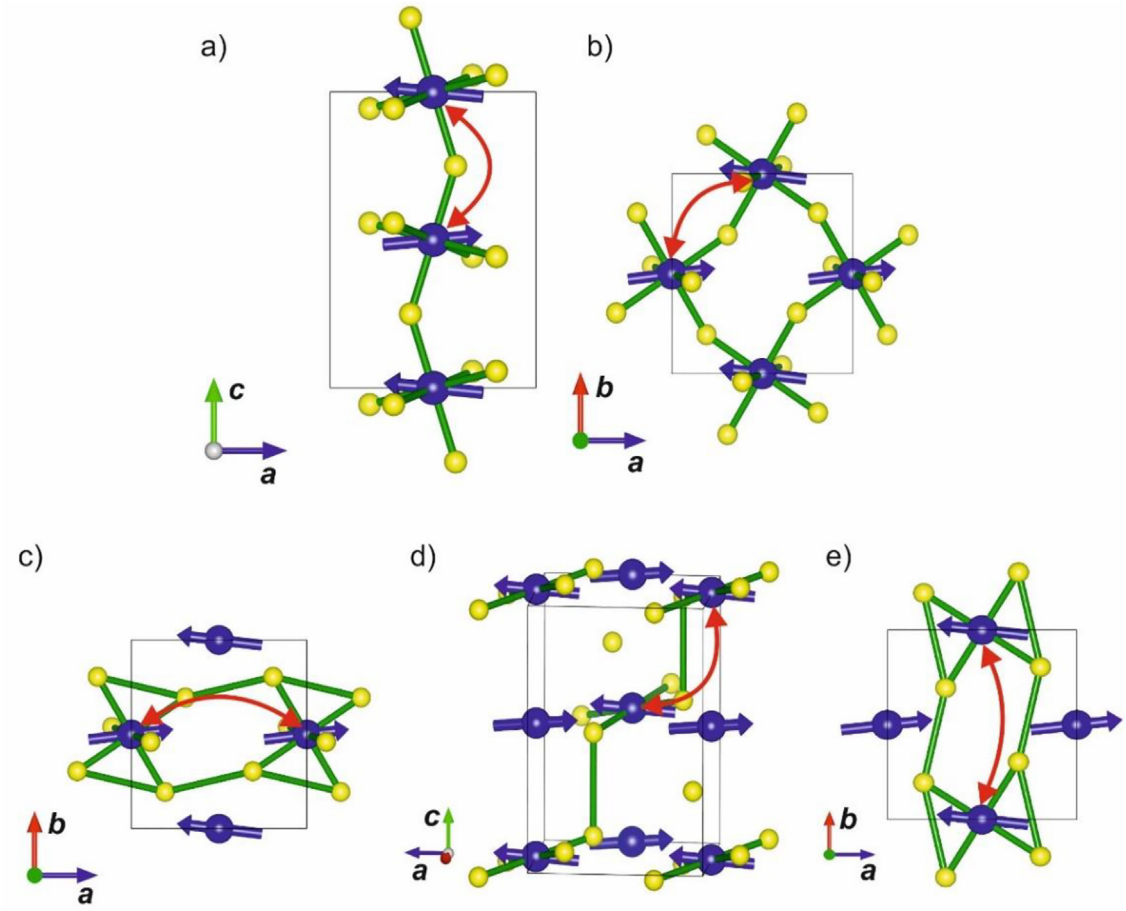

Fig. 5. The schemes of the interaction $HoFeO_3$ under consideration: a) and b) exchange paths of interaction J_c^{Fe} and J_{ab}^{Fe} with distances 3.810A and 3.842A, respectively; c) d) and e) exchange paths of interaction J_{nnn}^{Fe} with distances 5.282A, 5.409A and 5.591A, respectively. Blue spheres - Fe^{3+} ions, orange – O^{2-}. Red arrows show the exchange interaction paths. (For interpretation of the references to color in this figure legend, the reader is referred to the web version of this article.)

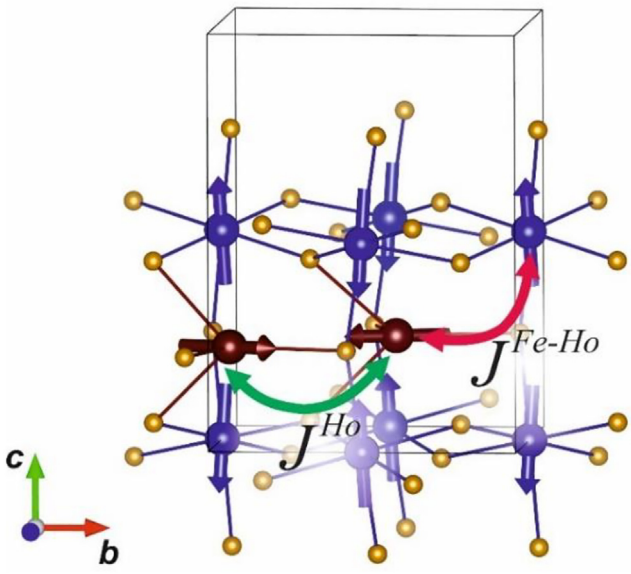

Fig. 6. Blue spheres show Fe ions. Orange – O. Red – Ho ions. Red arrow shows exchange paths J^{Fe-HO}. Green arrow – exchange J^{HO}. (For interpretation of the references to color in this figure legend, the reader is referred to the web version of this article.)

range of 0 ÷ 1 meV. At the temperature $T = 65$ K the value of splitting is $\Delta_{HGS} \approx 0.35(1)$ meV. The splitting value increases to $\Delta_{HGS} \approx 0.95(1)$ meV at $T = 35$ K, and then begins to decrease due to inset of Ho-Ho interaction, thus lowering the splitting value to $\Delta_{HGS} \approx 0.65(1)$ meV at the $T = 2.5$ K. This gives the evidence that interaction J^{Fe-Ho} and J^{Ho} must be of opposite sign since that provides the observed behavior of the level splitting energy. The similar situation was observed in experiments by optical spectroscopy [36,37], where the absorption lines splitting was $\Delta_{HGS} \approx 0.25$ meV at T = 100 K, at T = 20 K it was $\Delta_{HGS} \approx 0.88$ meV and at T = 1.2 K $\Delta_{HGS} \approx 0.61$ meV. The obtained values of J^{Fe-Ho} and J^{Ho} are presented at Table 1. These values and signs correlate well with the results from optical spectroscopy [36,37], that gives $J^{Fe-Ho} < 0.2$ meV, and by the Faraday balance measurements [25] that gives $J^{Fe-Ho} = 0.0215$ meV. In these cases, J^{Fe-Ho} exchange between the Fe and Ho sublattices and the J^{Ho} exchange in Ho sublattice also have opposite signs.

The exchange interaction J^{Fe-Ho} is comparatively small, nevertheless it influences considerably on our model calculations. Since this exchange couples the Fe and Ho subsystems, it contributes to the energy of the dispersion curves of both subsystems. In our experiments, we cannot clearly distinguish the dispersion branches from the Ho sublattice, but we are good at defining the dispersion curves corresponding to the Fe subsystem. Therefore, the influence of the J^{Fe-Ho} exchange value can be determined by the energy of the Fe dispersion curves. For example, for $J^{Fe-Ho} = 0.026$ meV, 0 meV, the calculated value of the energy gap (q = 1 0 1) is $\Delta = 3.82$ meV, 3.72 meV, respectively. While the calculated maximum energies for corresponding exchange values

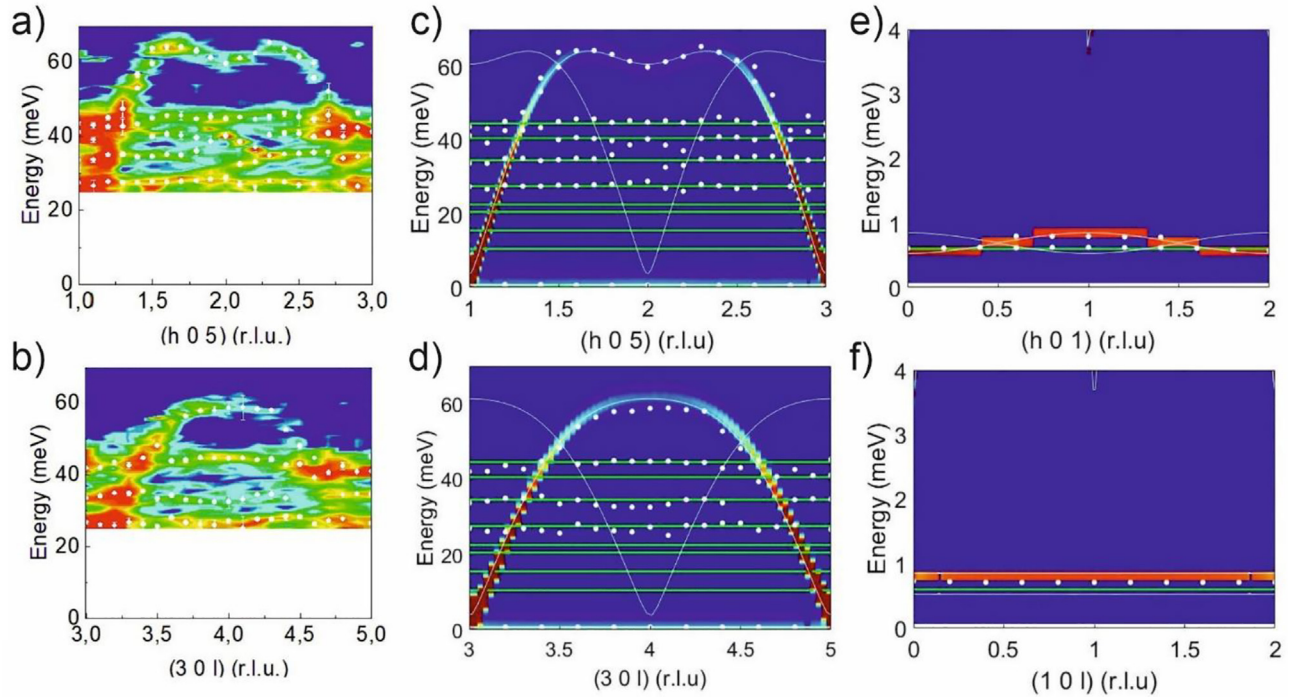

Fig. 7. a), b) High energy magnon dispersion measured at 2.5 K, the colors show the intensity, the white dots - positions of the inelastic peaks. c), d) Calculated high energy dispersion maps, white lines - calculated dispersion curves; green line – levels of the crystal field. e), f) calculated energy maps in the energy range 0–4 meV at T = 2.5 K; compare with Fig. 4. (For interpretation of the references to color in this figure legend, the reader is referred to the web version of this article.)

(at q = 1.68 0 1) differ very little: 64.11 meV, and 64.10 meV.

According to our simulations, dispersion curves associated with spin waves in the Ho sublattice should be in the energy range of 0 ÷ 1 meV. In the same energy range, the peaks from the transition in the exchange split crystal field level are present. The resolution of our measurements does not permit to make the perfect separation between the exact positions of peaks corresponding to inelastic scattering by spin waves in Ho sublattice. Nevertheless, the peak splitting is clearly seen at the energy scans at temperatures 35 K and 2.5 K and peak positions could be extracted. As example the energy scans at different temperatures are presented at Fig. 8, where one can see asymmetric peak at the region of 0.7 meV (Fig. 8b and c). This value is close to the position of the split level of the crystal field at low temperatures. Apparently this asymmetric peak broadening is due to the fact that the reflections from excitations of the Ho sublattice lie close to the peaks corresponding to the crystal field levels. At high temperatures, such a splitting is not observed (Fig. 8a). In this way, the calculated value of the Ho-Ho interaction, presented in Table 1, is the maximum possible estimate, on the basis of which the dispersion curves are reproduced in Fig. 7.

Single-ion anisotropy A leads to the appearance of a gap in the Fe magnon spectrum (Fig. 3). The easy-plane anisotropy Aab dominates in the Γ4 and Γ1 phases, thus forcing iron moments to lie in the ab plane [15]. With temperature decrease, the R-Fe interaction becomes more pronounced and below T_{SR2} it causes a redistribution of energy, and, therefore the change of anisotropy constants. In the Γ2 phase, the easy-axis anisotropy Ac becomes dominant that causes the orientation of iron moments mainly in the direction c [15]. The growth of Ac is confirmed by the experimental fact that the spectrum of magnons with high energies does not change at the spin-orientation transition, while the magnitude of the energy gap changes only. Such behavior can be understood if we assume the temperature dependence of the effective anisotropy constants $Aab\ (T)$ and $Ac\ (T)$. It can be seen at Fig. 9, where the energy gaps are shown at different temperatures. Gap values obtained were Δ_{65k}^{Fe} = 0.94 meV and Δ_{35k}^{Fe} = 1.04 meV – for the measurements in the Γ4 and Γ1 phases correspondingly, where the easy-plane anisotropy prevails, and their magnitude practically did not change through T_{SR1} transition. At the same time Δ_{15k}^{Fe} = 1.79 meV, $\Delta_{2.5k}^{Fe}$ = 3.82 meV – gaps in the Γ2 phase where easy-axis anisotropy dominates. A sharp increase in the energy gaps could be connected with growth of Ho^{3+} magnetic moment.

6. Conclusion

We report the neutron inelastic scattering study of the spin dynamics in $HoFeO_3$ at different temperatures corresponding to three magnetic ordering phases: Γ4, Γ1 and Γ2. The observed spectra were

Table 1
The parameters of exchange interactions (in meV) obtained in this work with the best fit of the data (Rw = 5.43), and similar parameters obtained for another orthoferrites for comparison.

Magnetic phase Γ4:	J_c^{Fe}	J_{ab}^{Fe}	J_{nnn}^{Fe}	J^{Fe-Ho}	J^{Ho}	D1	D2	Ac	Aab
$HoFeO_3$	4.901(5)	4.764(5)	0.150(7)			0.12(2)	0.08(2)	0	0.008(1)
$YFeO_3$ [21]	4.77		0.21			0.074	0.028	0.003	0.0055
$YFeO_3$ [38]	5.02	4.62	0.22			0.1447	0.1206	0.0025	0.0091
$YbFeO_3$ [31]	4.675		0.158			0.086	0.027	0	0.033
Magnetic phase Γ2:									
$HoFeO_3$	4.901(5)	4.764(5)	0.150(7)	−0.026(2)	0.035(5)	0.12(2)	0.08(2)	0.017(1)	0
$YbFeO_3$ [31]	4.675		0.158			0.086	0.027	0.023	0

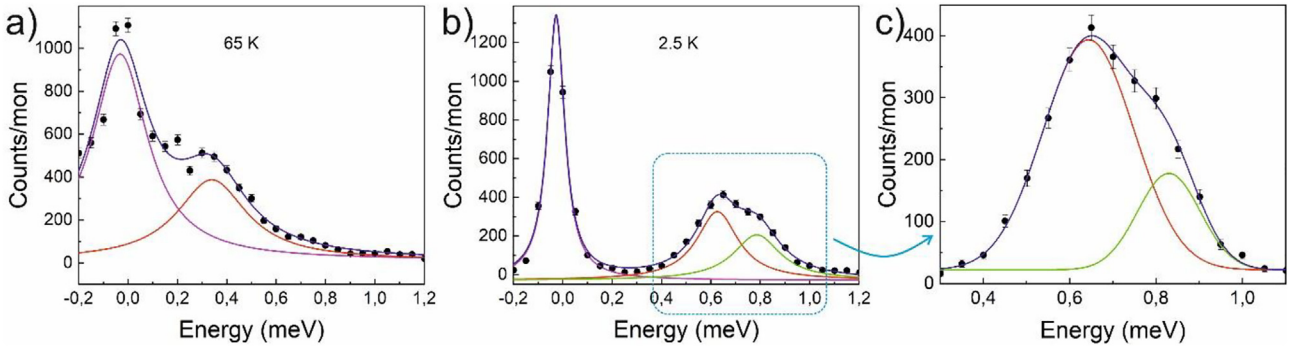

Fig. 8. a), b) – the energy scans in the energy range of −0.2 to 1.2 meV at temperatures of 65 K and 2.5 K, respectively. The pink line is the peak corresponding to the elastic scattering of neutrons, the red line – to the level of the crystal field, the green line – to the Ho magnons. Selected region c) – enlarged fragment of the 2.5 K scan. (For interpretation of the references to color in this figure legend, the reader is referred to the web version of this article.)

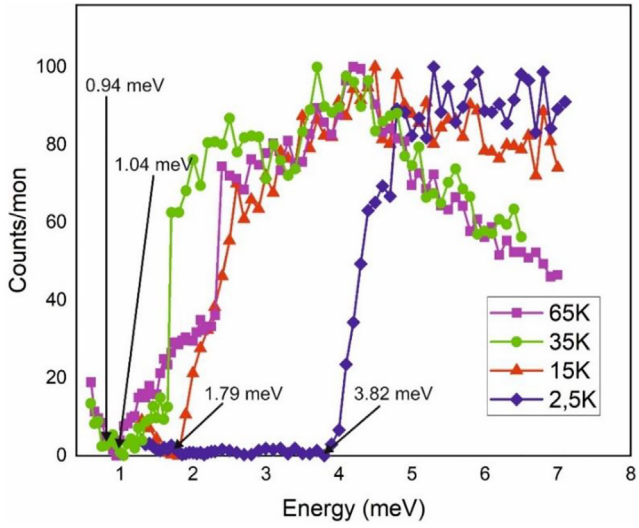

Fig. 9. Energy gaps measured at q = [1 0 1] at different temperatures.

analyzed in the frames of the linear spin-wave theory based on the magnetic structure, derived from the elastic neutron scattering [15]. The values of the parameters of exchange interactions within the Fe-subsystem were obtained, which are in a good agreement with similar values in other orthoferrites. We show that the anisotropy constants *Aab* and *Ac* of the iron sublattice in Γ4 and Γ1 phases keep their values, while in the Γ2 phase the ratio between them change itself for the score of growth of *Ac*, thus leading to the increase of anisotropy energy with temperature decrease. This provides the increase of the energy gap in spin-wave spectrum of Fe^{3+} magnetic system. Evaluations of exchange interactions within the Ho-subsystem and between Fe and Ho subsystems were made.

CRediT authorship contribution statement

A.K. Ovsyanikov: Methodology, Software, Formal analysis, Investigation, Writing - original draft. **I.A. Zobkalo:** Conceptualization, Methodology, Validation, Writing - review & editing, Supervision. **W. Schmidt:** Validation, Investigation, Formal analysis. **S.N. Barilo:** Resources. **S.A. Guretskii:** Resources. **V. Hutanu:** Validation, Writing - review & editing, Supervision.

Declaration of Competing Interest

The authors declare that they have no known competing financial interests or personal relationships that could have appeared to influence the work reported in this paper.

Acknowledgments

The authors are grateful to S.V. Maleyev for the discussions on the consideration of CEF. This work was supported by the Russian Foundation for Basic Research grant # 19-52-12047, and DFG grant # SA 3688/1-1. The work of S.N.B. and S.A.G. was done under support of Belorussian Foundation for Basic Research grant # BRRFFI - NFENK 18K-022.

References

[1] R. White, J. Appl. Phys. 40 (1969) 1061.
[2] M. Marezio, J.P. Remeika, P.D. Dernier, Acta Cryst. B 26 (1970) 2008.
[3] W.C. Koehler, E.O. Wollan, M.K. Wilkinson, Phys. Rev. 118 (1960) 58.
[4] I.E. Dzyaloshinsky, J. Phys. Chem. Solids 4 (1958) 241.
[5] T. Moriya, Phys. Rev. 120 (1960) 91.
[6] A.K. Zvezdin, A.A. Mukhin, JETP Lett. 88 (2008) 505.
[7] Y. Tokunaga, S. Iguchi, T. Arima, Y. Tokura, Phys. Rev. Lett. 101 (2008) 097205.
[8] Y. Tokunaga, et al., Nat. Mat. 8 (2009) 558.
[9] B. Rajeswaran, et al., Europhys. Lett. 101 (2013) 17001.
[10] J.-H. Lee, Y.K. Jeong, J.H. Park, M.-A. Oak, H.M. Jang, J.Y. Son, J.F. Scott, Phys. Rev. Lett. 107 (2011) 117201.
[11] P. Mandal, V.S. Bhadram, Y. Sundarayya, C. Narayana, A. Sundaresan, C.N.R. Rao, Phys. Rev. Lett. 107 (2011) 137202.
[12] U. Chowdhury, S. Goswami, D. Bhattacharya, J. Ghosh, S. Basu, S. Neogi, Appl. Phys. Lett. 105 (2014) 052911.
[13] Y.Q. Song, W.P. Zhou, Y. Fang, Y.T. Yang, L.Y. Wang, D.H. Wang, Y.W. Du, Chin. Phys. B 23 (2014) 077505.
[14] Y. Tokunaga, T.A. Taguchi, Y. Tokura, Nat. Phys. 8 (2012) 838.
[15] T. Chatterji, M. Meven, P.J. Brown, AIP Adv. 7 (2017) 045106.
[16] A. Bhattacharjee, K. Saito, M. Sorai, J. Phys. Chem. Solids 63 (2002) 569.
[17] M. Shao, S. Cao, Y. Wang, S. Yuan, B. Kang, J. Zhang, A. Wu, J. Xu, J. Cryst. Growth 318 (2011) 947.
[18] O. Nikolov, I. Hall, K.W. Godfrey, J. Phys. Condens. Matter 7 (1995) 4949.
[19] S.M. Shapiro, J.D. Axe, J.P. Remeika, Phys. Rev. B 10 (1974) 2014.
[20] A. Gukasov, U. Steigenberger, S.N. Barilo, S.A. Guretskii, Phys. B 234–236 (1997) 760.
[21] S.E. Hahn, A.A. Podlesnyak, G. Ehlers, G.E. Granroth, R.S. Fishman, A.I. Kolesnikov, E. Pomjakushina, K. Conder, Phys. Rev. B 89 (2014) 014420.
[22] N. Koshizuka, S. Ushioda, Phys. Rev. B 22 (1980) 5394.
[23] N. Koshizuka, K. Hayashi, J. Phys. Soc. Jpn 57 (1988) 4418.
[24] R.M. White, R.J. Nemanich, C. Herring, Phys. Rev. B 25 (1982) 1822.
[25] T. Sakata, A. Enomura, Phys. Stat. Sol. (a) 52 (1979) 311.
[26] A.V. Kimel, A. Kirilyuk, P.A. Usachev, R.V. Pisarev, A.M. Balbashov, Th. Rasing, Nature 435 (2005) 655.
[27] A.V. Kimel, A. Kirilyuk, A. Tsvetkov, R.V. Pisarev, Th. Rasing, Nature 429 (2004) 850.
[28] T.N. Stanislavchuk, Y. Wang, S.-W. Cheong, A.A. Sirenko, Phys. Rev. B 95 (2017) 054427.
[29] T.N. Stanislavchuk, Y. Wang, Y. Janssen, G.L. Carr, S.-W. Cheong, A.A. Sirenko, Phys. Rev. B 93 (2016) 094403.
[30] R.C. LeCraw, R. Wolfe, E.M. Gyorgy, F.B. Hagedorn, J.C. Hensel, J.P. Remeika, J. Appl. Phys. 39 (1968) 1019.
[31] S.E. Nikitin, L.S. Wu, A.S. Sefat, K.A. Shaykhutdinov, Z. Lu, S. Meng, E.V. Pomjakushina, K. Conder, G. Ehlers, M.D. Lumsden, A.I. Kolesnikov, S. Barilo, S.A. Guretskii, D.S. Inosov, A. Podlesnyak, Phys. Rev. B 98 (2018) 064424.
[32] S. Artyukhin, M. Mostovoy, N.P. Jensen, D. Le, K. Prokes, V.G. de Paula, H.N. Bordallo, A. Maljuk, S. Landsgesell, H. Ryll, B. Klemke, S. Paeckel, K. Kiefer, K. Lefmann, L.T. Kuhn, D.N. Argyriou, Nat. Mater. 11 (2012) 694.
[33] S.N. Barilo, A.P. Ges, S.A. Guretskii, D.I. Zhigunov, A.A. Ignatenko,

A.N. Igumentsev, I.D. Lomako, A.M. Luginets, J. Crystal Growth 108 (1991) 314.
[34] https://www.ill.eu/sites/fullprof/.
[35] S. Toth, B. Lake, J. Phys. Condens. Matter 27 (2015) 166002.
[36] J.C. Walling, R.L. White, Phys. Rev. B 10 (1974) 4737.
[37] H. Schuhert, S. Hufner, R. Faulhaber, Z. Phys. 220 (1969) 280.
[38] K. Park, H. Sim, J.C. Leiner, Y. Yoshida, J. Jeong, S. Yano, J. Gardner, P. Bourges, M. Klicpera, V. Sechovský, J. Phys. Condens. Matter 30 (2018) 235802.
[39] K.P. Belov, A.K. Zvezdin, A.M. Kadomtseva, R.Z. Levitin, Sov. Phys. Usp. 19 (1976) 574.
[40] D. Treves, J. Appl. Phys. 36 (1965) 1033.

Breaking the magnetic symmetry by reorientation transition near 50 K in multiferroic magnetocaloric $HoFeO_3$

Ovsianikov, Aleksandr[1, 2]; Thoma, Henrik[1,3]; Usmanov, Oleg[2]; Brown, Penelope Jane[4]; Chatterji, Tapan[5]; Sazonov, Andrew[1,2]; Barilo, Sergey[6]; Peters, Lars[1]; Hutanu, Vladimir[1,3]

[1] Institute of Crystallography, RWTH Aachen University, D-52066 Aachen, Germany
[2] Petersburg Nuclear Physics Institute named by B.P.Konstantinov of NRC «Kurchatov Institute», Gatcina, Russian Federation.
[3] Jülich Centre for Neutron Science JCNS at Heinz Maier-Leibnitz Zentrum (MLZ), Forschungszentrum Julich GmbH, Germany
[4] 12 Little St. Marys Lane, Cambridge, CB2 1RR, UK.
[5] Institut Laue-Langevin, 6 rue Joules Horowitz, BP 156, 38042 Grenoble Cedex 9, France.
[6] GO National Science and Practice Center Academy of Sciences of Belarus in Materials Science, Minsk, Belarus.

Using the new polarized neutron diffraction (PND) setup at MLZ the spin reorientation transition in the magnetocaloric orthoferrite $HoFeO_3$ was studied at different wavelength. The various experiments provided reproducible results demonstrating high reliability of the used setup. We show that during the phase transition at T_{SR}=53 K in an external magnetic field applied along crystal c-axis, the ordered magnetic moment of the Fe sublattice rotates from the crystallographic direction b to a not just in the ab plane, but through z axis. This means that the applied field breaks the orthorhombic symmetry allowing some magnetization parallel to z within a short temperature region. Interestingly, this is the same temperature region where large magnetocaloric effect for $HoFeO_3$ was previously reported. A general model of the magnetic structure of $HoFeO_3$, unconstrained by the orthorhombic symmetry, would allow the magnitudes and directions of the moments on each of the 8 magnetic sublattices in the unit cell to be independent of one-another, leading to 24 independent magnetic parameters. PND measurements were used to determine the absolute sign of the Dzyaloshinskii-Moriya interaction (DMI) in the ab plane for the Fe magnetic sublattice at 65 K. DMI plays an important role in the energy balance of the system.

Index Terms – magnetic structure, spin reorientation transition, polarized neutron diffraction, Dzyaloshinskii-Moriya interaction.

I. Introduction

Multiferroicity at room temperature has been reported for some representatives of the rare-earth orthoferrites family RFeO3 (e.g. YFeO3, LuFeO3, SmFeO3)[1-4]. It brings these compounds close to being useful for potential applications in switching elements, sensors, memory and other advanced technical devices with low energy consumption. Dzyaloshinskii-Moriya interaction (DMI), which leads to a weak ferromagnetism (WF) in the Fe sublattice is proposed as one of possible reasons for the electric polarization in this materials. A spontaneous electric polarization in HoFeO3 occurs at elevated temperatures ~ 210 K [5]. In addition, a large magnetocaloric effect has been reported for $HoFeO_3$ at low temperatures [6,7], proposing this material as a promising candidate for the efficient magnetic cooling for the cryogenic gases liquefying technology. This further increase the interest on this compound and justifies detailed studies on the complex magnetic ordering processes in the rare-earth orthoferrites generally and in $HoFeO_3$ particularly.

Corresponding author: A. Ovsianikov
(e-mail: Aleksandr.Ovsianikov@frm2.tum.de).

FIG. 1 HERE

According to recent precise single-crystal neutron diffraction studies on $HoFeO_3$ in zero field its average crystal structure is described well by the orthorhombic space group *Pbnm* [8]. Below T_N= 637 K the Fe sublattice orders antiferromagnetically (AFM) with the strongest component along the a-axis, and a weak ferromagnetic component along the c-axis (magnetic phase Γ4). Two spin reorientation transitions have been reported in zero field (Fig. 1): at T_{sr1}=53 K where the Fe moments rotate in plane from a axis to b axis (magnetic phase Γ1) and at T_{sr2}=35 K where the strongest component of magnetic moments occurs along the c axis (magnetic phase Γ2). Ho orders at a temperatures below T_{NR}=4 K [8].

With applied magnetic field, a strong magnetocaloric effect was found in $HoFeO_3$ at lower temperatures. Three peaks in the entropy-change occur for a field variation of 0-7 T: ΔSM=9 J/Kg K at 53 K, ΔSM=15 J/Kg K at 10 K and ΔSM=18 J/Kg K at 3 K [6]. Apparently the first peak is associated with a spin reorientation in the Fe subsystems solely. The last one should related to the Ho ordering. While the second peak may be related with some processes including both the Ho and Fe magnetic subsystems. However, a recent polarized neutron diffraction study [9] showed an ordered antiferromagnetic moment of about 1.0 μB at the Ho positions with an applied external field of 9 T even above T_{sr1} e.g. at 70 K. Thus, it is important to fully understand the fine interplay between the Fe and Ho magnetic subsystems occurring during the phase transitions in applied external magnetic fields.

Polarized neutron diffraction (PND) is a powerful method to study the magnetic ordering on the microscopic level. It has

been applied in $HoFeO_3$ to determine the magnetic structure of Fe in Γ4 phase (70 K) with 9 T and to evidence Fe and Ho ordering in Γ2 phase (< 25 K) at 0.5 T [9]. Recently new PND setup was implemented at Heinz Maier-Leibnitz Zentrum (MLZ) in Garching Germany [10,11]. Here we report on the one of the first studies performed using this new setup. The goals of the present research are both to investigate the detailed temperature-field evolution of the magnetic reorientation phase transition from Γ4 to Γ1 near 50 K in $HoFeO_3$ and to check the reliability of the new PND option at different wavelength.

II. Experiment

PND experiments were performed on the diffractometer POLI at MLZ [12]. Cryogen-free 2.2 T, compact high-T_c superconducting magnet presented in Ref. [11] was employed. Two series of measurements were made to test also the feasibility of the used setup at different wavelengths: the first using a neutron wavelength of 1.15 Å and the second of 0.71 Å. Qualitatively and quantitatively the same results were obtained from both measurements denoting a reliable control over the neutron polarization even using a very short neutron wavelength on POLI. Large high quality single crystal of $HoFeO_3$ used in the previous neutron investigations [8,9] was taken for this study. The studied crystal was aligned with its [001] axis nearly parallel to the ω diffractometer axis (sample rotation axis) which is also the magnetic field axis and neutron polarization direction. Using a lifting detector, a set of in-plane and out-of-plane (hkl) Bragg reflections, with l = 0, −1 and −2, could be measured. The evolution with temperature and field was measured using a set of 70 pre-selected Bragg peaks, which obtained the strongest flipping ratios at 70 K. Discrete temperatures points between 47 and 57 K separated by 2 K steps and from 57 to 67 K separated by 5 K steps were used. Between each pair of adjacent temperatures, a zero-field cooling cycle was carried out. In such a cycle, the field was first reduced to zero (remanent field ~350 Oe), then the sample was heated to 70 K and finally cooled to the next higher required temperature before measuring the set of reflections at four field values: 0.15, 0.5, 1.0 and 2.2 T respectively.

III. Results

In the distorted perovskite structure of $HoFeO_3$, the reflections to which the Fe sublattices contribute comprise four sets of Bragg reflections designated as following: F: h + k even, l even; A: h + k even, l odd; C: h + k odd, l even and G: h + k odd, l odd [8,13]. In the magnetic scattering, each of these reflection types is characteristic for a different modulation of the moments on the 4 Fe sublattices (Table 1). In an initial analysis the projection M⊥ P of the

TABLE 1 HERE

FIG. 2 HERE

magnetic interaction vector M⊥ on the polarization direction P was calculated from the measured asymmetry A = (I+- I-)/(I++ I-) of each reflection. Here, I± denotes the measured intensity for the two antiparallel spin orientations of the incoming neutron beam in regard to the quantization axis of the field. The analysis results, illustrated in Fig. 2, are divided according to the reflection type. This analysis shows that the asymmetries in the F, C and A reflections have essentially the same behavior: they vary only weakly with temperature and the F and A reflections increase with increasing field. The asymmetries of the C reflections are hardly significant. The largest asymmetries are observed in the G reflections which depend strongly on both temperature and field (Fig.2). A significant asymmetry in the intensity of polarized neutron diffraction from an antiferromagnet with zero propagation vector can only arise if the two 180° domains are unequally populated. In the weak ferromagnetic Γ4 phase of $HoFeO_3$, stable between 56 and 700 K, the weak [001] axis ferromagnetism ensures that the domain with its ferromagnetic moment in the field direction will dominate. The sense of the DMI leading to weak ferromagnetism is given by the sum of the cross products of nearly antiparallel spins on interacting atoms. Therefore, antiferromagnetic components of the magnetic moments are always perpendicular to the ferromagnetic axis.

The asymmetry values for 275 Bragg reflections were measured at 65 K. Using these values, we could refine the precise orientation of the AFM moments of the Fe sublattice in $HoFeO_3$ in the Γ4 phase. Our results are in good agreement with the previously published magnetic structure at 70 K [8]. To follow the magnetic phase transition explicitly, the asymmetries of 70 selected peaks (mostly of G-type) were measured in 2 K steps between 67-47 K, and the resulting magnetic moment components for the Fe atoms calculated (Fig. 3). The experimentally measured asymmetry map for the exemplary G-type reflection (30-1) is shown in Fig. 4. As predominantly G-type reflections were measured, a precise calculation of the Ho magnetic moments was barely possible. Below 53 K in the lowest field (0.15 T), the magnitude of the x-component of the Fe moment decreases abruptly whilst that of the y-component increases. This behavior is consistent with the reorientation transition to the Γ1 structure observed in zero field. Further increasing the applied field lowers the temperature of the transition, until it does not occur within the scanned temperature range for 2.2 T. However, an attempt to fit the intermediate phase as a linear combination of different volume fractions of Γ1 and Γ4 phases did not lead to a converging solution.

Between 66 and 47 K, the magnetic scattering is dominated by the contributions from the ordered Fe moments, which have magnetic structure factors of the form:

$$M = \pm f(k)(m_1 - m_2 + m_3 - m_4) \qquad (1)$$

where $f(k)$ is the Fe magnetic form factor for the corresponding reflection and m_1, m_2, m_3 and m_4 are the magnetic moments of the Fe atoms. The leading + sign applies for h even and the − for h odd. If the Ho ordering is neglected, the x, y, and z components of the Fe magnetic moments, which

FIG. 3 HERE

contribute to each of the F, A, C and G modulations, can be determined from the differences between the asymmetries (A) of equivalent reflections of the corresponding type. The values of the x,y,z components of the G modulation of the Fe moments calculated from the least squares fits to both series of measurements are shown in Figure 3. At the highest temperature and only the x component of the magnetic moment contributes to the asymmetries in the G reflections independent of the applied field value, as it is expected for the Γ4 structure. With decreasing temperature, no significant changes occur until between 55 and 54 K the absolute values of the x components start to fall and the y and z components rise. Below this temperature, the effect of an increasing field becomes important. Increasing the field lowers the temperature at which

FIG. 4 HERE

the changes start to occur and it reduces the overall redistribution between the magnetic moment components. At 53 K a reorientation transition takes place in zero field as the magnetic symmetry changes from Γ4 to Γ1 and the Fe moments with G modulation reorient from x to y. The results suggest that the reorientation transition temperature falls with increasing field and in 2.2 T applied along the z direction, it is reduced to below 47 K and thus, not visible in Fig. 3.

The Γ1 symmetry of the AF1 phase does not allow an intrinsic ferromagnetic component in any direction and so applying a magnetic field should not favor one of the 180° domains over the other. However, the finite asymmetries observed in the data collected for the three lower fields in the temperature range 54-47 K and their relative reproducibility over several temperature cycles suggests, that the applied field still favors one of the 180◦ domains even below the reorientation transition. The persistence of a polarization dependent cross-section may indicate a field induced phase with a lower symmetry. The existence of a z component of the asymmetry in the G reflections suggests that the applied field breaks the magnetic symmetry of the Γ4 and Γ1 phase which do not allow some G-type magnetization parallel to z (Fig. 5). A general, unconstrained model of the magnetic structure of $HoFeO_3$

FIG. 5 HERE

would allow the magnitudes and directions of the moments on each of the 8 magnetic sublattices (Fe and Ho) in the unit cell to be independent of one-another, leading to 24 independent magnetic parameters. Thus, the external magnetic field changes the energy balance of the exchange interactions near the phase transition. It leads to the appearance of a new magnetic phase.

IV. Absolute sign of the DMI

In the Γ4 phase, the magnetic field aligns the WF moment along its direction. This lifts the degeneracy between 180◦ AFM domains since the orientation of the AFM structure to the weak ferromagnetic moment is fixed by the DMI. Conversely, the sign of the DMI can be determined by refining the precise orientations of the AFM moments in the Γ4 phase from PND data. In the general case, the asymmetric DMI D_{ij} for each spin pair s_i, s_j contributes to the energy as:

$$\Delta E = \sum_{i \neq j} D_{ij} \cdot (s_i \times s_j) \quad (2)$$

A general symmetry restrictions for the DMI vector has been developed by Thoma et al. in Ref. [14]. As the DMI is antisymmetric D_{21}=-D_{21}, it is important to precisely define (fix) the bond directions. Here we adopt atom position notation as used in Ref. [9]. By performing a proper averaging over the four Fe sublattices of the Γ4 structure, we could reduce the DMI interaction in HoFeO3 as follows. Starting with Fe1, it is connected to Fe2 within the ab-plane by D_{12}^{Fe} and to Fe4 along the c-axis by D_{14}^{Fe}. D_{12}^{Fe} and D_{14}^{Fe} are not related by symmetry and thus might have different values. D_{34}^{Fe} is connected by a two-fold inversion screw axis with D_{12}^{Fe}, leading to D_{34}^{Fe} =(0, D_{12y}^{Fe} , -D_{12z}^{Fe}). The averaged DMI vector between Fe2 and Fe3 is given by D_{23}^{Fe} =(D_{14x}^{Fe} , - D_{14y}^{Fe} , 0). Thus, equation (2) applied for the magnetic structure Γ4 can be written by two independent parameters D_{12}^{Fe} and D_{14}^{Fe} as:

$$\begin{aligned}\Delta E_{\Gamma 4}^{Fe} &= 4D_{12}^{Fe} \cdot (m^{Fe1} \times m^{Fe2}) + 2D_{14}^{Fe} \cdot (m^{Fe1} \times m^{Fe4}) \\ &+4D_{34}^{Fe} \cdot (m^{Fe3} \times m^{Fe4}) + 2D_{23}^{Fe} \cdot (m^{Fe2} \times m^{Fe3}) \\ &= -8m_x m_z \left(D_{14y}^{Fe-Fe} + 2D_{12y}^{Fe-Fe}\right)\end{aligned}$$

where m is the magnetic moment of Fe1. The refinement results at 65 K show a positive m_x and m_z, and a negligible small m_y. Thus, the sum of the DMI vector components D_{14y}^{Fe} and D_{12y}^{Fe} must be positive as well in order to minimize the DMI energy. These results on the DMI sign complements the findings of our previous work where numerical values for the DMI and exchange interactions were determined by inelastic neutron scattering [15].This previous study revealed DMI magnitudes of D_a^{Fe}=0.12 meV and D_c^{Fe}=0.08 meV for Fe subsystem and an exchange interaction strength of $J_{Fe\text{-}Ho}$= -0.026 meV between the Fe and Ho.

FIG. 6 HERE

V. Concluding remarks

PND at the instrument POLI at MLZ could be successfully applied to study the temperature evolution of the spin reorientation transition in $HoFeO_3$ near 50 K under applied magnetic fields up to 2.2 T along the c-axis. One observed that the transition from the Γ4 to the Γ1 phase, which takes place in zero field at 53 K, gets shifted to lower temperatures by increasing the field and is unreachable above 47 K under applied field of 2.2. T. Moreover it was observed that the spin reorientation from the b axis in the Γ4 phase to the a-axis in the Γ1 phase is not restricted just to the ab plane but accompanied with the occurrence of a significant component along the external field (c direction). This intermediate phase breaking

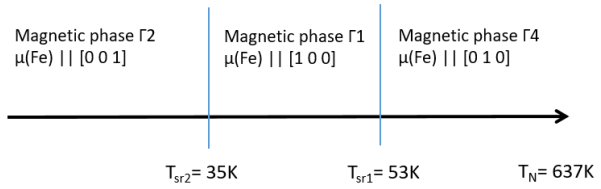

Fig. 1. Scheme of phase transitions in the Fe sublattice in zero magnetic field.

the magnetic symmetry could not be explained as a linear combination of the Γ4 and Γ1 phases and should be considered as a new low-symmetry magnetic phase. Using PND, a mapping of the new phase in the experimentally available temperature/field region could be done. Also using PND, the absolute positive sign of the DMI for the Fe-Fe interaction in the Γ4 phase could be determined. One may conclude that the competition between the external magnetic field, the asymmetric DMI and the isotropic exchange interactions between the Fe and Ho sublattice and inside the Fe sublattice leads to a complex picture of phase transitions in the rare-earth orthoferrites. In $HoFeO_3$, the exchange interactions inside the Fe sublattice and the DMI order the system into the magnetic phase Γ4 at room temperature. With decreasing temperature, the iron polarizes the holmium. It leads to a phase transition into the magnetic phase Γ1. External magnetic fields change this energy balance and break the magnetic symmetry such that a new intermediate phase appears. This complex behavior might cause the useful functionality observed in the rare-earth orthoferrites.

ACKNOWLEDGMENT

This work was supported in part by the Russian Foundation for Basic Research grant # 19-52-12047, and DFG grant #SA 3688/1-1. The work is based on the results obtained on instrument POLI, operated by the RWTH Aachen University in cooperation with FZ Juelich (Juelich-Aachen Research Alliance JARA).

REFERENCES

[1] J.-H. Lee, Y.K. Jeong, J.H. Park, M.-A. Oak, H.M. Jang, J.Y. Son, J.F. Scott, *Phys. Rev. Lett*. 107, 117201, 2011.
[2] P. Mandal, V.S. Bhadram, Y. Sundarayya, C. Narayana, A. Sundaresan, C.N.R. Rao, *Phys. Rev. Lett*. 107, 137202, 2011.
[3] U. Chowdhury, S. Goswami, D. Bhattacharya, J. Ghosh, S. Basu, S. Neogi, *Appl. Phys. Lett*. 105, 052911, 2014.
[4] Ke, Y.-J. et al. *Sci. Rep*. 6, 2016.
[5] K. Dey, A. Indra, S. Mukherjee, S. Majumdar, J. Strempfer, O. Fabelo, E. Mossou, T. Chatterji, and S. Giri. *Phys. Rev. B* 100, 214432, 2019.
[6] M. Shao et al. *Solid State Communications* 152, 947–950, 2012.
[7] M. Das, P. *Mandal AIP Conference Proceedings* 1942, 140007, 2018.
[8] T. Chatterji, M. Meven, P. J. Brown, *AIP ADVANCES* 7, 045106, 2017.
[9] T Chatterji1, A Stunault and P J Brown, *J. Phys.: Condens. Matter* 29, 385802, 2017.
[10] V. Hutanu*, Journal of large-scale research facilities*, vol. 1, p. A16, 2015.
[11] H. Thoma, H. Deng, G. Roth and V. Hutanu, *J. Phys.: Conf. Ser*. vol. 1316, p. 012016, 2019.
[12] H. Thoma, W. Luberstetter, J. Peters and V. Hutanu, *J. Appl. Crystallogr.*, vol. 51, no. 1, p. 17-26, 2018.
[13] Wollan E O and Koehler W C, *Phys. Rev* 100 545, 1959.
[14] H. Thoma, V. Hutanu, H. Deng, V. E. Dmitrienko, P. J. Brown, A. Gukasov, G. Roth, and M. Angst, *Phys. Rev. X*, 2021.
[15] A.K.Ovsianikov, I.A.Zobkalo, W.Schmidt, S.N.Barilo, S.A.Guretskii, V.Hutanu, *JMMM*, Volume 507, 166855, 2020.

TABLE I
Relative signs of the moments on the Fe sublattices contributing to the structure factors of reflections from HoFeO3.

Sublattice	Position			F	A	C	G
1	0	$\frac{1}{2}$	0	+	+	+	+
2	$\frac{1}{2}$	0	0	+	+	-	-
3	$\frac{1}{2}$	0	$\frac{1}{2}$	+	-	-	+
4	0	$\frac{1}{2}$	$\frac{1}{2}$	+	-	+	-

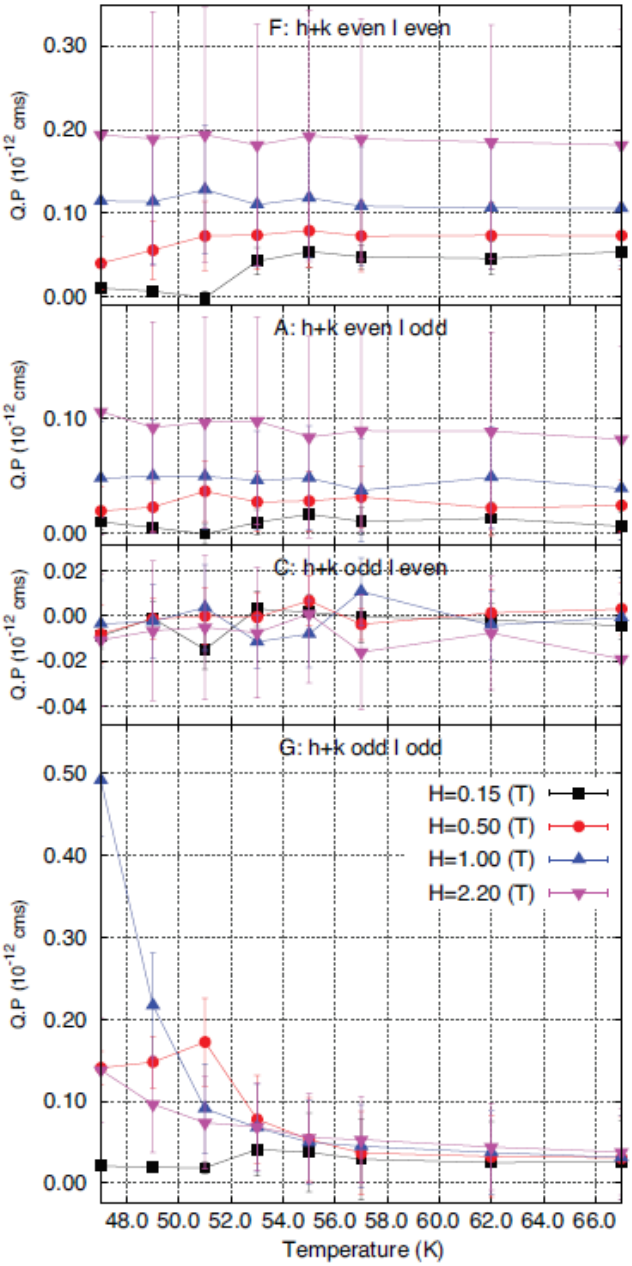

Fig. 2. Mean values of M⊥ P for the F, A, C and G reflections in $HoFeO_3$ measured in magnetizing fields of 0.15, 0.5,1.0 and 2.2 T respectively. The plotted error bars indicate the spread of the measured values in each reflection type.

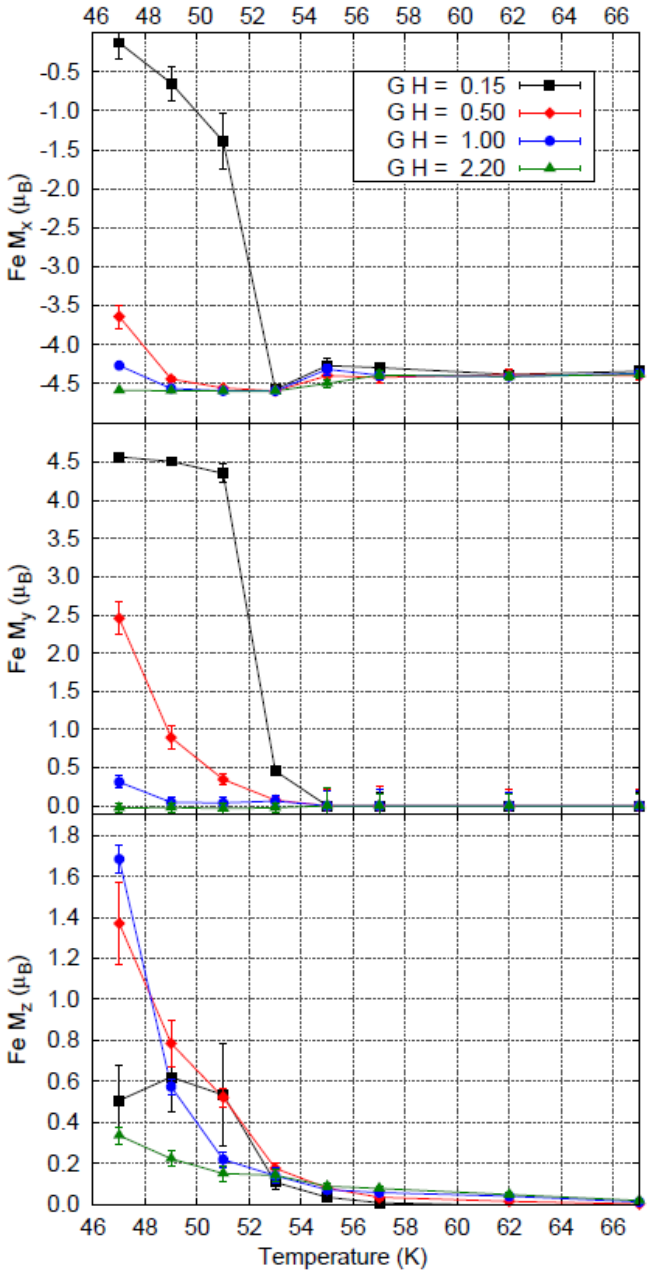

Fig. 3. Components of the G modulation of ordered magnetic moment in HoFeO3 calculated from sums and differences between the asymmetries of equivalent reflections

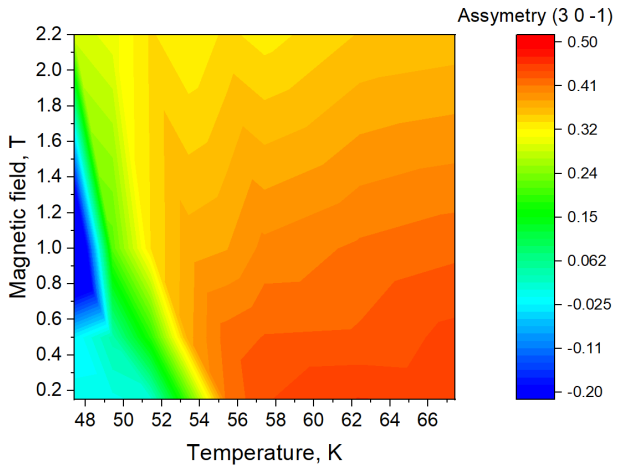

Fig. 4. Temperature/field map for the measured asymmetry of G-type peak (3 0 -1). The reddish area corresponds to the magnetic phase Γ4, blue to Γ1, celestial-greenish to the intermediate monoclinic magnetic phase.

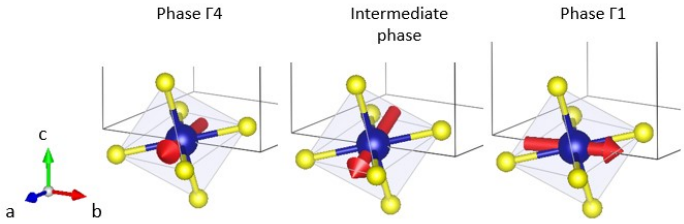

Fig. 5. Fe magnetic moment rotation by the reorientation phase transition in $HoFeO_3$ near 50 K with magnetic field B=0.5T along [001]. An intermediate phase braking orthorombic simmetry occurs between the magnetic phases Γ4 and Γ1. Here: blue balls - Fe ions, yellow - O, red arrows denote ordered magnetic moments.

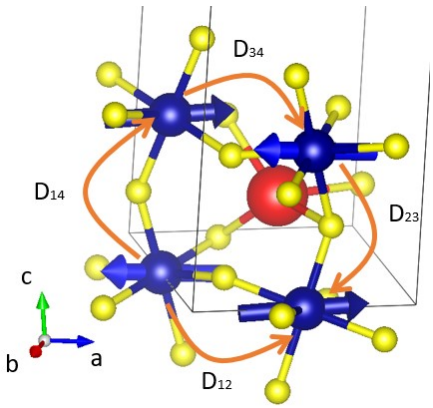

Fig. 6. Scheme of the DMI inside the Fe sublattice. Blue balls - Fe ions, red - Ho, yellow – O. Orange arrows show the paths with the same sing of the D_y^{Fe}.

Magnetic phase diagram of $HoFeO_3$ by neutron diffraction

A. K. Ovsianikov[1,2], O.V. Usmanov[1], I. A. Zobkalo[1], V. Hutanu[2,3], S.N. Barilo[4], N.A. Liubachko[4], K.A.Shaykhutdinov[5,6], K. Yu Terentjev[5], S.V. Semenov[5,6], T. Chatterji[7], M. Meven[2,3], P. J. Brown[7], G. Roth[2], L. Peters[2], H. Deng[3], A. Wu[8].

[1] Petersburg Nuclear Physics Institute by B.P. Konstantinov of NRC «Kurchatov Institute», 188300 Gatchina, Russia.

[2] Institute of Crystallography, RWTH Aachen University, 52066 Aachen, Germany

[3] Jülich Centre for Neutron Science at Heinz Maier- Leibnitz Zentrum, Lichtenbergstrae 1, 85747 Garching, Germany

[4] Scientific-Practical Materials Research Centre NAS of Belarus, 19 P. Brovki str., Minsk, 220072, Belarus;

[5] Kirensky Institute of Physics, Federal Research Center, Krasnoyarsk 660036, Russia

[6]Siberian Federal University, Krasnoyarsk, 660071, Russia

[7] Institut Laue-Langevin, 71 Avenue des Martyrs, CS 20156 - 38042 Grenoble Cedex 9, France

[8]Institute of Ceramic, Chinese Academy of Sciences, Shanghai 200050, China

Abstract

Neutron diffraction studies of $HoFeO_3$ single crystals were performed under external magnetic fields. The interplay between the external magnetic fields, Dzyaloshinsky-Moria antisymmetric exchange, isotropic exchange interactions between Fe and Ho sublattices and within the Fe sublattice provides a rich magnetic phase diagram. As the result of the balance of exchange interactions inside the crystal and external magnetic fields, we found 8 different magnetic phases, induced or suppressed dependent on the external field.

Introduction

Rare-earth orthoferrites $RFeO_3$ have been studied since the 60s of the last century [1 – 3]. These compounds belong to the orthorhombic *Pnma* space group and have high Néel temperatures in the region $T_N = 620 – 740$ K. Below T_N, the iron subsystem orders antiferromagnetically with a weak ferromagnetic component. With temperature decrease, the influence of the *R* ion leads to spin-reorientation (SR) transitions, which take place in the case of magnetic rare-earth ions. There are no such transitions for the non-magnetic ions *R* = Y, La, Lu [4]. The amount and features of SR transitions vary for different magnetic *R* ions, as well as the characteristic temperatures T_{SR}. The temperature of spin-reorientation transitions ranges from $T_{SR} = 37$ K for $DyFeO_3$ [5] to $T_{SR} =$ 480 K for $SmFeO_3$ [6]. For compounds with *R* = Dy, Sm, Tm, Er, Yb, only one SR transition is reported while in $TmFeO_3$ and $ErFeO_3$ an additional intermediate mixed phase [7, 8] is observed. Several SR transitions were detected in crystals with *R* = Ho, Tb [9, 10]. Spontaneous ordering of the rare-earth sublattice takes place below $T_{NR} \sim 10$ K. Thus, the family of rare-earth orthoferrites is very suitable for studying the magnetic interaction in systems containing both 3*d* and 4*f* ions.

The interest in these compounds increased strongly after the prediction and subsequent discovery of their multiferroic properties. Symmetry analysis showed that orthoferrites may have ferroelectric polarization at temperatures below T_{NR} [11]. Indeed, experiments have confirmed the

presence of a dielectric polarization below the magnetic ordering temperature T_{NR} = 5 – 10 K in $DyFeO_3$ and $GdFeO_3$ [5, 12]. However, lately electric polarization in $DyFeO_3$ was observed at higher temperature, around T_{SR} = 50 – 60 K [13]. In $HoFeO_3$ spontaneous electric polarization emerges at ~ 210 K [14]. In other orthoferrites like $SmFeO_3$, $YFeO_3$ and $LuFeO_3$, electric polarization was reported even at room temperature [15 – 17]. This brings these compounds close to being useful for potential applications in switching elements, sensors, memory and other advanced technical devices with low energy consumption [18-20]. The mechanism leading to the emergence of ferroelectric polarization at high temperatures in $RFeO_3$ compounds is not yet understood. The Dzyaloshinskii-Moriya interaction (DMI) [21], which leads to weak ferromagnetism in the Fe3+ sublattice, could be regarded as one of the possible causes of polarization [22]. The distortion of the Fe-oxygen octahedra could play a decisive role here as it leads to a broken local symmetry.

Also, orthoferrites $RFeO_3$ show interesting anisotropic magnetocaloric phenomena. The magnetocaloric effect (MCE) describes the temperature change of magnetic materials in an adiabatic process caused by magnetic entropy change ΔS_M under external magnetic field. In $TmFeO_3$, the entropy change ΔS_M has a maximum of ~ 12 J/kg K at 17 K under applied field of 7 T along the *c* axis; in $TbFeO_3$ ΔS_M reaches a value of ~ 25 J/kg K at ~ 12 K in an applied field of 7 T along the *a* axis [23]. This is, most likely, due to a spin orientation transition of the Fe subsystems. In $HoFeO_3$ the entropy change ΔS_M has some extremums with values equal to 9 J/kg K at temperature T = 53 K, ΔS_M = 15 J/kg K and ΔS_M = 18 J/kg K in the external field of 7 T at temperatures T = 10 K and T = 3 K respectively [24]. The first peak is also associated with a spin orientation transition in the Fe subsystem, while the second and third ones could be associated with some spin orientation transitions in the holmium subsystem. The richness of these observations clearly calls for a study of the (H, T) phase diagram of $HoFeO_3$ in external magnetic fields. This will give a better understanding of the processes inside Ho subsystem, which are presumably related to these entropy jumps ΔS_M. In addition, the external magnetic field will lead to changes of the energy balance and influence the exchange interaction and anisotropy inside the holmium and iron subsystems.

The crystal structure of $HoFeO_3$ is described by the space group #62 IT [25], *Pnma* (or *Pbnm* in another setting). Below T_N = 647 K, the Fe^{3+} the sublattice shows an antiferromagnetic order with the strongest component along the *c*-axis, and a weak ferromagnetic component along the *b* axis [1, 9]. As it was observed recently, the compound has two spin-reorientation transitions at T_{SR1} = 53 K where the moments of the Fe^{3+} ions rotate in plane from the *c* axis to the *a* axis and one at T_{SR2} = 35 K where the strongest component of the magnetic moment is directed along the *b* axis [9]. The Ho^{3+} ordering takes place at a temperature of $T_{NR} \approx$ 10 K [26 – 28].

Experimental

The high quality single crystals of $HoFeO_3$ used for the neutron and magnetic studies have been grown by the flux method [29] and using the optical floating zone technique (FZ-4000, Crystal Systems Corporation) with the natural isotopes. Single crystal with parallelepiped-like shape and dimensions of 5×4×6 mm^3 was used for the neutron studies. The orientation and quality of the crystal obtained was controlled using the Laue technique, a typical X-ray Laue image of the $HoFeO_3$ crystal is presented in Fig. 1. Crystals for the macroscopic, X-Ray and Neutron measurements were taken from the same batch. X-Ray studies were performed at the Rigaku SmartLab diffractometer at the Petersburg Nuclear Physics Institute (PNPI). Measurements of the

magnetic properties were carried out at the Krasnoyarsk Regional Center of Research Equipment of Federal Research Center «Krasnoyarsk Science Center SB RAS» on the vibrating sample magnetometer Quantum Design PPMS – 9T and Lakeshore VSM 8604.

The neutron diffraction experiments were performed at the Heinz Maier- Leibnitz Zentrum (MLZ) on the polarized neutron diffractometer POLI [30, 31]. Instrument POLI is a versatile two axes single crystal diffractometer, which can make measurements with polarized and non-polarized neutrons. For the present studies we used a non-polarized setup with the 8 T dedicated magnet. The sample was mounted in a cryomagnet, fixed on a sample stick with the glue from two sides and mechanically clamped between two aluminum plates to prevent sample rotation in the strong fields at low temperatures. In these measurements, the crystal *b*-axis was oriented vertically, while the *a* and *c* axes were laying in the horizontal scattering plane.

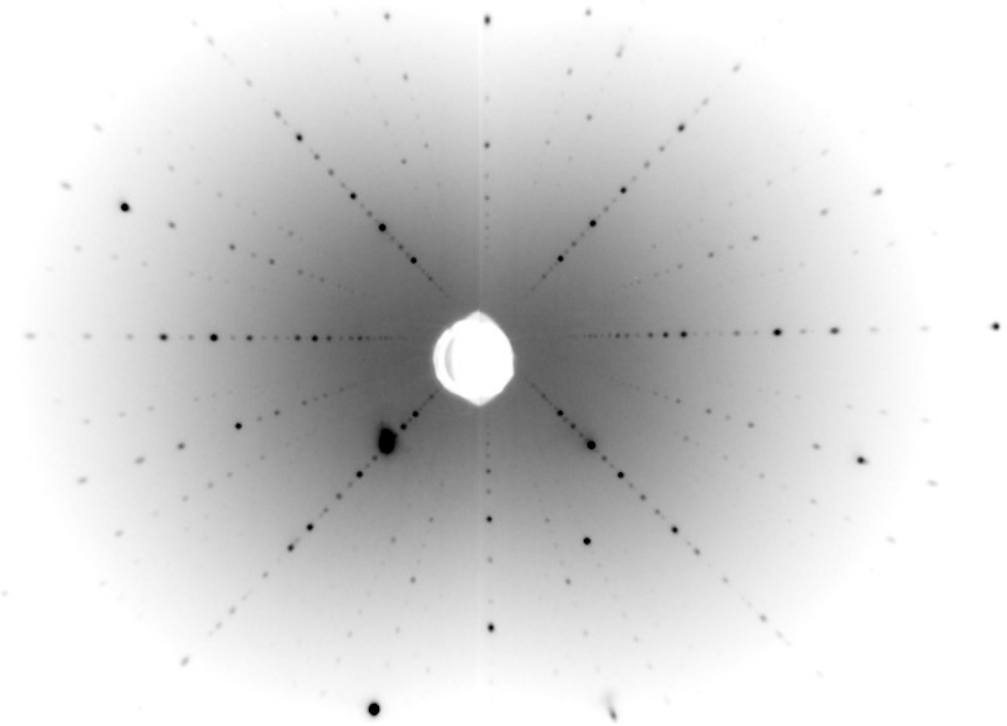

Figure 1. Typical X-ray Laue-photograph of the single crystal $HoFeO_3$ perpendicular to [010] direction, showing the high quality of the crystal.

The magnetic field was applied vertically, along the *b*-axis of the crystal. For the measurements the crystal was cooled down slowly in zero field. The measurements of the temperature dependences of 8 peaks corresponding to four different types of magnetic ordering were performed in the temperature range 2 – 68 K with 2 K steps upon heating for 7 different constant fields: 0.5, 1.25, 2.25, 3.5, 5, 6.5, 8 T. The phase transition shows only small temperature hysteresis.

Crystal structure studies

Powder X-Ray diffraction studies were performed at different temperatures – 300 K, 40 K and 7 K. The refinement of the obtained XRD patterns was performed for space group *Pnma* as well as for its subgroups. For this treatment, the FullProf suite [32] was used. For all temperatures parameters describing the quality of fit (like χ^2, R_f) did not change significantly when the lower symmetry subgroups were considered. Hence, there is no evidence for a change of symmetry of

the crystal structure in this temperature interval. The crystal structure (Fig. 2a) was therefore refined in space group *Pnma* at all temperatures. The most significant changes in the ion positions between 300 K and 7 K (Table 1) were observed for oxygen O_1. Through this anion, the super-exchange interaction along the *b* axis takes place (Fig. 2b). The exchange paths and exchange bond angles at 300 K and 7 K are presented at Table 2. It is noteworthy that both path lengths (d) and bond angles (γ) for the exchange through O_1 change their values to a much greater extent than those for the exchange through O_2, corresponding to an interaction in the *ac* plane. Interestingly, the Fe^{3+} single ion anisotropy constants change their ratio from $Ab < Aac$ at 300 K to $Ab > Aac$ below 35 K [33]. This could be connected with such change of super-exchange bonds.

Table 1. Crystal structure of $HoFeO_3$ at 300 K, 7 K, *Pnma* , X-ray powder data

300 K		a = 5.5908(1)Å, b = 7.6016(2) Å, c = 5.2778(1) Å, χ^2 = 2.37		
		x	y	z
Fe	4(b)	0	0	0.5
Ho	4(c)	0.0680(3)	0.25	0.9790(4)
O_1	4(c)	0.479(2)	0.25	0.077(2)
O_2	8(d)	0.344(2)	0.058(1)	0.696(2)
7 K		a = 5.5825(1) Å, b = 7.5845(1) Å, c = 5.2680(1) Å, χ^2 = 4.31		
		x	y	z
Fe	4(b)	0	0	0.5
Ho	4(c)	0.0693(3)	0.25	0.9790(5)
O_1	4(c)	0.445(2)	0.25	0.097(3)
O_2	8(d)	0.319(2)	0.061(1)	0.697(2)

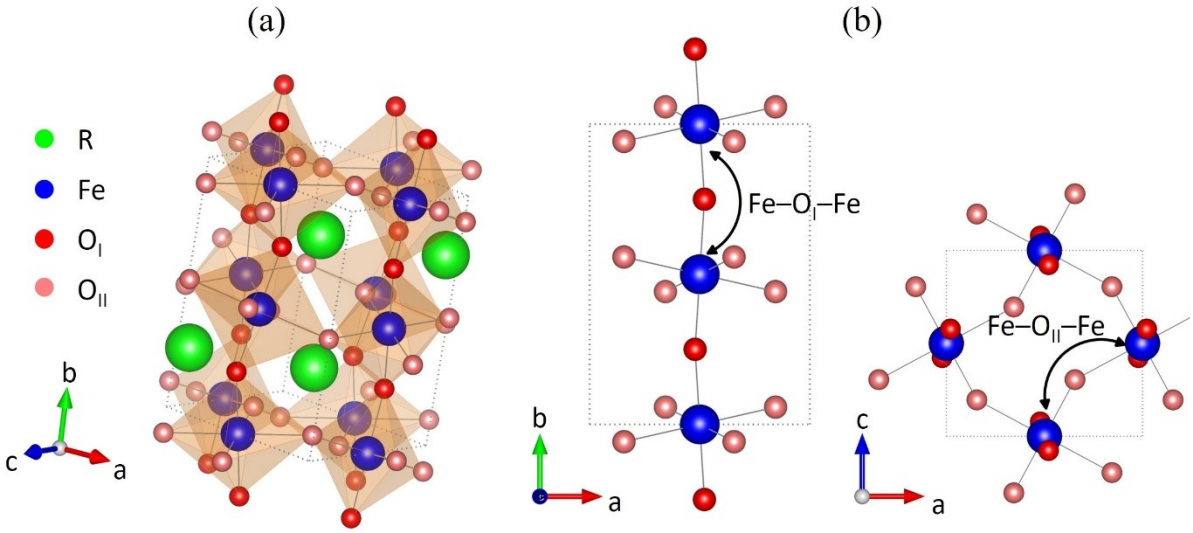

Figure 2. (a) Crystal structure $RFeO_3$; (b) Exchange paths for the nearest neighbors in the Fe sublattice. The configuration Fe–O_I–Fe corresponds to an exchange along the *b* axis, the configuration Fe–O_{II}–Fe – to an exchange in the *ac* plane.

Table 2. Exchange paths parameters at 300 K and 7 K.

	Fe-O_1-Fe		Fe-O_2-Fe	
	d	γ	d	γ
300 K	3.894 (8) Å	154.9° (7)	4.107 (14) Å	138.6°(5)
7 K	3.976 (10) Å	145.1° (9)	4.057 (16) Å	142.2°(6)

Magnetization studies

The temperature dependence of the magnetization, measured in the range 4 – 860 K, is presented in Fig. 3a. These magnetization measurements were performed on a $HoFeO_3$ single crystal at an external magnetic field H = 1 kOe, parallel to the b-axis. The two distinct features correspond to the Néel temperature $T_N \approx 647$ K (in good agreement with previous works [1, 3]) and to the emergence of a spin-reorientation transition in the temperature range 48 – 58 K. In order to find possible magnetic transitions in the temperature range of 2 – 100 K, the dependences of $M(T)$ at different magnetic fields were also measured (Fig. 3b). It can be seen from Fig. 3b, that a feature corresponding to spin-reorientation transition in the range 48 – 58 K is observed only at a field H = 1 kOe whereas at larger fields, these dependencies become monotonous in this temperature range. The only feature of the $M(T)$ dependence noticable for the field H = 30 kOe is the leveling-off at T = 4.2 K.

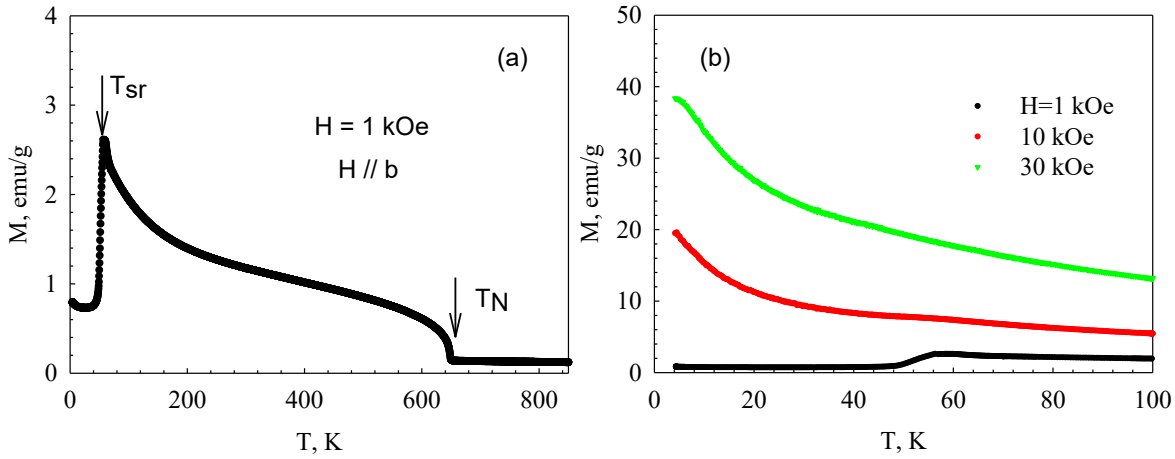

Figure 3. (a) Temperature dependence of the $HoFeO_3$ single crystal magnetization (~1kOe); (b) reduced temperature interval, M (T) for 3 different external magnetic fields.

In order to search for new features in the phase diagram of $HoFeO_3$ in the temperature range of 2 – 100 K we also measured there in detail the isotherms of the field dependences of magnetization.

Fig. 4 shows the results of measurement data of $M(H)$ in fields up to 90 kOe. It can be seen that the high-field part of the $M(H)$ dependence is linear over the entire temperature range below and above the spin-reorientation transition. The kink at small fields corresponds to the reorientation of the iron moments, and in high fields the main contribution to the magnetization comes from holmium.

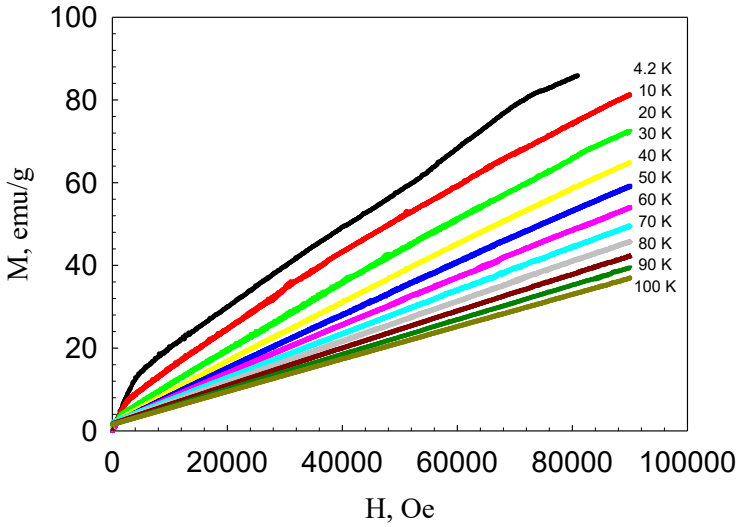

Figure 4. Field dependence of the $HoFeO_3$ single crystal magnetization at different temperatures.

The behavior of the magnetization M(H) in the region of the spin-reorientation transition at low magnetic fields was studied in detail (see Fig. 5), magnetic field H was parallel to b axis of the crystal. It can be seen from the Figure that, at temperatures above the spin-reorientation transition, the $M(H)$ dependences saturate rapidly, since at $T > T_{SR}$ the easy axis of the crystal is b axis. At $T < T_{SR}$, already c is the easy axis, and the magnetization process occurs in a wider range of fields. A small slope above the saturation of the iron moments corresponds to the influence of the paramagnetic holmium.

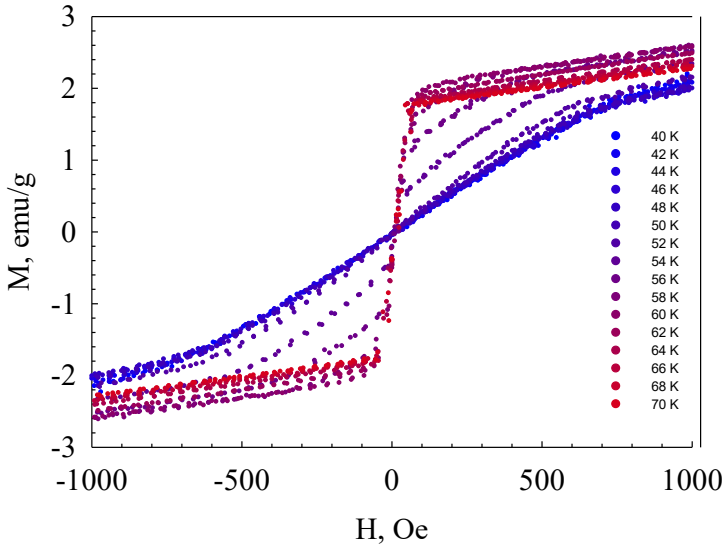

Figure 5. Field dependence of the $HoFeO_3$ single crystal magnetization in the temperature range close to T_{SR}.

At Figure 6 the results of the magnetization measurements along different crystallographic directions at room temperature are presented. The magnetization hysteresis with field along *b* axis connected with weak ferromagnetic component directed along *b* under the environmental condition. While the hysteresis along *c* is due to the weak magnetic component induced by the field. The spontaneous SR transition in $HoFeO_3$, which results in the reorientation of weak magnetic component from *b* to *c* axis, takes place due to the very weak Fe-Ho exchange interaction. Then weak magnetic field will be enough to induce the same reorientation transition and hysteretic behavior similar to that one for field along *b*. The difference in the shape and magnitude of the hysteresis for these two cases reflects anisotropy of the crystal. These results are in good agreement with studies of the magnetization shown in ref. [34].

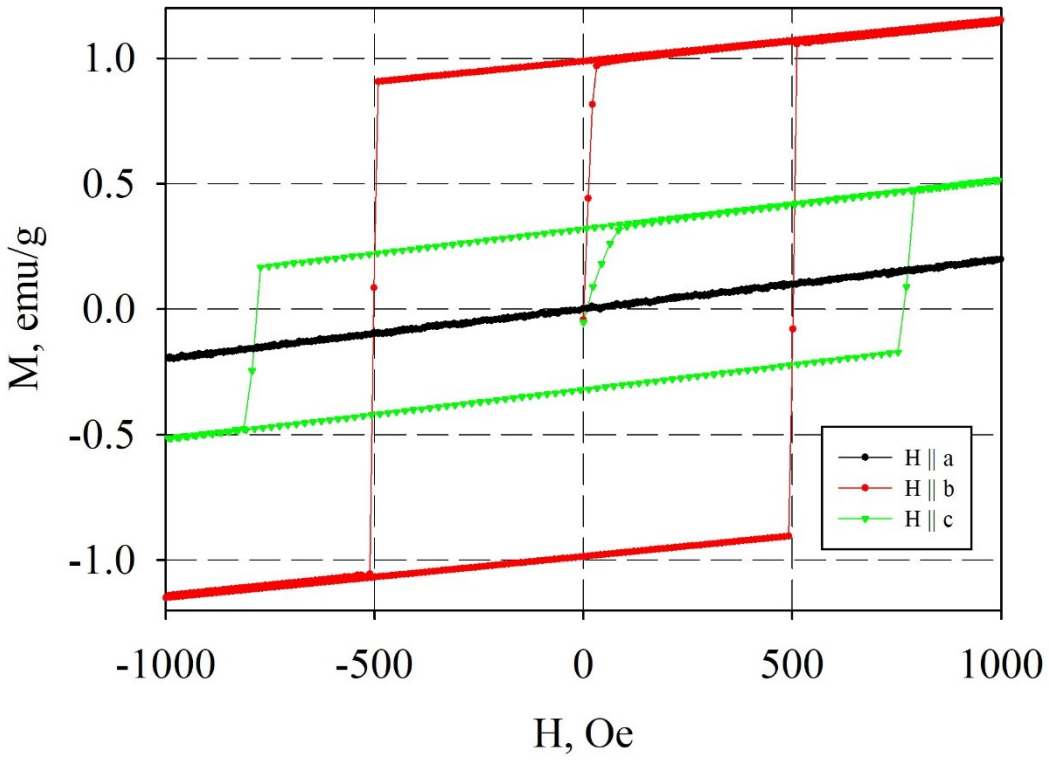

Figure 6. Field dependence of $HoFeO_3$ single crystal magnetization at room temperature.

Magnetic symmetry analysis

For the analysis of the magnetic scattering, the program k-SUBGROUPSMAG [35] from the Bilbao Crystallographic Server (BCS) [36 – 38] was used. The magnetic symmetry of the subgroups of space group *Pnma* with the propagation vector $\boldsymbol{k}$ = 0 0 0 can be described by the combination of eight one-dimensional irreducible representations (IR). Their designation in BCS notation is the following: $\Gamma_1^+, \Gamma_2^+, \Gamma_3^+, \Gamma_4^+, \Gamma_1^-, \Gamma_2^-, \Gamma_3^-, \Gamma_4^-$.

Within the Fe sublattice, the main interaction is the isotropic exchange interaction between the nearest neighbors. As the crystal cell contains four non-equivalent magnetic Fe atoms there are four types of possible collinear ordering of the Fe subsystem, which can be expressed by means of the following Bertaut notation [39]:

$$\mathbf{F} = \mathbf{S}1 + \mathbf{S}2 + \mathbf{S}3 + \mathbf{S}4,$$
$$\mathbf{G} = \mathbf{S}1 - \mathbf{S}2 + \mathbf{S}3 - \mathbf{S}4,$$
$$\mathbf{C} = \mathbf{S}1 + \mathbf{S}2 - \mathbf{S}3 - \mathbf{S}4,$$

$$\mathbf{A} = \mathbf{S}1 - \mathbf{S}2 - \mathbf{S}3 + \mathbf{S}4,$$

where **G** describes the main antiferromagnetic component of the magnetic structure, **F** is the ferromagnetic vector and weak antiferromagnetic components **C** and **A** describe the canting of the magnetic moments. DMI leads to a canting of the sublattices and the appearance of more complex structures, which can be described using the components of collinear types of ordering. For the Fe subsystem, the decomposition of the full magnetic representation Γ^{Fe} has the form:

$$\Gamma^{Fe} = \sum n_{\nu}^{Fe} gm_{\nu} = 3\Gamma_1^+ \oplus 3\Gamma_2^+ \oplus 3\Gamma_3^+ \oplus 3\Gamma_4^+ \quad (1)$$

For the Ho subsystem the full magnetic representation Γ^{Ho} looks like

$$\Gamma^{Ho} = \sum n_{\nu}^{Ho} gm_{\nu} = 1\Gamma_1^+ \oplus 2\Gamma_1^- \oplus 2\Gamma_2^+ \oplus 1\Gamma_2^- \oplus 2\Gamma_3^+ \oplus 1\Gamma_3^- \oplus 1\Gamma_4^+ \oplus 2\Gamma_4^- \quad (2)$$

In the general case the magnetic moment of an atom j in cell L with its coordinates $\boldsymbol{R}$ and propagation vectors $\boldsymbol{k}$ may be written as a Fourier series:

$$\boldsymbol{m}_j = \sum_{\boldsymbol{k}} \boldsymbol{S}_{\boldsymbol{k}j} \cdot e^{-2\pi i \boldsymbol{k}\boldsymbol{R}} \quad (3)$$

The vectors $\boldsymbol{S}_{kj}$ are the Fourier components of the magnetic moment $\boldsymbol{m}_j$. They can be written as a linear combination of basics functions of irreducible representations:

$$\boldsymbol{S}_{kj} = \sum_{a,m} C_{a,m} \boldsymbol{V}_{a,m}(\boldsymbol{k}, \nu|j) \quad (4)$$

where the $C_{a,m}$ are the coefficients of the linear combinations, and the basic vectors $\boldsymbol{V}_{a,m}(\boldsymbol{k}, \nu|j)$ are constant vectors referred to the basis of the direct cell. The index a varies from 1 up to the dimension of the IRs. The index m varies from 1 up to the number corresponding to the number of times the representation Γ_ν is contained in the magnetic reducible representation Γ. By varying these coefficients, one can obtain all classes of magnetic structures corresponding to the symmetry of the propagation vector.

Full magnetic representation includes all irreducible magnetic representations of the subgroups of the parent group #62 for the rare-earth and iron sublattices. Table 3 shows the irreducible representations corresponding to magnetic groups and possible types of magnetic ordering for the sites Fe and Ho. Magnetic groups of lower symmetry within the orthorhombic space group can be described using the direct sum of these representations. For example, the magnetic space group *Pnm2₁* is described by the representation $\Gamma = \Gamma_1^+ \oplus \Gamma_4^-$.

Table 3. The irreducible representations and corresponding magnetic groups in the *Pnma* setting.

	Parent space group *Pnma*		
Irreducible representations	Magnetic group	Site of Fe	Site of Ho
Γ_1^+	*Pnma*	$G_x C_y A_z$	C_y
Γ_2^+	*Pn'm'a*	$C_x G_y F_z$	$C_x \quad F_z$
Γ_3^+	*Pnm'a'*	$F_x A_y C_z$	$F_x \quad C_z$

Γ_4^+	*Pn'ma'*	$A_x F_y G_z$	F_y
Γ_1^-	*Pn'm'a'*		$A_x \quad G_z$
Γ_2^-	*Pnma'*		A_y
Γ_3^-	*Pn'ma*		G_y
Γ_4^-	*Pnm'a*		$G_x \quad A_z$

Magnetic scattering dependence on magnetic field

In the $HoFeO_3$ unit cell, the Fe^{3+} ions occupy the special position 4*b* that provides some special conditions for the contribution of different magnetic modes to Bragg reflections with corresponding Miller index parity. Thus, to reflections with $h + l$ even, k odd, only mode **A** gives a contribution, to reflections with k even, $h + l$ odd, only type **C** contributes, $h + l$ even, k even – only type **F**, $h + l$ odd, k odd, only type **G**. For the studies, two Bragg reflections for each magnetic mode were chosen: (113) and (311) for type **A**, (201) and (102) for type **C**, (002) and (200) for type **F**, (011) and (110) for type **G**. The temperature dependences of their integral intensities were measured in the external magnetic field. For all of these reflections a change in intensity with the temperature was observed. Fig. 7a shows the temperature dependence of (011) reflection intensity for all measured fields. At Fig. 7b the temperature dependences of (201) reflection for fields 0.5 T and 8 T are shown. One can see that the boundaries of the phase transitions shift down in temperature with an increase of external magnetic field. The increase of the (011) intensity at zero magnetic field in the temperature range 35 – 50 K definitely is owing to formation of phase Γ_1, which exists in that temperature range [9]. A dip in the intensity of (011) reflection in the temperature range of 50 – 55 K appears at field of 0.5 T, which is not observed at zero field (Fig. 7a). That means that the field leads to the formation of an intermediate phase during the transition below T_{SR1} = 53 K. The increase of intensity still persists at fields 0 – 1.25 T and disappears with further increase in the magnetic field. No (011) intensity increase was observed below T_{SR1} at the fields ≥ 2.25 T and temperature range 35-50K, where phase Γ_1 exists at zero field. Which means that phase Γ1 is suppressed by the field. The sharp increase in the intensity of the (201) reflection, which indicates an increase of the magnetic moment of holmium, shifts to higher temperature in high fields (Fig. 7b).

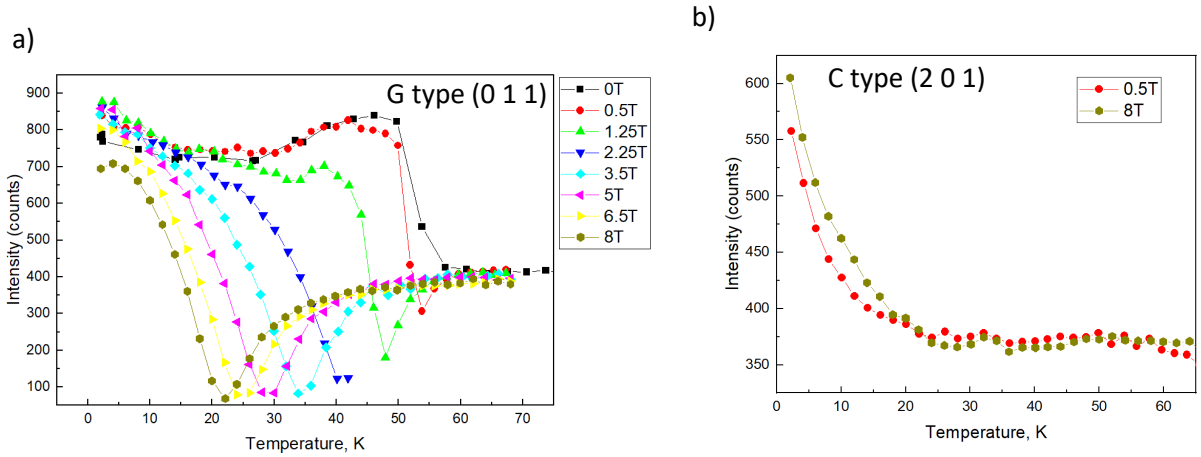

Figure 7. Temperature dependence of the integrated intensities of reflections: a) (011) of type **G** and b) (201) of type **C** in the different magnetic fields.

For magnetic structure refinement, we considered the magnetic representations shown in Table 1 and the results of refinement from reference [9]. In this way we obtained a set of magnetic phases that can be described by different magnetic representations as well as by different directions and magnitudes of the components of the magnetic moments. The resulting phase diagram is shown in Figure 8. The corresponding descriptions of the phases are given in Table 4. The magnetic moment values shown in Table 4 are rough estimates that we got when fitting 8 reflections. To refine the crystal extinction parameters, we measured these 8 peaks in zero field and used the known parameters of the magnetic moments from [9]. For all measurements in an external magnetic field, we fixed the obtained values of extinction and fitted the values of magnetic moments. We consider phases to be different also in the case they are described by the same set of irreducible presentations but with coefficients $C_{a,m}$ having different signs. Obviously, the boundaries between phases are only approximate, owing to comparatively high e.s.d.s of our magnetic structure refinements.

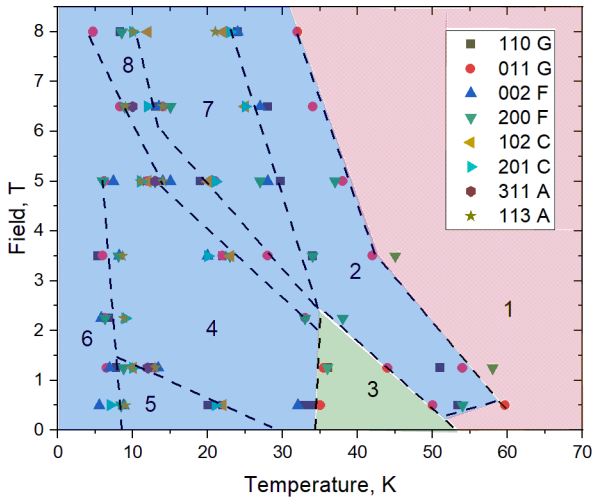

Figure 8. Magnetic phase diagram of $HoFeO_3$. Dotted line – boundary between different magnetic phases . Color area – region that are described by different magnetic representation of the Fe subsystems: red – Γ_4^+, green – Γ_1^+, blue – Γ_2^+. The numbers indicate phases as they are mentioned in the text.

Table 4. Estimates of the magnetic moments components of Fe and Ho in different magnetic phases. Magnetic moment values are given in μ_B.

Magnetic representation:		$\Gamma_4^+ \oplus \Gamma_1^-$	$\Gamma_2^+ \oplus \Gamma_2^-$	$\Gamma_1^+ \oplus \Gamma_1^-$	$\Gamma_2^+ \oplus \Gamma_2^-$	$\Gamma_2^+ \oplus \Gamma_2^-$	$\Gamma_2^+ \oplus \Gamma_3^-$	$\Gamma_2^+ \oplus \Gamma_2^-$	$\Gamma_2^+ \oplus \Gamma_2^-$
Magnetic phase		*Pn'a'2₁*	*P2₁'2₁'2₁*	*P2₁2₁2₁*	*P2₁'2₁'2₁*	*P2₁'2₁'2₁*	*Pn'a2₁'*	*P2₁'2₁'2₁*	*P2₁'2₁'2₁*
Phase number Temperature Field		1 60 K 0.5 T	2 40 K 5 T	3 40 K 0.5 T	4 30 K 0.5 T	5 15 K 0.5 T	6 5 K 0.5 T	7 20 K 6.5 T	8 11 K 6.5 T
Fe	Mx	0	0	4.2(1)	0	0	0	0	0
	My	-0.7(2)	-3.3(4)	0	-4.5(1)	-4.8(3)	-5.2(9)	-3.3(3)	-4.3(8)
	Mz	-4.23(8)	-1.8 (7)	1.2(5)	0.2 (5)	0.2 (5)	0.2 (5)	-2.6(9)	-1.1(6)

Ho	Mx	0	1.7(8)	-0.8(3)	2.2(6)	2.1(2)	5.4(1)	2.6(8)	3.4(2)
	My	0	0	0	0.9(6)	1.4(3)	0	0	0.4(5)
	Mz	0	0	-0.3(2)	1.6(5)	-2.3(3)	3.3(2)	-2.1(1.0)	1.0(6)
R factor		1.12	4.41	1.81	2.18	0.96	1.20	5.40	0.86

The best fit of phase 2 is obtained using representation $\Gamma = \Gamma_4^+$ with non-zero magnetic moment components of the iron subsystem. Nevertheless, previous studies using polarized neutrons [40] show that the *y*-component of the magnetization corresponding to the G-type reflections emerges during the transition from phase 1 to phase 3. Also, it was shown that an external magnetic field with B = 9 T at the temperature T = 70 K induces a magnetic moment around 1 μB on Ho^{3+} [41]. Therefore, the magnetic space group $P2_1'2_1'2_1$ was used to describe the magnetic structure in magnetic fields. This phase is described by the representation $\Gamma = \Gamma_2^+ \oplus \Gamma_2^-$ which resolves the existence of the *y* component for G-type reflections and magnetic moments on the Ho^{3+} ions. The groups $Pn'a'2_1$ and $Pn'a2_1'$ are non-centrosymmetric and polar groups. The groups $P2_1'2_1'2_1$ and $P2_12_12_1$ are non-centrosymmetric and non-polar groups. Table 4 clearly shows that at temperatures above T_{SR1} = 53 K (where only the iron subsystem is ordered) and at temperatures below T_{NR} = 10 K (where the holmium has its own moment alignment) the system is in a higher symmetrical phase. Temperature range $T_{NR} < T < T_{SR1}$ is supposedly characterized by the interactions between the Fe- and Ho-subsystems and within the Ho subsystem. Along with that, the external field shifts down the temperature of the magnetic phase transitions. In addition, as can be seen from the phase diagram, an increase of the external field leads to transitions from the low-symmetry phase (№ 2 or № 3) to a highly symmetric phase (№ 1). The same situation was observed in $DyFeO_3$ where an external field leads to a transition from phase $P2_12_12_1$ to $Pn'a'2_1$ at temperatures around T_{NR} [5]. However, in the case of $HoFeO_3$ this transition goes through an intermediate phase $P2_1'2_1'2_1$.

Phase transitions in weak magnetic fields

With an external magnetic field, the full magnetic Hamiltonian of $HoFeO_3$ will have the form:

$$H = H^{Fe-Fe} + H^{Fe-Ho} + H^{Ho-Ho} + H_{ext} \qquad (5)$$

The complex interplay, balance and competition of these interactions provide the observed sequence of phase transitions. In phase 1 (configuration Γ4), the interactions within the Ho subsystem and between the Ho and Fe subsystems can be neglected. In the absence of an external field, the Ho^{3+} ions are in the exchange field of the Fe^{3+} ordered subsystem, which induces an ordered magnetic moment on the holmium ions. At a temperature around T_{SR1} = 53 K, the exchange interactions and easy-plane anisotropy in the *ac* plane play a main role within the iron subsystem [33]. The strongest super-exchange interaction is along the iron chains: J_b = 4.9 meV, the interaction in the *ac* plane is slightly weaker: J_{ac} = 4.76 meV [33]. However, the easy-plane anisotropy stabilizes the system and the moments on the iron sublattice lie in the *ac* plane with a small canting due to DMI. At T_{SR1}, the exchange interaction Fe-Ho increases to a level sufficient to rotate the Fe moment in the *ac* plane which yields the Γ1 structure – phase 3 in our notation.

It can be seen that already in a weak magnetic field above 0.5 T along the *b* axis, $HoFeO_3$ has an additional intermediate phase and transitions are shifted to lower temperature. It seems

likely that the external field induces an additional ordered magnetic moment on the Ho^{3+} ions which in turn produces an additional contribution to exchange interaction J_{ij}^{Fe-Ho} between the Fe and Ho subsystems. The increase of the Fe-Ho exchange interaction produced by a field of 0.5 T provides the transition from phase 1 to phase 2. This is clearly visible in the temperature dependence of reflection (011) as a drop of its intensity, which takes place due to rotation of the Fe magnetic moment in the direction along the *b* axis. A magnetic field higher than 0.5 T influences the iron sublattice much stronger, leading to the essential changes in the alignment of the Fe moments. In this case, the iron subsystem produces a field opposite to the external one. Therefore, the temperature of transition from phase 1 to phase 2 decreases with the increase of the field. The behavior of the Ho magnetic moments reflects the competition between the external magnetic field and internal field from the Fe-sublattice. At low external field, the main influence on the Ho sublattice is exerted by the field from Fe-sublattice; thus interaction J_{ij}^{Fe-Ho} rotates the iron magnetic moments from phase 1 to phase 3 through the *b* direction (see Fig. 9).

Since holmium has a highly anisotropic g-factor (g_x = 6.7, g_y = 1.6, g_z = 3.5) [42], at fields higher than B = 2.5 T, the external field holds the Ho moments along *x* direction mainly and the anisotropic interaction J_{ij}^{Fe-Ho} holds the iron magnetic moment close to the *b* axis. Thus phase 3 is suppressed by the field.

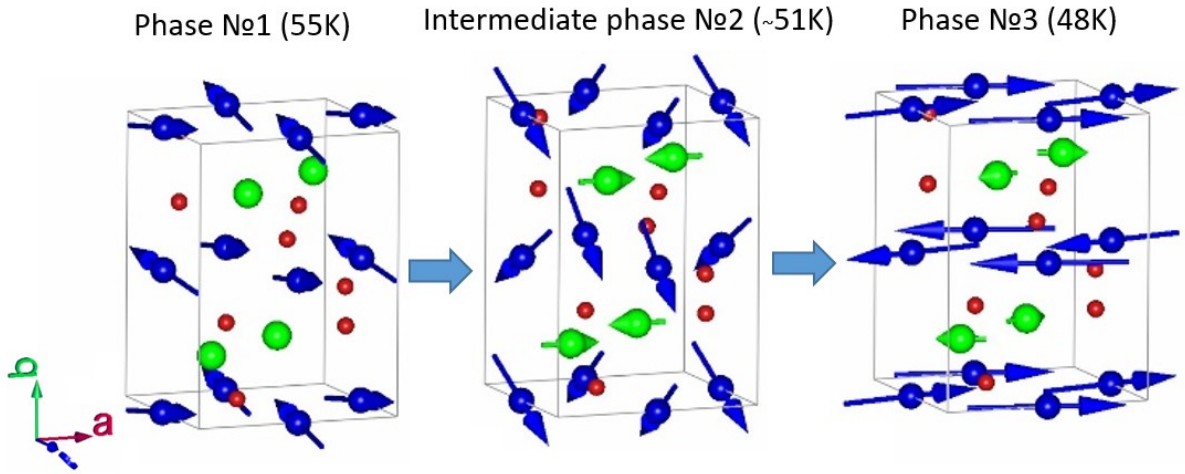

Figure 9. Scheme of magnetic structure evolution by the reorientation phase transition in $HoFeO_3$ near 50 K with magnetic field 0.5 T along [010]. Blue arrows - Fe^{3+} ions, green – Ho^{3+}, orange spheres – O^{2+}.

Low temperature phase transitions

At the temperature T_{SR2} = 35 K the increase of the induced magnetic moment of the Ho subsystem provides a subsequent increase of the exchange interaction J_{mn}^{Ho} which leads to a new redistribution of the energy balance. This gives a new phase - phase 4, where the Fe^{3+} moments turn closer towards the *b* direction and the system described by magnetic representation $\Gamma = \Gamma_2^+ \oplus \Gamma_2^-$ as well as for phase 2, but with a more distinct contribution from the Ho subsystem. Below T_{SR2} the exchange interactions Ho-Ho and Ho-Fe become progressively more important:

$$H^{Fe-Ho} + H^{Ho-Ho} = \sum_{ij} S_i^{Fe} \cdot J_{ij}^{Fe-Ho} \cdot s_j^{Ho} - \sum_{mn} s_m^{Ho} \cdot J_{mn}^{Ho} \cdot s_n^{Ho} \quad (6)$$
$$+ \sum_{ij} D_{ij}^{Fe-Ho} \cdot (S_i^{Fe} \times s_j^{Ho}) - \sum_{mn} D_{mn}^{Ho-Ho} \cdot (s_m^{Ho} \times s_n^{Ho}) \sum_i s_i^{Ho} \cdot \boldsymbol{Hext}$$

where J_{ij} is the isotropic exchange, $\boldsymbol{D}_{ij}^{N-M}$ the Dzyaloshinsky vectors which could consist of antisymmetric exchange and single ion anisotropy, $\boldsymbol{S}_i^{Fe}$ the effective spin operator of Fe, and $\boldsymbol{s}^{Ho}$ the Ho spin moment operator:

$$\boldsymbol{s}^{Ho} = (g_j - 1)\boldsymbol{J} \tag{7}$$

where g_j is the Lande factor, $\boldsymbol{J}$ the total angular moment.

It has been established that the exchange interactions Ho-Ho and Ho-Fe have different signs [33, 43]. An increase of the ordered magnetic moment on holmium ions leads to an increase of the contribution to the energy from the exchange Ho-Ho. Most likely, the similarity of Ho-Ho and Ho-Fe interactions is, probably, the reason of the transition at T = 24 K (in this work, and T = 20 K in [9]) to phase 5, where the direction of the ferromagnetic component of Ho changes its sign (see Fig. 10a).

A magnetic field above 1 T destroys this balance, and suppresses this phase also (Fig. 10b). At temperature T_{NR} = 10 K Ho^{3+} spontaneous magnetic ordering takes place. It leads to a new rebalancing of the energy: the exchange interaction within the rare-earth subsystem is already strong enough to hold its magnetic moment mainly along the Ho^{3+} easy axis x and not to follow the influence of iron sublattice and external field. Therefore, below T_{NR} = 10 K, the Ho^{3+} moment along the hard axis $m_y \approx 0$, and the ferromagnetic component m_z of Ho^{3+} changes sign again (phase 6, Fig. 10a).

As it can be seen, fields above 2 T has a significant influence on the Ho-sublattice. At a field of B = 2.5 T, the energy of the external magnetic field is higher than the energy of Fe-Ho interaction. In this way, at temperatures above 35 K, phase 3 disappears. Simultaneously, external fields higher than 2 T are strong enough to induce y component of the magnetic moment on the Ho^{3+} ions. In this way a new phase 7 with strong canting of the Fe moments on that sublattice is formed,

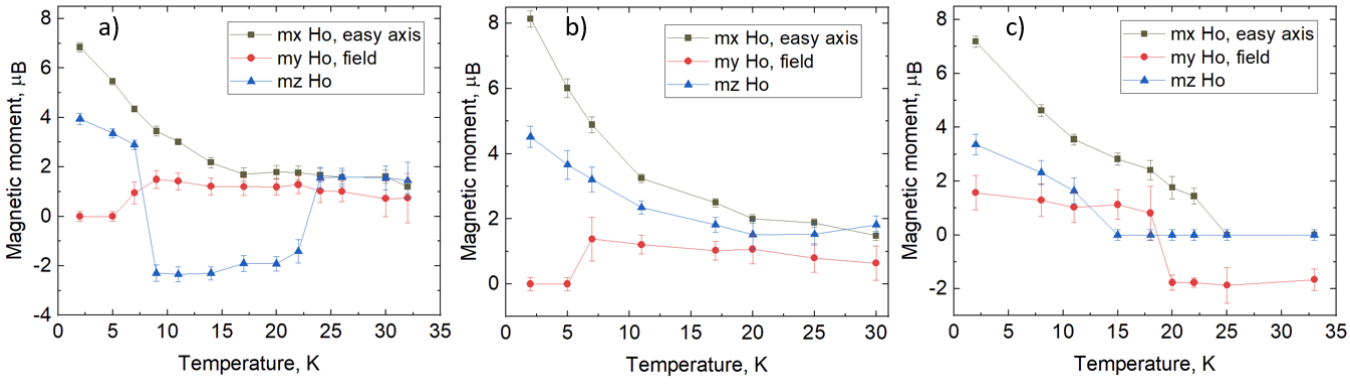

Figure 10. Temperature dependence of the x, y and z components of the Ho magnetic moments in fields of a) 0.5 T, b) 1.25 T and c) 5 T.

Phase 8 is an intermediate phase, where the Fe moments have a large component along the b with a significant ferromagnetic component along c. A fields above 4 T lead to a canting of the Ho moments and gives a non-zero y-component of the Ho magnetic moment (Fig. 10c). The

magnetic structures corresponding to the different magnetic phases at 20 K are shown in Figure 11.

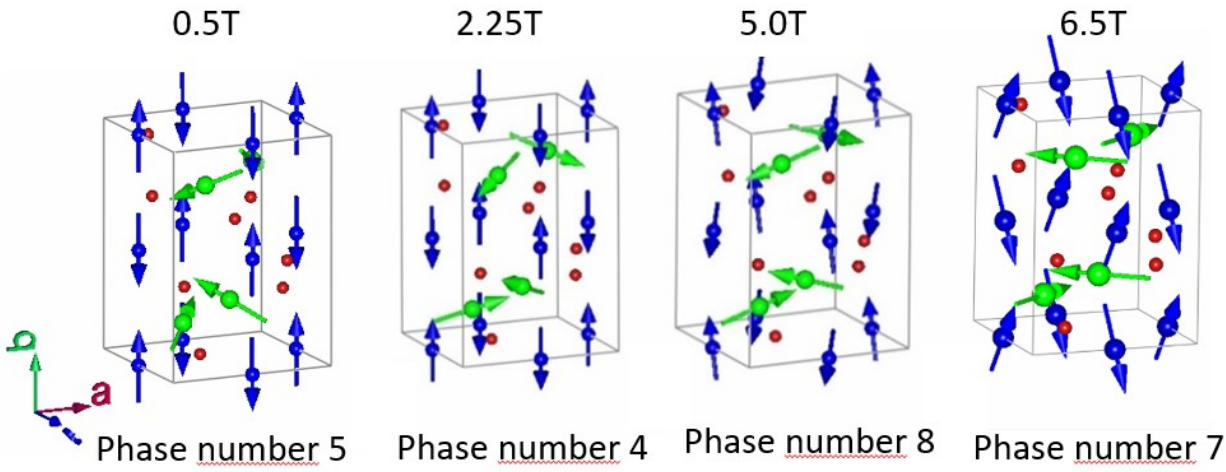

Figure 11. Schematic representation of the magnetic structures of HoFeO3 at temperature T = 20 K with increasing magnetic field (B ∥ b). Blue arrows - Fe^{3+} ions, green – Ho^{3+}, orange spheres – O^{2+}.

Conclusion

Our studies demonstrate that $HoFeO_3$ has a rich phase diagram in an external magnetic field. The approach to the phase definition, adopted in this work is different from the conventional one, when magnetic phases described by the same set of irreducible representation considered to be the same, notwithstanding of coefficients signs. Phases defined by our approach bear different magnetic and, possibly, other different physical properties which led us to consider them to be different. The competition between the external magnetic field, the antisymmetric DMI and isotropic exchange interactions between the Fe and Ho sublattice and within the Fe sublattice leads to a complex picture of phase transitions in the rare-earth orthoferrite $HoFeO_3$. According to our considerations we can outline 8 different magnetic phases, induced or suppressed by the magnetic field. The richness of this phase diagram is the result of a very delicate balance of exchange interactions in the crystal and the external magnetic field. Such complex behavior may cause the useful functionality of rare-earth orthoferrites. The obtained results are in good agreement with the results from inelastic neutron scattering experiments [33], from which the values of exchange interactions were calculated and also with measurements of the magnetic entropy change where peaks of ΔS_M lie near the spin reorientation transition between phases 1 or 2 and 3; phases 4, 5 and 6 [24].

Acknowledgments

This work was supported by the Russian Foundation for Basic Research grant # 19-52-12047, and DFG grant # SA 3688/1-1. Neutron Experiments were performed at the instrument POLI jointly operated by RWTH Aachen University and Forschungszentrum Jülich at MLZ within JARA-FIT collaboration.

References

[1] W.C. Koehler, E.O. Wollan, M.K. Wilkinson, Phys. Rev. 118 (1960) 58.
[2] M. Marezio, J.P. Remeika, P.D. Dernier, Acta Cryst. B 26 (1970) 2008.
[3] R. White, J. Appl. Phys. 40 (1969) 1061.
[4] K. Park, H. Sim, J. C Leiner, Y. Yoshida, J. Jeong, S. Yano, J. Gardner, P. Bourges, M. Klicpera, V. Sechovský, M. Boehm and J. Park, J. Phys.: Condens. Matter 30 (2018) 235802.
[5] Y. Tokunaga, S. Iguchi, T. Arima, and Y. Tokura, Phys. Rev. Lett. 101 (2008) 097205.
[6] S. Chaturvedi, P. Shyam, A. Apte, J. Kumar, A. Bhattacharyya, A. M. Awasthi, and S. Kulkarni, Phys. Rev. B 93, (2016) 174117.
[7] A. Bombik, B. Leśniewska, A.W Pacyna, J. Magn. Magn. Mater. 214 (2000) 243.
[8] L. T. Tsymbal, et al., Low Temp. Phys. 31 (2005) 277.
[9] T. Chatterji, M. Meven, P.J. Brown, AIP Adv. 7 (2017) 045106.
[10] S. Artyukhin, M. Mostovoy, N. Jensen, et al., Nat. Mater. 11 (2012) 694.
[11] A.K. Zvezdin, A.A. Mukhin, JETP Lett. 88 (2008) 505.
[12] Y. Tokunaga, et al., Nat. Mat. 8 (2009) 558.
[13] B. Rajeswaran et al., Europhys. Lett. 101 (2013) 17001.
[14] K. Dey, A. Indra, S. Mukherjee, S. Majumdar, J. Strempfer, O. Fabelo, E. Mossou, T. Chatterji, and S. Giri, Phys. Rev. B 100 (2019) 214432.
[15] J.-H. Lee, Y.K. Jeong, J.H. Park, M.-A. Oak, H.M. Jang, J.Y. Son, J.F. Scott, Phys. Rev. Lett. 107 (2011) 117201.
[16] P. Mandal, V.S. Bhadram, Y. Sundarayya, C. Narayana, A. Sundaresan, C.N.R. Rao, Phys. Rev. Lett. 107 (2011) 137202.
[17] U. Chowdhury, S. Goswami, D. Bhattacharya, J. Ghosh, S. Basu, S. Neogi, Appl. Phys. Lett. 105 (2014) 052911.
[18] Zvezdin, A. K. & Kotov, V. A. Modern Magnetooptics and Magnetooptical Materials (IOP, Bristol, 1997).
[19] A. Kimel, A. Kirilyuk, P. Usachev, et al., Nature 435 (2005) 655.
[20] X. X. Zeng, R. Wang, X. Q. Xi, B. Li, and J. Zhou, Opt. Express 26 (2018) 17056.
[18] I. E. Dzyaloshinsky, J. Phys. Chem. Solids 4 (1958) 241.
[21] T. Moriya, Phys. Rev. 120 (1960) 91.
[22] A. Moskvin, Condensed Matter 4 (2019) 84.
[23] YJ. Ke, XQ. Zhang, Y. Ma, et al., Sci. Rep. 6 (2016) 19775.
[24] M. Shao et al., Solid State Comm.152 (2012) 947.
[25] International Tables for Crystallography (2006). Vol. A, Space group 62, pp. 298–299.
[26] A. Bhattacharjee, K. Saito, M. Sorai, J. Phys. Chem. Solids 63 (2002) 569.
[27] M. Shao, S. Cao, Y. Wang, S. Yuan, B. Kang, J. Zhang, A. Wu, J. Xu, J. Cryst. Growth 318 (2011) 947.
[28] O. Nikolov, I. Hall, K.W. Godfrey, J. Phys. Condens. Matter 7 (1995) 4949.
[29] S.N. Barilo, A.P. Ges, S.A. Guretskii, D.I. Zhigunov, A.A. Ignatenko, A.N. Igumentsev, I.D. Lomako, A.M. Luginets, J. Crystal Growth 108 (1991) 314.
[30] V. Huţanu, M. Meven, E. Lelièvre-Berna, G. Heger, Physica B 404 (2009) 2633.
[31] V. Hutanu, Journal of large-scale research facilities 1 (2015) A16.
[32] J. Rodriguez-Carvajal, Physica B 192 (1993) 55.
[33] A.K. Ovsyanikov, I.A .Zobkalo, W. Schmidt, S.N. Barilo, S.A. Guretskii, V. Hutanu, , J. Magn. Magn. Mater. 507 (2020) 1.
[34] K.K. Bamzai & Monita Bhat, Integrated Ferroelectrics 158 (2014) 108.
[35] J.M. Perez-Mato, S.V. Gallego, E.S. Tasci, L. Elcoro, G. de la Flor, and M.I. Aroyo, Annu.

Rev. Mater. Res. (2015), 45:13.1-13.32.
[36] M. I. Aroyo, J. M. Perez-Mato, D. Orobengoa, E. Tasci, G. de la Flor, A. Kirov, Bulg. Chem. Commun. 43 (2011) 183.
[37] M. I. Aroyo, J. M. Perez-Mato, C. Capillas, E. Kroumova, S. Ivantchev, G. Madariaga, A. Kirov & H. Wondratschek , Z. Krist. 221 (2006) 15.
[38] M. I. Aroyo, A. Kirov, C. Capillas, J. M. Perez-Mato & H. Wondratschek, Acta Cryst. A62, (2006) 115.
[39] E. F. Bertaut, Magnetism (Academic, New York, 1963).
[40] A. Ovsianikov et al., IEEE Transactions on Magnetics, 58(2) (2022) 1.
[41] T. Chatterji et al., 2017 J. Phys.: Condens. Matter 29 (2017) 385802.
[42] Schuchert, H., Hüfner, S. & Faulhaber, Z. Physik 220 (1969) 280.
[43] John C. Walling and Robert L. White Phys. Rev. B 10 (1974) 4737.

Journal of Magnetism and Magnetic Materials 563 (2022) 170025

Contents lists available at ScienceDirect

Journal of Magnetism and Magnetic Materials

journal homepage: www.elsevier.com/locate/jmmm

Inelastic neutron studies and diffraction in magnetic fields of $TbFeO_3$ and $YbFeO_3$

A.K. Ovsianikov [a,b,*], O.V. Usmanov [b], I.A. Zobkalo [b], W. Schmidt [c], A. Maity [d], V. Hutanu [a,e], E. Ressouche [f], K.A. Shaykhutdinov [g,h], K. Yu Terentjev [g], S.V. Semenov [g,h], M. Meven [a,e], G. Roth [a], L. Peters [a]

[a] Institute of Crystallography, RWTH Aachen University, Jägerstraße 17 – 19, 52066 Aachen, Germany
[b] Petersburg Nuclear Physics Institute by B.P. Konstantinov of NRC «Kurchatov Institute», Orlova roshcha 1, 188300 Gatchina, Russia
[c] Forschungszentrum Jülich GmbH, Jülich Centre for Neutron Science at Institut Laue-Langevin, 71 Avenue des Martyrs, CS 20156 - 38042 Grenoble Cedex 9, France
[d] Heinz Maier-Leibnitz Zentrum, Technical University of Munich, 85747 Garching, Germany
[e] Forschungszentrum Jülich GmbH, Jülich Centre for Neutron Science at Heinz Maier- Leibnitz Zentrum, Lichtenbergstraße 1, 85747 Garching, Germany
[f] Université Grenoble Alpes, Grenoble INP, Commissariat à l'énergie atomique et aux énergies alternatives, Interdisciplinary Research Institute of Grenoble -Modeling and Exploration of Materials Laboratory, 38000 Grenoble, France
[g] Kirensky Institute of Physics, Federal Research Center, Krasnoyarsk 660036, Russia
[h] Siberian Federal University, Krasnoyarsk 660071, Russia

ARTICLE INFO

Keywords:
Neutron diffraction
Orthoferrites
Crystal structure
Exchange interaction

ABSTRACT

Investigations of the orthoferrites $TbFeO_3$ and $YbFeO_3$ were performed by neutron inelastic scattering and neutron single crystal diffraction in magnetic fields. The low temperature evolution of energy gaps was explored for both compounds and considered from the point of view of changes of rare earth ion anisotropy. Exchange parameters between nearest neighbors for Fe^{3+} in $TbFeO_3$ were obtained. The magnetic phase diagram for $YbFeO_3$ was obtained and discussed as a result of the energy balance between Heisenberg exchange interactions, Dzyaloshinsky-Moriya interaction, anisotropy and external magnetic field.

1. Introduction

The rare earth orthoferrite family $RFeO_3$, where R is a rare earth element, demonstrates a remarkable variety of magnetic properties. Its compounds crystallize in an orthorhombic perovskite structure with the space group *Pnma*. At the Neel temperature which is typically in the range $T_N = 600 \div 700$ K, the iron magnetic moments form a canted antiferromagnetic phase [1,2], where the Dzyaloshinsky-Moriya interaction (DMI) is responsible for the canting of the Fe-sublattice. With temperature decrease, increasing exchange interaction between Fe^{3+} and R^{3+} ions leads to a rebalance of energies of the magnetic interactions, which causes spin reorientation transitions [3–5]. Different combinations of DMI and rare-earth ions with different ionic radii and filling of outer shells lead to a variety of magnetic effects. Rare earth orthoferrites are nowadays well known as multiferroics - materials with large magnetoelectric (ME) coupling. This phenomenon allows the control of spontaneous polarization by a magnetic field and spontaneous magnetization by an electric field. Electric polarization was experimentally observed in $DyFeO_3$ and $GdFeO_3$ below the magnetic ordering temperature of R moments $T_{N,R} = 5 – 10$ K [6,7]. For $HoFeO_3$ the characteristic temperature of polarization was reported to be ~210 K [8]. Futhermore, in $SmFeO_3$, $YFeO_3$ and $LuFeO_3$ ferroelectric polarization was observed at room temperature [9–11]. In addition, these compounds show the magnetocaloric effect (MCE), which is described as a temperature change of magnetic materials in an adiabatic process caused by magnetic entropy change ΔS_M under external magnetic field. This effect appears in the vicinity of the phase transitions. $GdFeO_3$ demonstrates the record value of MCE in the rare earth orthoferrites family: $\Delta S_M = -52.5$ J/kg K at a field change of 0 – 9 T [12]. $TbFeO_3$ also has a large $\Delta S_M = -20$ J/kg K for the field directions along *a* and *c*, and $\Delta S_M = -3$ J/kg K for the field direction along *b* [13]. This means that $TbFeO_3$ has a strong magnetocaloric anisotropy. Such a huge variety of different magnetic properties make these compounds promising candidates for industrial applications.

Space group *Pnma* describes the crystal structure of $TbFeO_3$, where Tb and Fe take the positions 4c and 4b respectively. At $T_N = 650$ K the Fe

* Corresponding author.
E-mail address: Aleksandr.Ovsianikov@frm2.tum.de (A.K. Ovsianikov).

https://doi.org/10.1016/j.jmmm.2022.170025
Received 8 July 2022; Received in revised form 6 September 2022; Accepted 28 September 2022
Available online 5 October 2022

spins order antiferromagnetically along the *c* direction with a small canting along the *b* direction. This high temperature phase (HT) is described by the magnetic representation Γ_4^+ [14] in the notation of Bilbao Crystallographic Server (see Table 1) [15–19]. At lower temperatures, the Fe sublattice polarizes Tb sublattice and induces magnetic moment on Tb^{3+} ions. This Fe-R interaction produces a spin-reorientation transition at $T_{SR1} = 8.5$ K; below this temperature the iron magnetic moment rotates towards the *b* direction. In the temperature range $T = 3$–6 K a low-temperature (LT) magnetic phase with configuration Γ_2^+ emerges [20]. At $T_N^{Tb} \sim 3$ K, the Tb subsystem goes to its own spontaneous alignment [13]. This leads to a second spin-reorientation transition below $T_{SR2} = 3$ K, providing a second low-temperature magnetic phase (LT), where magnetic moments of iron return to a phase represented by Γ_4^+ while the Tb-sublattice is described by the representation Γ_4^- [15]. This situation is very close to the scheme of phase transitions in $YbFeO_3$ where the Fe-sublattice at $T \sim 8$ K has the same sequence of transitions between the phases HT and LT with corresponding representations of Fe-subsystems Γ_4^+ and Γ_2^+ through a mixed phase (MP) $\Gamma_4^+ \oplus \Gamma_2^+$. [21]. However, Yb^{3+} ions order below $T \sim 1$ K [22] and the reverse transition to Γ_4^+ in this compound was not reported so far. Thus, $TbFeO_3$ and $YbFeO_3$ constitute a suitable showcase for comparative studies of the evolution of exchange interactions leading to spin reorientation transition. Also, it should be noted that all phase transitions pass a mixed phase (MP) in a small temperature range.

2. Experimental

High quality twin-free single crystals of $TbFeO_3$ and $YbFeO_3$ were grown by optical floating zone technique using a FZ-4000 (Crystal Systems Corporation) furnace. The shape of the crystals used in the experiments is close to a parallelepiped with approximate dimensions 5 × 7 × 5 mm^3 with the longest dimension along the *b*-axis. The crystal structure was refined with X-ray-data from the Rigaku SmartLab diffractometer at Petersburg Nuclear Physics Institute (PNPI). The crystal structure as well as geometrical the exchange path parameters of $TbFeO_3$ and $YbFeO_3$ at room temperature and at 4 K for $TbFeO_3$ and at 5 K for $YbFeO_3$ are presented in the Tables 2 and 3.

Neutron diffraction studies were performed at the thermal neutron diffractometer D23 at the Institut Laue-Langevin (ILL). The inelastic neutron scattering experiments were performed at the Heinz Maier-Leibnitz Zentrum (MLZ) on the thermal neutron spectrometer PUMA [23] and on the cold neutron spectrometer IN12 at ILL.

Since Fe^{3+} ions take the *4b* position (0 0 0.5) in the *Pnma* unit cell, this situation provides some convenient conditions for the analysis of the contributions of different magnetic configurations to Bragg reflections which corresponds to definite Miller index parity. Thus, to reflections with $h + l$ even, *k* odd, only mode **A** contributes, to reflections with *k* even, $h + l$ odd, only type **C** contributes, to $h + l$ even, *k* even – only type **F** and to $h + l$ odd, *k* odd, only type **G**. The magnetic configurations here are denoted follow the Bertaut notation [24] with four types of possible collinear ordering of the Fe subsystem, expressed by:

F = **S**1 + **S**2 + **S**3 + **S**4,
G = **S**1 − **S**2 + **S**3 − **S**4,
C = **S**1 + **S**2 − **S**3 − **S**4,
A = **S**1 − **S**2 − **S**3 + **S**4,

For the studies, two Bragg reflections for each magnetic configuration were chosen: (1 1 3) and (3 1 1) for type **A**, (2 0 1) and (1 0 2) for type **C**, (0 0 2) and (2 0 0) for type **F**, (0 1 1) and (1 1 0) for type **G**.

Table 1
The irreducible representations and the corresponding magnetic groups in *Pnma* setting for propagation vector $\boldsymbol{k} = (0\,0\,0)$.

	Parent space group *Pnma*		
Irreducible representations	Magnetic group	Fe sites	R sites
Γ_1^+	*Pnma*	$G_x\ C_y\ A_z$	C_y
Γ_2^+	*Pn'm'a*	$C_x\ G_y\ F_z$	$C_x\ F_z$
Γ_3^+	*Pnm'a'*	$F_x\ A_y\ C_z$	$F_x\ C_z$
Γ_4^+	*Pn'ma'*	$A_x\ F_y\ G_z$	F_y
Γ_1^-	*Pn'm'a'*		$A_x\ G_z$
Γ_2^-	*Pnma'*		A_y
Γ_3^-	*Pn'ma*		G_y
Γ_4^-	*Pnm'a*		$G_x\ A_z$
$\Gamma_4^+ \oplus \Gamma_4^-$	$P2_1'2_1'2_1$	$A_x\ F_y\ G_z$	$G_x\ F_y\ A_z$

Table 2
Crystal structure and exchange path parameters of $TbFeO_3$ at $T = 300$ K and 4 K (*Pnma*), X-ray powder data.

$TbFeO_3$		300 K ($\chi^2 = 3.19$)	4 K ($\chi^2 = 3.19$)
a [Å]		5.5996(3)	5.5919(1)
b [Å]		7.6404(4)	7.6345(2)
c [Å]		5.3273(2)	5.3306(1)
Fe 4(b)	x	0.0	0.0
	y	0.0	0.0
	z	0.5	0.5
Tb 4(c)	x	0.0631(4)	0.0644(4)
	y	0.25	0.25
	z	−0.0158(8)	−0.0174(8)
O1 4(c)	x	0.466(4)	0.481(5)
	y	0.25	0.25
	z	0.118(4)	0.136(5)
O2 8(d)	x	0.275(4)	0.273(4)
	y	0.073	0.058(2)
	z	(2)	0.297(4)
		0.265(5)	
Fe-O1-Fe, J_b^{Fe} (Fig. 1)	ang. [deg]	141.8 ± 1.2	138 ± 1.4
	dist. [Å]	4.044 ± 0.011	
			4.088 ± 0.014
Fe-O2-Fe, J_{ac}^{Fe} (Fig. 1)	ang. [deg]	146.6 ± 0.9	149.9 ± 1.0
	dist. [Å]		
		4.030 ± 0.042	4.000 ± 0.042

Table 3
Crystal structure and exchange path parameters of $YbFeO_3$ at $T = 300$ K and at 5 K (*Pnma*), X-ray powder data.

$YbFeO_3$		300 K ($\chi^2 = 2.69$)	5 K ($\chi^2 = 1.60$)
a [Å]		5.5620(4)	5.5563(2)
b [Å]		7.5709(6)	7.5545(3)
c [Å]		5.2317(4)	5.2222(2)
Fe 4(b)	x	0.0	0.0
	y	0.0	0.0
	z	0.5	0.5
Yb 4(c)	x	0.0727(5)	0.0724(4)
	y	0.25	0.25
	z	0.9752(6)	0.9783(6)
O1 4(c)	x	0.376(6)	0.368(4)
	y	0.25	0.25
	z	0.092(6)	0.136(4)
O2 8(d)	x	0.341(4)	0.344(3)
	y	0.073(3)	0.073(2)
	z	0.668(4)	0.662
			(3)
Fe-O1-Fe, J_b^{Fe} (Fig. 1)	ang. [deg]	132.2 ± 1.7	123.2 ± 1.1
	dist. [Å]	4.142 ± 0.020	
			4.294 ± 0.015
Fe-O2-Fe, J_{ac}^{Fe} (Fig. 1)	ang. [deg]	131.4 ± 1.2	130.3 ± 0.8
	dist. [Å]		
		4.19 ± 0.04	4.202 ± 0.024

3. Model

Currently, there is a generally accepted model Hamiltonian [25,26] for describing exchange interactions in the Fe sublattice of $RFeO_3$:

$$H^{Fe-Fe} = \sum_{ij} S_i^{Fe} \bullet J_{ij}^{Fe} \bullet S_j^{Fe} + \sum_i S_i^{Fe} \bullet A_i^{Fe} \bullet S_i^{Fe} + \sum_{mn} S_m^{Fe} \bullet D_{mn}^{Fe} \bullet S_n^{Fe} \quad (1)$$

with S_i^{Fe}: effective spin operator, J_{ij}^{Fe}: isotropic exchange interactions,

A_i^{Fe}: single ion anisotropy, D_{mn}^{Fe}: DMI parameter. The effective spin operator S_i^{Fe} is related to the total magnetic moment of Fe^{3+} as $m_{Fe} = g_s \mu_\beta S^{Fe}$ with $g_s = 2$: spin g-factor, μ_β: Bohr magneton. The interaction between nearest neighbors (i and j) J_{ij}^{Fe} consists of the interaction along the b direction J_b^{Fe} and the one within the ac plane J_{ac}^{Fe}. As has been shown in [25], the differences between these parameters can be as much as 10%, despite the very small geometrical differences in the exchange paths between the interacting atoms (see tables 2, 3). The interaction between next nearest neighbors J_{nnn}^{Fe} includes all interactions via two oxygen anions (Fig. 1). Two antisymmetric exchange constants D1 and D2 responsible for the canting along the b and a from the full DM tensor are enough to describe DMI in orthoferrites [27,28]. The energy gap in the magnon spectrum of Fe ions originates from single ion anisotropy. Using a standard linear spin-wave approach and an average value of exchange interaction in $RFeO_3$, we built a pre-simulated energy map and planed our inelastic neutron scattering experiment accordingly in the high-energy range (Fig. 2). As can be seen in Fig. 2 the scanning ranges were $\Delta E = 20$–40 meV for constant Q-scan (red line) and $\Delta q = 1.0$–1.4 r.l.u. for constant E-scan (green line).Then scan modes of the measurements were chosen in order to achieve a better resolution for the measurements of magnons at low energy as well as at the high energy scale. Modeling and calculation were performed in the program SpinW [29].

At low temperatures, the contribution of the Hamiltonian terms corresponding to the Fe-R and R-R exchange interactions becomes important, that lead to a rebalancing of the total energy. Thus in the case of $TbFeO_3$ below $T_N^{Tb} \sim 3$ K the Tb^{3+} ions spontaneous magnetic ordering takes place which gives the following contribution to the Hamiltonian:

$$H^{Fe-Tb} + H^{Tb-Tb} = \sum_{ij} S_i^{Fe} \bullet J_{ij}^{Fe-Tb} \bullet s_j^{Tb} + \sum_{mn} s_m^{Tb} \bullet J_{mn}^{Tb-Tb} \bullet s_n^{Tb} \quad (2)$$

where s^{Tb} – the Tb spin moment operator $s^{Tb} = \left(g_j - 1\right)\mathbf{J}$ with g_j: Landé factor, **J**: total angular moment.

4. Results and discussion

4.1. $TbFeO_3$, $YbFeO_3$: inelastic neutron scattering studies

High-energy excitations in a $TbFeO_3$ single crystal were studied at PUMA (MLZ) [23], a thermal neutron spectrometer, the low energy range was explored at IN12 (ILL). The measurements at PUMA were performed at temperatures corresponding to different magnetic phases: at the temperatures $T = 15$ K and $T = 5$ K, which correspond to the magnetic representations Γ_4^+ and Γ_2^+ of the Fe-sublattice, respectively. All measurements were performed around the node $\boldsymbol{q} = (3\,1\,0)$ and in the energy range 5 – 75 meV. Following the strategy of the measurements obtained from our pre-simulation, in the experiment we used the "constant-E" mode for measurements around the center of the Brillouin zone (Fig. 3a). The "constant-q" mode was used for measurements in the high-energy range of the dispersion curves and the refinement of the positions of magnon peaks near the energies that correspond to the levels of the crystal field (Fig. 3b). This strategy allowed us to achieve a better resolution for the low energy magnons and to avoid an influence excitations of the RE (rare earth) crystal-field energy levels, which are associated with peaks around 15 meV, 25 meV [30] and 35 meV that are clearly visible in Fig. 3b.

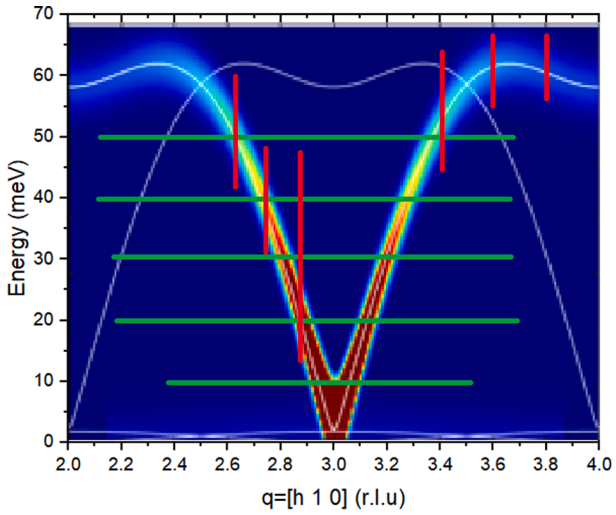

Fig. 2. Scheme of the measurement on a pre-simulated energy map. Colors from red to blue show the intensity; white lines: calculated dispersion curves, green lines: supposed scans with constant E, red lines: those with constant $\boldsymbol{q}$.

For low-energy transfers the measurements on IN12 were performed around node [0 1 0] along the h direction, where h was varied between 0 and 0.8 at $T = 2$ K. During this experiment we returned to "constant-q" mode scans, where the scans were made in the energy range 0–2 meV with energy steps of $\Delta E = 0.05$ meV along the scan. In the same way, the temperature dependence of the energy gap was measured in the temperature range $T = 2$–10 K at $q = (1\,1\,0)$.

For $YbFeO_3$ the low-energy map at IN12 was obtained around node (1 1 0) by measuring along h and k directions at $T = 2$ K. During the experiment we used scans in "constant-q" mode, where the measurements of scan were made in the energy range 0 – 2 meV with energy

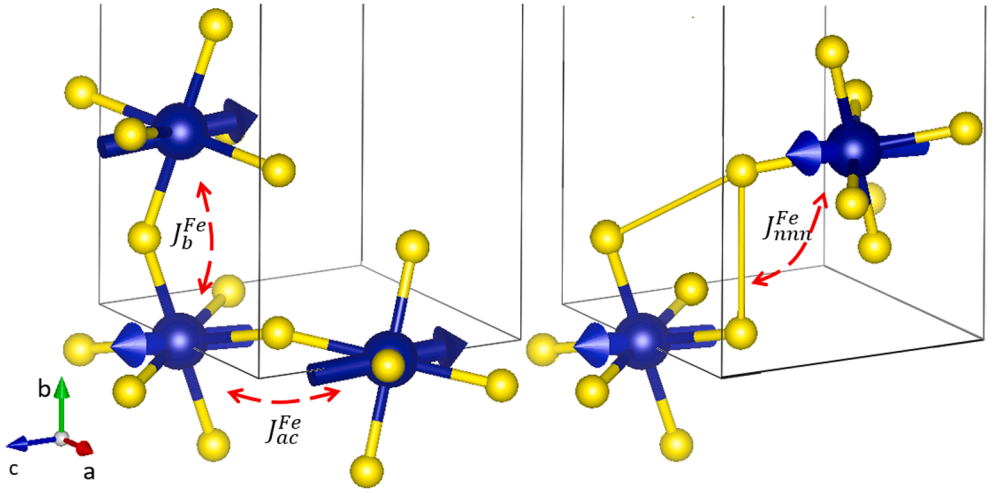

Fig. 1. Scheme of the exchange interaction inside the iron sublattice. Blue spheres: Fe^{3+} ions, yellow: O^{2-}, red arrow: direction of the exchange interaction.

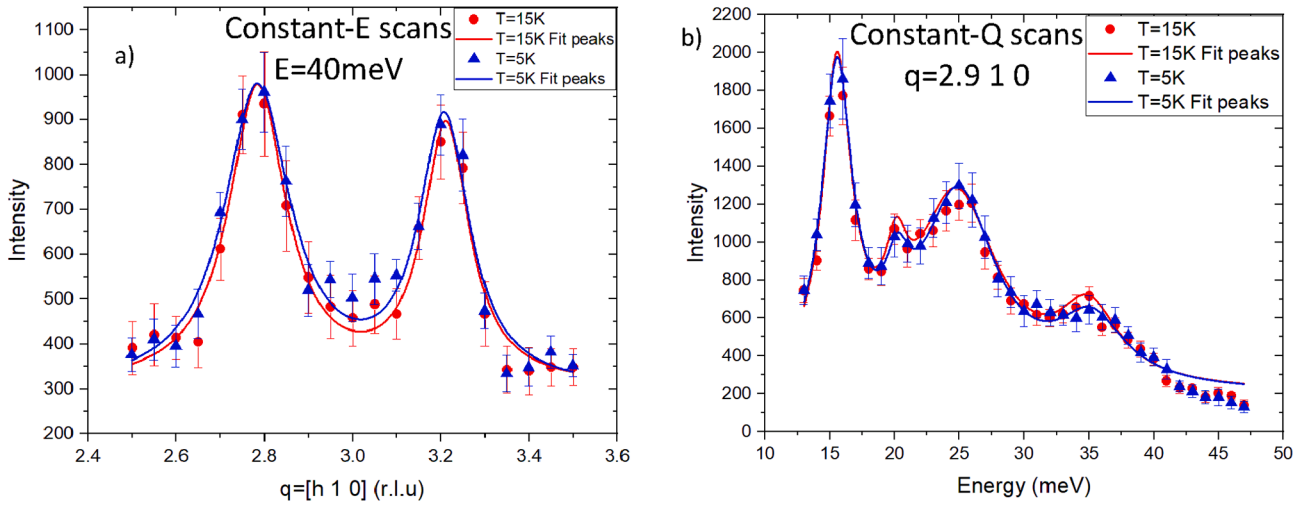

Fig. 3. Typical inelastic neutron scattering scans on $TbFeO_3$, obtained at PUMA at T = 15 K and T = 5 K: a) measurement in "constant-*E*" mode, b) measurement in "constant-$\boldsymbol{q}$" mode.

steps of ΔE = 0.1 meV. For a more accurate determination of the energy gaps, some of the measurements were made with an energy step ΔE = 0.05 meV. The absence of Yb energy levels and of parasitic effects allowed to measure the magnon peaks very accurately.

In $TbFeO_3$ the exchange interactions inside the Fe-sublattice determine the magnetic structure at temperatures above $T_{SR1} = 8.5$ K. The magnetic moments of iron lie within the *ac* plane with a small canting along the *b* direction. The magnetic structure of the Fe-sublattice is described by the magnetic representation Γ_4^+ (HT phase). The results of the experimental data fitting based on Hamiltonian (1) are shown in Table 4. Below $T_{SR1} = 8.5$ K the Fe magnetic moments turn towards the *b* direction. The magnetic structure of Fe-sublattice is described by the magnetic representation Γ_2^+ (LT phase). Fig. 3 shows clearly that the intensities of inelastic neutron scattering from the Fe-subsystem does not change between in the two different phases. Obviously, this means that the exchange interactions inside the Fe-sublattice remain the same. At low temperatures when still $T > T_{SR1}$, the Tb^{3+} ions have an induced ordered magnetic moment which leads to the emergence of the exchange interaction between the Tb and Fe-sublattices J_{ij}^{Fe-Tb}. It is generally accepted that this exchange interaction is responsible for a spin-reorientation transition. However, the strength of the J_{ij}^{Fe-Tb} interaction is not large to change the dispersion curves. Below $T_{SR2} = 3$ K, the arrangement of the magnetic moments of iron returns to the phase represented by Γ_4^+ (LT' phase). This behavior of the Fe-sublattice is different from the one in $YbFeO_3$. The compound $YbFeO_3$ has only one spin-reorientation transition from the phase corresponding to Γ_4^+ to the phase represented by Γ_2^+ around $T_{SR} = 7.5$ K, which takes place through the mixed phase. We suppose that this difference leads to the observed differences in the temperature dependences of the energy gaps and, consequently, in the values of the single ion anisotropy (Table 5). Fig. 4a shows an example of the $YbFeO_3$ scan at temperature $T = 10.8$ K. The second derivative of the intensity (Fig. 4b) shows the points of sharp change in the function. The position of the peak on the graph of the 2nd derivative corresponds to the value of the energy gap. Thus, the temperature dependences of the energy gap for $TbFeO_3$ and $YbFeO_3$ were obtained (Fig. 4 c and d). In $TbFeO_3$ one can see a sharp increase of the energy gap below $T_{SR2} = 3$ K, while in $YbFeO_3$ a similar sharp increase of the energy gap is observed already below $T_{SR} = 7.5$ K. This means that the exchange interaction J_{ij}^{Fe-Tb} does not strongly influence the values of the exchange interactions within the Fe-sublattice. The strong magnetic moment on the Tb^{3+} ions below $T_N^{Tb} \sim 3$ K increases the energy gap in the spectrum of magnons corresponding to excitations of the Fe^{3+}-ions, which stabilizes the system. At the same time in $YbFeO_3$ the exchange interaction J_{ij}^{Fe-Yb} is strong enough to influence the Fe-sublattice and the energy gap increases just below the spin-reorientation transition.

Table 4
The parameters of the exchange interactions in $TbFeO_3$ (in meV) obtained in this work, and parameters obtained for other orthoferrites for comparison.

Compounds/ Magnetic phase	J_b^{Fe}	J_{ac}^{Fe}	J_{nnn}^{Fe}	D1	D2
$TbFeO_3$	4.77 (1)	4.55 (2)	0.10(2)	0.13 (3)	0.10 (3)
$YbFeO_3$ [26]	4.675	4.675	0.15	0.086	0.027
$HoFeO_3$ [28]	4.90 (5)	4.76 (5)	0.150 (7)	0.12 (2)	0.08 (2)
$YFeO_3$ [25]	5.02	4.62	0.22	0.14	0.12

$YbFeO_3$ and $TbFeO_3$ have dispersion curves in the same low energy range. Fig. 5a and 5c show typical scans and energy maps for $YbFeO_3$. The scans have just one peak, which corresponds the excitation of the magnon. Intensities on the map show an almost dispersionless curve in the direction $\boldsymbol{q} = [0\ 1\ l]$ and some dispersion in the direction $\boldsymbol{q} = [0\ k\ 1]$. Our experiment partially repeats the experiment presented in ref. [26] and results are in good agreement with it.

The energy scan of $TbFeO_3$ at $\boldsymbol{q} = (0.2\,1\,0)$ (Fig. 5b) shows peaks around $E_1 = 0.78$ meV, $E_2 = 1.00$ meV and several weak peaks. The first peak at $E_1 = 0.78$ meV corresponds to crystal electric field (CEF) splitting of the ground doublet of Tb^{3+} [31]. It can be seen (Fig. 5d) that in the range $\boldsymbol{q} = (0\,1\,0.3–0.5)$, the positions of the magnon peak and the CEF peak are close each other.

We obtained the value of interaction $J_{ij}^{Tb-Tb} \approx 0.20(3)$ meV according to our estimates within the linear spin wave theory model. This value of the exchange interaction is close to those in other $RFeO_3$ (R = Dy, Er, Tm) compounds [32]. The resulting model of the energy map made with the parameters obtained by fitting is shown in Fig. 5d. The emergence of the rare earth interaction J_{ij}^{Tb-Tb} leads to a second spin-reorientation transition at $T_{SR2} = 3$ K. Probably, the interactions J_{ij}^{Tb-Tb} and J_{mn}^{Fe-Tb} have opposite signs, the same situation as it was established for $HoFeO_3$ [28,33]. Thus, the energy of the exchange interaction within the Tb subsystem to some extent compensates the energy of the exchange interaction between the Fe and Tb subsystems. This is the reason, the Fe-subsystem returns to the Γ_4^+ phase, which is, apparently, the energetically most stable. The further increase of the ordered magnetic moment on the Tb^{3+} ions leads to an increase of the single ion anisotropy of the Fe^{3+} ions. The hierarchy of exchange interactions in $TbFeO_3$ can be

Table 5
Single ion anisotropies (in meV) in the different magnetic phases.

Compounds	$TbFeO_3$			$YbFeO_3$ [30]		$HoFeO_3$ [28]		$YFeO_3$ [25]
Magnetic phase	Γ_4^+ HT	Γ_2^+ LT	Γ_4^+ LT`	Γ_4^+ HT	Γ_2^+ LT	Γ_4^+ HT	Γ_2^+ LT	Γ_4^+ HT
A_{ac}	0.007	0	0.012	0.033	0	0.008	0	0.0091
A_b	0	0.0076	0	0	0.023	0	0.017	0.0025

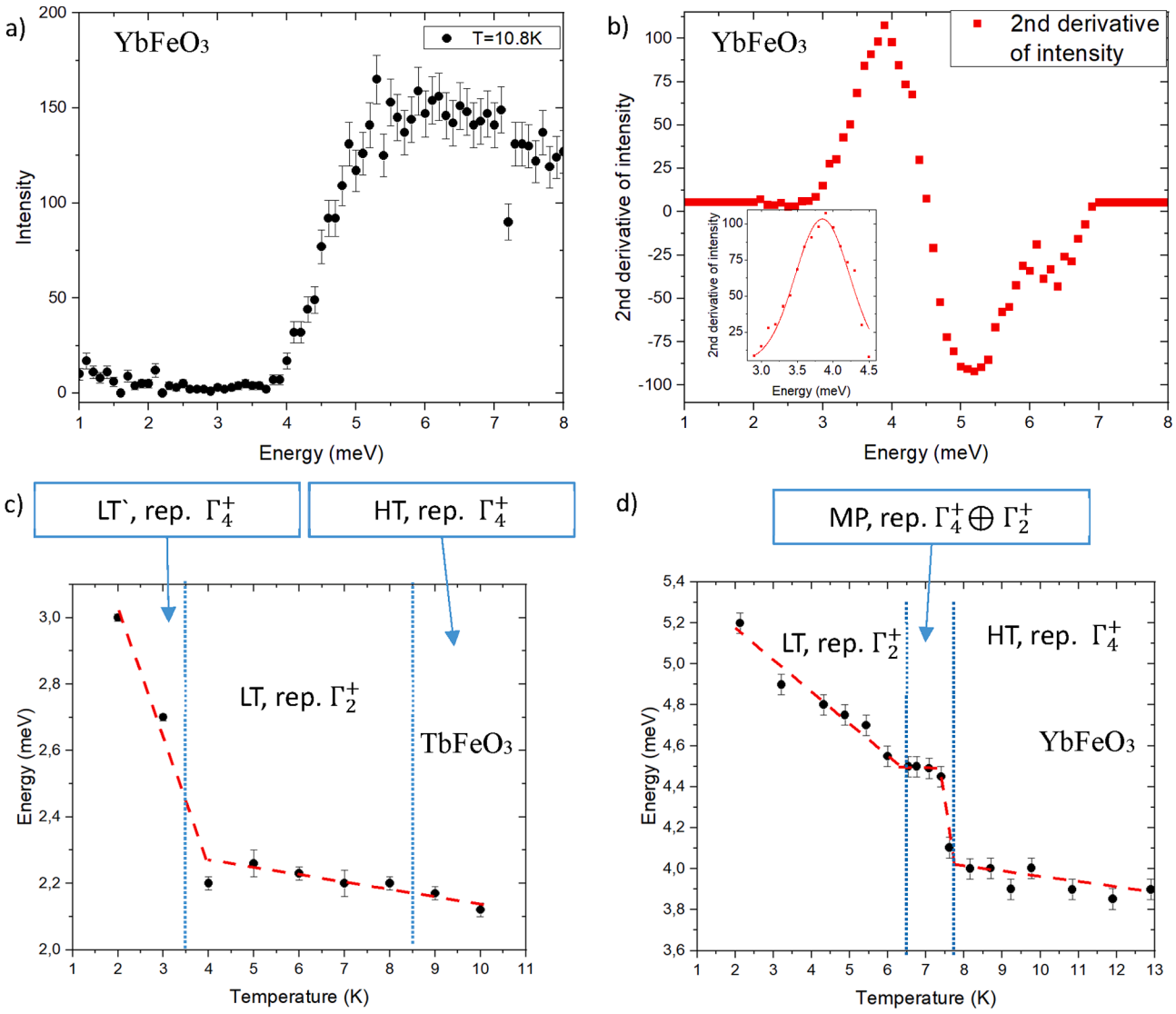

Fig. 4. a) Typical inelastic neutron scattering scans on $YbFeO_3$, obtained at IN12 at $T = 5$ K. b) The second derivative of the intensity. The inset shows the fitting of the peak corresponding to the energy gap. c) and d) Temperature dependences of the energy gaps for $TbFeO_3$ and $YbFeO_3$ respectively. Blue lines: phase-boundaries; dots: measured energies; red dashed lines: a guide to the eyes. The text inscribed refers to the irreducible representations for the Fe-sublattice.

described in the following way: $J_{ij}^{Fe-Fe} > J_{ij}^{Tb-Tb} > J_{ij}^{Tb-Fe}$. The strong J_{ij}^{Fe-Fe} interaction orders the system below $T_N = 650$ K and the competition between J_{ij}^{Tb-Tb} and J_{ij}^{Tb-Fe} defines the subsequent phase transitions. In contrast to that, in $YbFeO_3$ exists another hierarchy sequence of exchange interactions: $J_{ij}^{Fe-Fe} > J_{ij}^{Fe-Yb} > J_{ij}^{Yb-Yb}$ [26], which leads to only one spin-reorientation transition.

4.2. *$YbFeO_3$: diffraction in the magnetic field*

The Neutron diffraction experiments were performed at the thermal neutron diffractometer D23 (ILL). In the first part of the experiment we measured the temperature dependence of eight Bragg reflections – two for each type of the magnetic ordering modes A, C, F and G. The measurements were performed in the temperature range from 2 K to 50 K at cooling and heating in an applied external magnetic field. Three discrete field values of the constant magnetic field B were applied along the c axis: 0.2, 0.5 and 1 T. In the second part of experiment, the fields were directed close to the easy axis of magnetization [1 0 1]. For this field direction temperature dependences of twenty Bragg reflections were measured for five discrete field values: 0.25, 0.5, 1, 1.5 and 3 T.

The integrated intensities of the measured reflections of all types changed with temperature and field. Fig. 6a,b shows the temperature dependences of the G type reflections (1 –1 0) and (1 –3 0) for the various fields as an example. As shown earlier the results of our X-Ray refinements confirm that the crystal structure of the compound remains

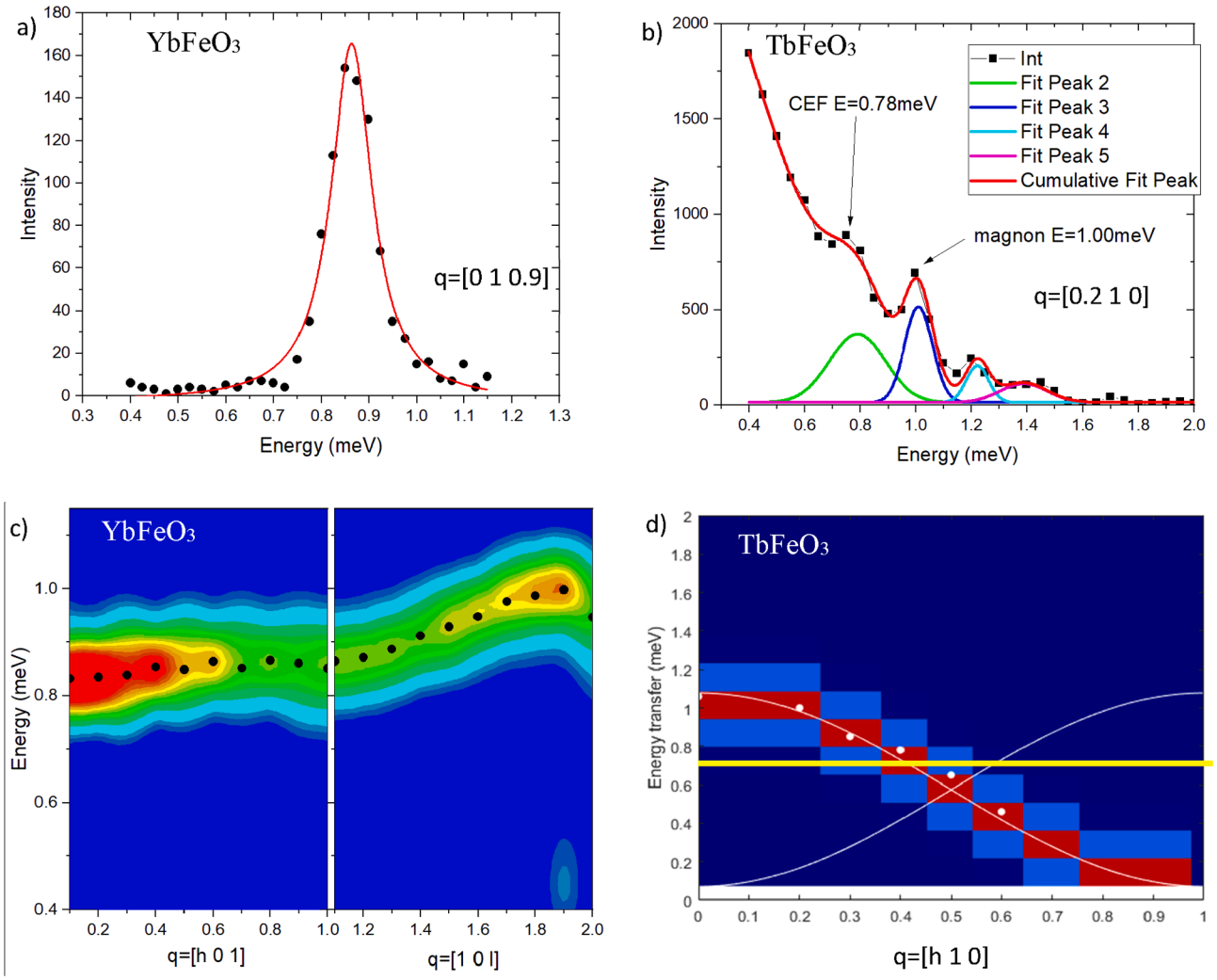

Fig. 5. a, b) Typical energy scans of inelastic neutron scattering fitted by Gaussian for $YbFeO_3$ and $TbFeO_3$, respectively. Black dots: measured intensities, red line: cumulative fit peak. c) Measured map $YbFeO_3$. Black dots: positions of inelastic peaks; colors from red to blue show the intensities. d) Simulated map $TbFeO_3$. White dots: positions of inelastic peaks; white line: model of dispersion curves; yellow line: CEF level; colors from red to blue show the intensity.

unchanged (*Pnma*). Therefore, the change in intensities corresponds to changes in the magnetic structure of the compound from which we can construct the phase diagram. The positions of the phase boundaries can be found by differentiating the temperature dependences of the intensities of every peak. Critical points of the derivative show changes in the system. Thus, the positions of these points in the temperature - field coordinate system lead to the magnetic phase diagram. It can be seen, that for $YbFeO_3$ the application of an external field along the directions either [0 0 1] or [1 0 1] increases the temperature of the phase transition from Γ_4^+ to Γ_2^+ (Fig. 6c,d). The mechanism of this change can be explained as follows. The ordered magnetic moment of the Yb subsystem, induced by the iron magnetic lattice, lies within the ac plane with a deviation of 28 degrees from the *c*-axis [34,35]. The external field is in the same plane, close to the direction of the Yb^{3+} magnetic moment, thus increasing the effective ordering of the Yb^{3+} ion subsystem. This leads in turn to an increase of the exchange interaction J_{ij}^{Fe-Yb} at higher temperatures, which shifts the phase transition. The large difference of one order of magnitude for the exchange interactions $J_{ij}^{Fe-Yb} > J_{ij}^{Yb-Yb}$ [26] does not allow the formation of new magnetic phases for this direction of the external field.

According to previous neutron diffraction studies performed on $TbFeO_3$ single crystals [14], quite another situation takes place there with $J_{ij}^{Tb-Tb} > J_{ij}^{Tb-Fe}$. The application of a magnetic field B up to 4 T along direction [0 1 0] led to a decrease of temperature of the phase transition from Γ_4^+ to Γ_2^+ and to the appearance of new magnetic phases: an incommensurate phase, a domain wall disordered phase which is described by representation configuration $\Gamma_4^+ \oplus \Gamma_4^-$ as the low temperature phase formed below $T_N^{Tb} \sim 3$ K [14]. However, the opposite situation takes place in $HoFeO_3$ where J_{ij}^{Ho-Ho} J_{ij}^{Ho-Fe} [28]. In the low-temperature phase, where the Fe-sublattice is described by representation Γ_2^+, the competition between exchange interactions leads to a rotation of the Ho magnetic moment direction and the formation of several phases, differing in magnetic moment directions [5,36,37]. An external magnetic field suppresses some of these magnetic phases for field values below 2 T and produces new field induced magnetic phases above 2 T. This comparison demonstrates clearly how the ratio between the magnitudes of the exchange interactions influences the spin-reorientation transitions and how the external magnetic field changes the internal energy balance.

5. Conclusion

We have performed neutron studies on the orthoferrites $YbFeO_3$ and $TbFeO_3$ by triple-axis neutron spectroscopy as well as neutron and X-ray diffraction. The obtained exchange parameters between nearest neighbors for Fe^{3+} in $TbFeO_3$ have different values for the exchange within

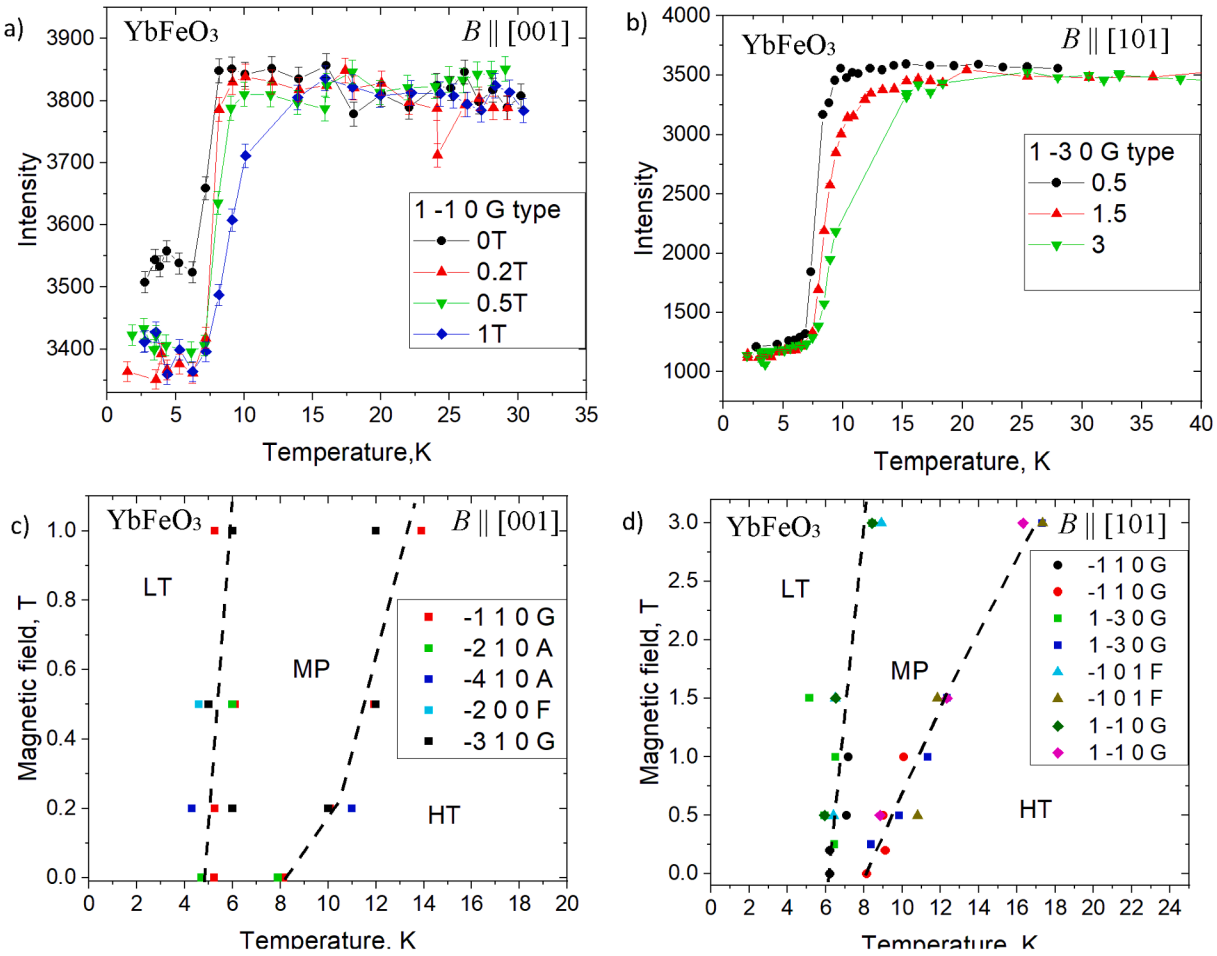

Fig. 6. a, b) Temperature dependence of the integrated intensities of reflections (1–1 0) and (1–3 0) of type G of $YbFeO_3$ for field along [0 0 1] and [1 0 1], respectively. c, d) Magnetic phase diagram of $YbFeO_3$ for fields along [0 0 1] and [1 0 1], respectively. Dotted line: phase boundaries. HT: high-temperature phase with magnetic representation Γ_4^+ of the Fe-sublattice, MP: mixed phase with magnetic representation $\Gamma_4^+ \oplus \Gamma_2^+$, LT: low-temperature phase with magnetic representation Γ_2^+.

the *ac* plane and along the *b*-axis: 4.55(2) meV against 4.77(1) meV. Dzyaloshinsky coefficients responsible for the canting along *b* and *a* were extracted. The change in the energy gap at low temperatures was explored for both compounds. Combining both methods of inelastic neutron scattering and neutron diffraction in external magnetic fields allowed us to show the influence of the energy balance on the phase transitions in the two compounds. The obtained phase diagram for $YbFeO_3$ is discussed as a result of the energy balance between the exchange interactions, DMI, anisotropy and external magnetic field. The exchange within the Fe-subsystems is the strongest one, playing the main role in the whole temperature range below T_N. But other acting forces can influence the magnetic structure significantly. DMI leads to a spin canting, single-ion anisotropy stabilizes the system. For $YbFeO_3$ the interaction within the Yb-subsystem is not sufficient to change qualitatively the balance of energy. This leads to an increase of the anisotropy of the system only. External fields along the [1 0 1] direction produce additional polarization of the Yb subsystem, which provides the increase of the temperature of the spin-reorientation transition. In contrast, for $TbFeO_3$ the strength of the interaction within the Tb-subsystems J_{ij}^{Tb-Tb} nearly compensates the strength of the interaction between the two subsystems J_{ij}^{Tb-Fe}. This leads to an additional spin-reorientation transition. An external field along the [0 1 0] direction can compete with the energy of J_{ij}^{Tb-Tb} and new, field induced magnetic phases are formed in $TbFeO_3$. Such a different behavior depending on the selected rare-earth ion, makes the magnetic phase diagrams of orthoferrites so rich and lets them appear as promising materials for use in technical applications.

CRediT authorship contribution statement

A.K. Ovsianikov: Investigation, Visualization, Writing – original draft, Writing – review & editing. **O.V. Usmanov:** Investigation. **I.A. Zobkalo:** Conceptualization, Methodology, Project administration. **W. Schmidt:** Investigation. **A. Maity:** Investigation. **V. Hutanu:** Investigation, Methodology, Project administration. **E. Ressouche:** Investigation. **K.A. Shaykhutdinov:** Investigation. **K. Yu Terentjev:** Investigation. **S.V. Semenov:** Investigation. **M. Meven:** Supervision. **G. Roth:** Project administration. **L. Peters:** Supervision.

Declaration of Competing Interest

The authors declare that they have no known competing financial interests or personal relationships that could have appeared to influence the work reported in this paper.

Data availability

No data was used for the research described in the article.

Acknowledgments

This work is supported by the Russian Foundation for Basic Research

grant # 19-52-12047, and DFG grant # SA 3688/1-1. The neutron Experiments were performed at the instruments PUMA (MLZ), IN12 (ILL) and D23 (ILL). The authors express their gratitude to A. Bykov for his assistance to the XRD measurements.

References

[1] R.L. White, J. Appl. Phys. 40 (1969) 1061.
[2] D. Treves, J. Appl. Phys. 36 (1965) 1033.
[3] K. Park, H. Sim, J.C. Leiner, Y. Yoshida, J. Jeong, S. Yano, J. Gardner, P. Bourges, M. Klicpera, V. Sechovský, M. Boehm, J. Park, J. Phys.: Condens. Matter 30 (2018).
[4] S. Chaturvedi, P. Shyam, A. Apte, J. Kumar, A. Bhattacharyya, A.M. Awasthi, S. Kulkarni, Phys. Rev. B 93 (2016), 174117.
[5] T. Chatterji, M. Meven, P.J. Brown, AIP Adv. 7 (2017), 045106.
[6] Y. Tokunaga, S. Iguchi, T. Arima, Y. Tokura, Phys. Rev. Lett. 101 (2008), 097205.
[7] Y. Tokunaga, et al., Nat. Mat. 8 (2009) 558.
[8] K. Dey, A. Indra, S. Mukherjee, S. Majumdar, J. Strempfer, O. Fabelo, E. Mossou, T. Chatterji, S. Giri, Phys. Rev. B 100, 214432 – Published 26 December 2019.
[9] J.-H. Lee, Y.K. Jeong, J.H. Park, M.-A. Oak, H.M. Jang, J.Y. Son, J.F. Scott, Phys. Rev. Lett. 107 (2011), 117201.
[10] P. Mandal, V.S. Bhadram, Y. Sundarayya, C. Narayana, A. Sundaresan, C.N.R. Rao, Phys. Rev. Lett. 107 (2011), 137202.
[11] U. Chowdhury, S. Goswami, D. Bhattacharya, J. Ghosh, S. Basu, S. Neogi, Appl. Phys. Lett. 105 (2014), 052911.
[12] M. Das, S. Roy, P. Mandal, Phys. Rev. B 96 (2017), 174405.
[13] Y.-J. Ke, X.-Q. Zhang, Y. Ma, Z.-H. Cheng, Anisotropic magnetic entropy change in $RFeO_3$ single crystals (R = Tb, Tm, or Y), Sci. Rep. 6 (1) (2016).
[14] S. Artyukhin, M. Mostovoy, N.P. Jensen, D. Le, K. Prokes, V.G. de Paula, H. N. Bordallo, A. Maljuk, S. Landsgesell, H. Ryll, B. Klemke, S. Paeckel, K. Kiefer, K. Lefmann, L.T. Kuhn, D.N. Argyriou, Solitonic lattice and Yukawa forces in the rare-earth orthoferrite $TbFeO_3$, Nat. Mater. 11 (8) (2012) 694–699.
[15] E.F. Bertaut, J. Chappert, J. Mareschal, J.P. Rebouillat, J. Sivardiere, Solid State Commun. 5 (1967) 293.
[16] M.I. Aroyo, J.M. Perez-Mato, D. Orobengoa, E. Tasci, G. de la Flor, A. Kirov, Bulg. Chem. Commun. 43 (2) (2011) 183–197.
[17] M.I. Aroyo, J.M. Perez-Mato, C. Capillas, E. Kroumova, S. Ivantchev, G. Madariaga, A. Kirov, H. Wondratschek, Z. Krist. 221 (1) (2006) 15–27.
[18] M.I. Aroyo, A. Kirov, C. Capillas, J.M. Perez-Mato, H. Wondratschek, Acta Cryst. A62 (2006) 115–128.
[19] J.M. Perez-Mato, S.V. Gallego, E.S. Tasci, L. Elcoro, G. de la Flor, M.I. Aroyo, Annu. Rev. Mater. Res. (2015).
[20] K.P. Belov, A.K. Zvezdin, A.M. Kadomtseva, N.B. Krynetskii, A.A. Mukhin, Metamagnetic phase transitions and instability of magnetic structure in rare-earth orthoferrites, Zh. Eksp. Teor. Fiz. 76 (April 1979) 1421–1430.
[21] Ya. B. Bazaliy, L.T. Tsymbal, G.N. Kakazei, V.I. Kamenev, P.E. Wigen, Phys. Rev. B 72, 174403 – Published 1 November 2005.
[22] P. Radhakrishna, J. Hammann, M. Ocio, P. Pari, Y. Allain, Antiferromagnetic ordering in the ytterbium aluminum perovskite $YbAlO_3$, Solid State Commun. 37 (1981) 813.
[23] Heinz Maier-Leibnitz Zentrum, PUMA: Thermal three axes spectrometer, J. Large-Scale Res. Facil. 1 (2015) A13. https://doi.org/10.17815/jlsrf-1-36.
[24] E.F. Bertaut, Magnetism, Academic, New York, 1963.
[25] K. Park, H. Sim, J.C. Leiner, Y. Yoshida, J. Jeong, S. Yano, J. Gardner, P. Bourges, M. Klicpera, V. Sechovský, J. Phys.: Condens. Matter (2018).
[26] S.E. Nikitin, L.S. Wu, A.S. Sefat, K.A. Shaykhutdinov, Z. Lu, et al., Phys. Rev. B 98 (2018), 064424.
[27] V.P. Plakhty, Y.P. Chernenkov, M.N. Bedrizova, Solid State Connnun. 47 (5) (1983) 309–312.
[28] A.K. Ovsianikov, I.A. Zobkalo, W. Schmidt, S.N. Barilo, S.A. Guretskii, V. Hutanu, JMMM 507 (1 August 2020).
[29] S. Toth, B. Lake, J. Phys.: Condens. Matter 27 (2015), 166002.
[30] A. Gukasov, U. Steigenberger, S.N. Barilo, S.A. Guretskii, Phys. B 234–236 (1997) 760–761.
[31] J.D. Gordon, G. Gorodetsky, R.M. Hornreich, JMMM 3 (4) (1976) 288–294.
[32] I. Ameri, A. Boularaf, F. Drief, A. Zaoui, S. Kacimi, JMMM, Volume 537, 2021, 168214, ISSN 0304-8853, https://doi.org/10.1016/j.jmmm.2021.168214.
[33] J.C. Walling, R.L. White, Phys. Rev. B 10 (1974) 4737.
[34] H. Schuhert, S. Hufner, R. Faulhaber, Z. Phys. 220 (1969) 280.
[35] S.R. Brown, I. Hall, J. Phys.: Condens. Matter 5 (1993) L99.
[36] A. Ovsianikov, H. Thoma, O. Usmanov, P.J. Brown, T. Chatterji, A. Sazonov, S. Barilo, L. Peters, V. Hutanu, IEEE Trans. Magn. 58 (2) (Feb 2022), https://doi.org/10.1109/TMAG.2021.3082324.
[37] A.K. Ovsianikov, O.V. Usmanov, I.A. Zobkalo, V. Hutanu, S.N. Barilo, N.A. Liubachko, K.A. Shaykhutdinov, K. Yu Terentjev, S.V. Semenov, T. Chatterji, M. Meven, P.J. Brown, G. Roth, L. Peters, H. Deng, A. Wu, JMMM, Available online 5 May 2022, 169431. https://doi.org/10.1016/j.jmmm.2022.169431.